Final Report for AOARD Grant FA2386-10-1-4126 "Human-Robot Interaction: Intention Recognition and Mutual Entrainment"

August 18, 2012

Name of Principal Investigators: Professor Kazuhiro Kosuge

- **e-mail address:** kosuge@irs.mech.tohoku.ac.jp
- **Institution:** Tohoku University
- **Mailing Address:** Department of Bioengineering and Robotics
  Graduate School of Engineering
  Tohoku University
  6-6-01 Aoba, Aramaki, Aoba-ku,
  Sendai 980-8579, JAPAN
- **Phone:** +81-22-795-6914
- **Fax:** +81-22-795-6914

Period of Performance: 08/31/2010 - 08/30/2012

Abstract

Waltz is a typical example of physical human-human interaction (pHHI) in a well-structured environment, which makes waltz a good start point for understanding pHHI and physical human-robot interaction (pHRI). Waltz involves two dancers. Understanding of the female dancer's abilities in dancing may help designing robots that can physically interact with human in intuitive ways. Therefore, our goal is to reproduce the female dancer's abilities with a robot in pHRI. We focus on the lower level interaction in pHRI, i.e., coupled dynamics. We propose a framework which covers modeling, analysis,

Report Documentation Page

Form Approved
OMB No. 0704-0188

1. REPORT DATE	2. REPORT TYPE	3. DATES COVERED
15 OCT 2012	**Final**	**31-08-2010 to 30-08-2012**

4. TITLE AND SUBTITLE
Human-Robot Interaction: Intention Recognition and Mutual Entrainment

5a. CONTRACT NUMBER
FA23861014126

5b. GRANT NUMBER

5c. PROGRAM ELEMENT NUMBER

6. AUTHOR(S)
Kazuhiro Kosuge

5d. PROJECT NUMBER

5e. TASK NUMBER

5f. WORK UNIT NUMBER

7. PERFORMING ORGANIZATION NAME(S) AND ADDRESS(ES)
Tohoku University,6-6-01 Aramaki Aza Aoba,Sendai 980-8579,Japan,JP,980-8579

8. PERFORMING ORGANIZATION REPORT NUMBER
N/A

9. SPONSORING/MONITORING AGENCY NAME(S) AND ADDRESS(ES)
AOARD, UNIT 45002, APO, AP, 96338-5002

10. SPONSOR/MONITOR'S ACRONYM(S)
AOARD

11. SPONSOR/MONITOR'S REPORT NUMBER(S)
AOARD-104126

12. DISTRIBUTION/AVAILABILITY STATEMENT
Approved for public release; distribution unlimited

13. SUPPLEMENTARY NOTES

14. ABSTRACT
Waltz is a typical example of physical human-human interaction (pHHI) in a well-structured environment. Waltz involves two dancers. The goal is to reproduce the female dancer's abilities with a robot in pHRI. The project focused on the lower level interaction in pHRI, i.e., coupled dynamics, and proposed a framework which covers modeling, analysis, human state sensing and robot control in developing a cooperative female robot dancer. The two dancers' coupled dynamics was modeled as two physically connected inverted pendulums. Stability of this two pendulum system was analyzed. The human state was measured by two laser range sensors, while the measurement noise and bias were corrected by a Kalman filter. Several candidate robot controllers were discussed and evaluated in experiments.

15. SUBJECT TERMS

16. SECURITY CLASSIFICATION OF:			17. LIMITATION OF ABSTRACT	18. NUMBER OF PAGES	19a. NAME OF RESPONSIBLE PERSON
a. REPORT	b. ABSTRACT	c. THIS PAGE			
unclassified	**unclassified**	**unclassified**	**Same as Report (SAR)**	**65**	

human state sensing and robot control in developing a cooperative female robot dancer. We model the two dancers' coupled dynamics as two physically connected inverted pendulums. Stability of this two-pendulum system is analyzed. The human state is measured by two laser range sensors, while the measurement noise and bias are corrected by a Kalman filter. Several candidate robot controllers are discussed and evaluated in experiments. Our contributions include:

1. A model for describing dancers' coupled dynamics in waltz;
2. Implementation of poly-quadratic stability condition in proving the two-LIPM system's stability;
3. A novel method which uses LRF to infer human's timing in pHRI, and a Kalman-filter-based method for estimating the state of human;
4. Analysis and validation of several robot controllers.

1 Introduction

Today, a vast variety of robots have been created to help human. To realize this design goal, robots must interact with the external world. Depending on the requirements of tasks, robots may interact with diversified objects, including human. Because of the extremely complicated nature of human, a large field of study is dedicated to understanding, designing, and evaluating robot systems for human-robot interaction (HRI) [1].

HRI can be on the cognitive level (cognitive human-robot interaction, cHRI [2]) and physical level (physical human-robot interaction, pHRI [3]). As in the near future human and robot are expected to cooperate within the shared workspace in industrial and domestic applications, pHRI is drawing increasing attention and has become one of the major focuses in robotics research.

Because human has the strong ability to cooperate with each other, we could assume that for the same task, the pHHI (physical human-human interaction) may have superior performance than the pHRI. Besides performance, we may have more "natural" user experience in pHHI than in pHRI. Due to the above reasons, understanding the pHHI could help the researchers to create more cooperative robots to enhance the pHRI performance [4].

Among the millions of pHHI, we select waltz as the subject of our study. One reason is that waltz is a real-world, interesting pHHI; a waltz partner robot which has desired pHRI performance has the potential to be socially adopted for entertainment and rehabilitation purposes [5]. Another reason

Figure 1: One developed dance partner robot [6]

is that waltz is the pHHI in well-structured environment, the simple environment and simple context knowledge make waltz a good start point for understanding pHHI and pHRI. Therefore, the pHHI and pHRI of waltz have attracted our attention.

Waltz involves a male dancer (usually the leader) and a female dancer (usually the follower). Understanding the female dancer's ability in pHHI may help improving a robot's performance in pHRI; Therefore, our research is to develop a robot which can cooperatively dance with a human leader with playing the female dancer's role. A prototype developed in earlier stage is shown in Fig. 1 [6].

The pHHI and the pHRI can be divided into two levels:

Intention estimation Waltz has a fixed set of motion patterns, i.e., dance steps. During dancing, when the leader selects the next step, the follower must estimate the leader's intention.

Coupled dynamics The follower's body dynamics are coupled with the leader's, hence the follower must adapt herself to the coupled body dynamics.

To reproduce the pHHI of waltz in pHRI, the dance partner robot should also be able to carry on the two tasks.

The higher level interaction, i.e., intention recognition, has been intensively investigated in our earlier work [6, 7] and other researchers' studies [8–11]. In contrast, the lower level interaction, i.e., coupled dynamics, is still not well-understood. In the field of robotics, some dance robots that can interact with human have also been demonstrated by Khatib et al. [12], Oudeyerand et al. [13], and Setiawan et al. [14], etc. These works have realized pHRI from the engineering perspective. At the same time, model and analysis of the coupled dynamics are still not investigated.

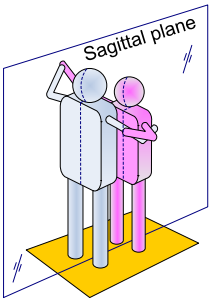

Figure 2: Dancers' coupled body dynamics in sagittal plane are studied

Aside from the pHRI in dance, numerous methods have been proposed in other pHRI-related applications. Colgate et al. analyzes the coupled stability between a linear manipulator and a linear, passive environment, but the explicit modeling of human dynamics is not implemented [15]. Kazerooni models the pHRI between a human arm and a robot extender, and uses small gain theorem to design the robot controller which has the guaranteed stability, but only the human arm is modeled, with linear, low-pass-filter type transfer functions [16]. The coupled dynamics in pHRI has been intensively investigated in the field of haptics (between a human operator and a haptic display), teleoperation (between a human operator and a robot master), and human assistance [17–23], in which coupled dynamics in pHRI has been thoroughly, quantitatively studied and used for controller designs. However, because of their specific applications, only human arm dynamics are modeled with some passive, impedance-type models, while the arm dynamics are very different from a dancer's body dynamics in waltz. In contrast, human's body dynamics in waltz are close to a walking biped, whose dynamics are not strictly stable or passive.

Therefore, to understand the dancers' coupled dynamics in waltz and utilize the knowledge obtained to enhance pHRI, new models, new analysis and design approaches are needed.

On modeling the coupled dynamics in waltz, we focus on two dancers' body dynamics in sagittal plane (Fig. 2). Hence the limitation of the simplification is that dancers' rotational motions are not considered; however, this one-dimensional simplified case enable us to better understand the fundamentals in pHHI and pHRI. Similar one-dimensional simplifications also appeared in literature in coordinated teleoperation [24], haptic human-robot interaction [25], and human-robot-human cooperation [4], etc.

Because our goal is developing a dance partner robot, we aim to address three issues:

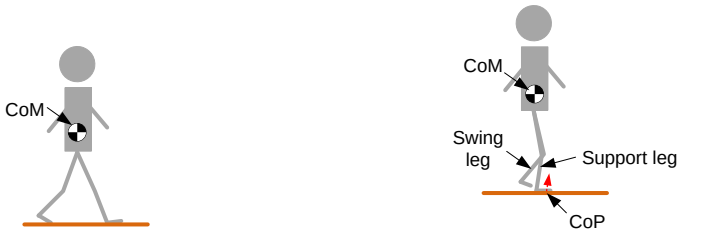

(a) Double-support phase (b) Single-support phase

Figure 3: Illustration of terms related with walking

Modeling: The coupled dynamics in waltz are to be modeled;

Analysis: System characteristics of the model are to be analyzed;

Control: Based on the characteristics of the coupled dynamics, robot controllers are to be designed.

2 Approach and Results

2.1 Modeling

2.1.1 A single dancer's model

Human's body dynamics in waltz can be described by a bipedal walking model; therefore here we briefly list some terms related with walking:

Single-support phase: The period of time when only one foot is in contact with ground, as shown in Fig. 3(b).

Double-support phase: The period of time when both feet are in contact with ground, as shown in Fig. 3(a).

Support leg: During single-support phase, the support leg is in contact with ground while supporting the body weight, as shown in Fig. 3(b).

Swing leg: During single-support phase, the swing leg is traveling in the air; the swing leg has no contact with the ground, as shown in Fig. 3(b).

Center of mass (CoM): The weighted average position of all the mass in human body, as shown in Fig. 3.

(a) Simplified human walking model (b) Linear inverted pendulum

Figure 4: LIPM as a simplified model

Center of pressure (CoP): The weighted average position of all the pressure on the contact surface between human's support foot and ground, as shown in Fig. 3(b).

A simplified model of walking is linear inverted pendulum (LIPM, [26]). Consider a simplified human body model in sagittal plane (Fig. 4(a)). The origin of the coordinate frame is at human's CoP (center of pressure). By applying several constraints on the walking system [26], we can convert the system into an inverted pendulum as shown in Fig. 4(b). This system has linear dynamics defined by [26]

$$\ddot{x} = \frac{g}{z}x + \frac{1}{m}f \tag{1}$$

where x is the position of LIPM's CoM (center of mass) with respect to LIPM's CoP, z is the height of CoM, g is gravity acceleration, m is mass of the body, and f is the external force.

Because of the instability of LIPM, a balance controller is needed. The balance controller intermittently resets x, i.e., this inverted pendulum can instantaneously reset its CoP to keep balance. Let $\{t_k\}$ be the set of moments at which the CoP resets; let $\dot{x}^-$, $\dot{x}^+$ be the CoM velocity before and after t_k; let x^-, x^+ be the CoM's relative position (with respect to CoP) before and after t_k. The LIPM with its controller can be viewed as an impulsive dynamical system [27]:

$$\begin{cases} \ddot{x} &= (g/z)x, \ t \notin \{t_k\} \\ x^+ &= h_{\text{bal}}(x^-, \dot{x}), \ t \in \{t_k\} \end{cases} \tag{2}$$

The function h_{bal} in (2) is the balance controller. There are many candidates for the balance controller h_{bal}. Here a proposed controller [28] is implemented, with x is reset by

$$x^+ = -\frac{t_\tau C_\tau}{S_\tau}\dot{x}(kT) + \frac{t_\tau}{S_\tau}v_d(k+1) \tag{3}$$

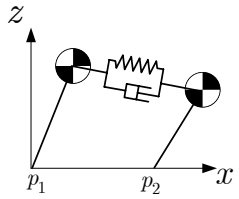

Figure 5: Dancers' model as two inverted pendulums

where $v_d(k+1) = \dot{x}(kT_p+T_p)$ is a reference input which represents the desired velocity at t_{k+1}; $t_\tau = \sqrt{z/g}$, $C_\tau = \cosh(T_p/t_\tau)$, $C_\tau = \cosh(T_p/t_\tau)$, and T_p is the period of the CoP reset.

To test whether the LIPM can be used in modeling a waltz dancer, we compare a professional female dancer's motions with the model-generated trajectories. Results of comparison support the use of LIPM, while details of the experiments can be found in [29].

2.1.2 Model of the coupled dynamics

The physical interaction of waltz involves two dancers. If each dancer is modeled by an LIPM, then the two physically coupled dancers can be modeled by two spring-damper-connected LIPMs, as shown in Fig. 5. Without loss of generality, we can consider the left LIPM as the leader, and the right LIPM as the follower. Let x_l^g and x_f^g be the leader's and the follower's CoM positions . Let p_l^g and p_f^g be their CoP positions, all with respect to the global frame. Defining a state vector $\boldsymbol{x}$:

$$\boldsymbol{x} = [x_l, \dot{x}_l, x_f, \dot{x}_f, q]^T \tag{4}$$

where $x_l = x_l^g - p_l^g$, $x_f = x_f^g - p_f^g$ are the leader's and the follower's relative positions of CoM with respect to their CoPs. $q = x_f^g - x_l^g - d_{\text{spring}}$, d_{spring} is the spring's natural length. k_c and d_c are constants of the spring and the damper. Dynamics of the two-LIPM system are:

$$\begin{cases} \dot{\boldsymbol{x}} &= \boldsymbol{A}\boldsymbol{x}, \ t \notin \{t_k^l\} \cup \{t_k^f\} \\ \boldsymbol{x}^+ &= \boldsymbol{H_l}\boldsymbol{x}^- + \boldsymbol{B_l}v_d^l, \ t \in \{t_k^l\} \\ \boldsymbol{x}^+ &= \boldsymbol{H_f}\boldsymbol{x}^- + \boldsymbol{B_f}v_d^f, \ t \in \{t_k^f\} \end{cases} \tag{5}$$

where $\{t_k^l\}$ and $\{t_k^f\}$ are the leader's and the follower's respective CoP reset moments. v_d^l and v_d^f are the leader's and the follower's desired velocities at

$\{t_k^l\}$ and $\{t_k^f\}$, respectively. Matrix $\boldsymbol{A}$ is defined as

$$\boldsymbol{A} = \begin{pmatrix} 0 & 1 & 0 & 0 & 0 \\ \frac{g}{z_l} & -\frac{d_c}{m_l} & 0 & \frac{d_c}{m_l} & \frac{k_c}{m_l} \\ 0 & 0 & 0 & 1 & 0 \\ 0 & \frac{d_c}{m_f} & \frac{g}{z_f} & -\frac{d_c}{m_f} & -\frac{k_c}{m_f} \\ 0 & -1 & 0 & 1 & 0 \end{pmatrix} \tag{6}$$

where z_l, z_f are the leader's and the follower's CoM heights and m_l, m_f are their body mass. $\boldsymbol{H_l}$, $\boldsymbol{H_f}$, $\boldsymbol{B_l}$, and $\boldsymbol{B_f}$ are the matrix forms of (3), with

$$\boldsymbol{H_l} = \left(\begin{array}{cc|c} 0 & -C_l t_{\tau_l}/S_l & \multirow{2}{*}{$\mathbf{0}_{2\times 3}$} \\ 0 & 1 & \\ \hline \multicolumn{2}{c|}{\mathbf{0}_{3\times 2}} & \boldsymbol{I}_{3\times 3} \end{array}\right) \tag{7}$$

$$\boldsymbol{H_f} = \left(\begin{array}{c|ccc} \boldsymbol{I}_{2\times 2} & \multicolumn{3}{c}{\mathbf{0}_{2\times 3}} \\ \hline & 0 & -C_f t_{\tau_f}/S_f & 0 \\ \mathbf{0}_{3\times 2} & 0 & 1 & 0 \\ & 0 & 0 & 1 \end{array}\right) \tag{8}$$

and $\boldsymbol{B_l} = [t_{\tau_l}/S_l, 0, 0, 0, 0]^T$, $\boldsymbol{B_f} = [0, 0, t_{\tau_f}/S_f, 0, 0]^T$. $\boldsymbol{H_l H_f} = \boldsymbol{H_f H_l} = \boldsymbol{H}$. Symbols like $t_{\tau_{l,f}}$, $C_{l,f}$ and $S_{l,f}$ are defined similarly as in (3). Interaction force between the two LIPMs is denoted by f, with $f = \boldsymbol{c_c x}$, where

$$\boldsymbol{c_c} = [0, d_c, 0, -d_c, -k_c] \tag{9}$$

2.2 Analysis

2.2.1 System model with synchronization errors

Since the coupled dynamics have been modeled by (5), we can analyze system stability. In our earlier work, by assuming two dancers' CoP resets are precisely synchronized, stability of the simplified dynamics has been analyzed [30]. However, in real applications two dancers' timing errors (or synchronization error) are inevitable. Therefore, it is necessary to consider the effect of timing error on system stability.

Let the leader's and the follower's k-th CoP reset moment be t_k^l and t_k^f (Fig. 6). Because in pHRI the follower is a robot, we can keep $t_k^f > t_k^l$ for all k, i.e.,

$$0 < t_k^f - t_k^l \triangleq \delta t_k^f \leq \overline{\delta t_f}, \forall k \tag{10}$$

where δt_k^f is the follower's timing error in following the leader, and $\overline{\delta t_f}$ is δt_k^f's upper bound.

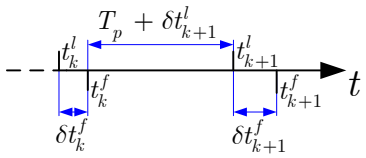

Figure 6: Timing errors of the leader and the follower

Consider the timing error of the human leader and the robot following, we have

$$-\overline{\delta t_l}/2 \leq \delta t^l_{k+1} \triangleq t^l_{k+1} - t^f_k - T_p \leq \overline{\delta t_l}/2, \forall k \tag{11}$$

The assumptions of bounded timing errors, i.e., $0 < \delta t^f_k \leq \overline{\delta t_f}$ and $-\overline{\delta t_l}/2 \leq \delta t^l_k \leq \overline{\delta t_l}/2$ are reasonable because if δt^f_k or δt^l_k grows unbounded, the two dancers would be unable to dance together.

System dynamics from t^{f+}_k to t^{f+}_{k+1} consists four transitions, namely

1. From t^{f+}_k to t^{l-}_{k+1}, during which there is no CoP reset moment; system dynamics are continuous;
2. From t^{l-}_{k+1} to t^{l+}_{k+1}, the leader's CoP reset moment with impulsive dynamics;
3. From t^{l+}_{k+1} to t^{f-}_{k+1}, continuous dynamics;
4. From t^{f-}_{k+1} to t^{f+}_{k+1}, the follower's CoP reset moment with impulsive dynamics.

According to (5), (10), (11), we have

$$\begin{aligned} \boldsymbol{x}(t^{f+}_{k+1}) &= \boldsymbol{H_f} e^{\boldsymbol{A}\delta t^f_{k+1}} \boldsymbol{H_l} e^{\boldsymbol{A}(T_p+\delta t^l_{k+1})} \boldsymbol{x}(t^{f+}_k) \\ &\quad + \boldsymbol{H_f} e^{\boldsymbol{A}\delta t^f_{k+1}} \boldsymbol{B_l} v^l_d + \boldsymbol{B_f} v^f_d \end{aligned} \tag{12}$$

Equation (12) describes a discrete linear system. Its homogeneous form is:

$$\boldsymbol{x}(t^{f+}_{k+1}) = \boldsymbol{A^*_d}(\delta t^l_{k+1}, \delta t^f_{k+1}) \boldsymbol{x}(t^{f+}_k) \tag{13}$$

where

$$\boldsymbol{A^*_d}(\delta t^l_{k+1}, \delta t^f_{k+1}) = \boldsymbol{H_f} e^{\boldsymbol{A}\delta t^f_{k+1}} \boldsymbol{H_l} e^{\boldsymbol{A}(T_p+\delta t^l_{k+1})} \tag{14}$$

and the entries of $\boldsymbol{A^*_d}(\delta t^l_{k+1}, \delta t^f_{k+1})$ depend on δt^l_{k+1} and δt^f_{k+1}, which are both time-varying.

2.2.2 Stability of the coupled dynamics

To analyze the stability of the uncertain, time-varying system in (13), we introduce a stability condition proposed by Daafouz et al. [31]. To apply this stability condition, firstly the time-varying matrix $\boldsymbol{A_d^*}(\delta t_k^l, \delta t_k^f)$ is to be converted into a linear matrix polytope with the following form:

$$\boldsymbol{A_d^*}(\delta t_k^l, \delta t_k^f) = \sum_{i=1}^{N} \xi_i(k) \boldsymbol{A_i} \tag{15}$$

$$\xi_i(k) \geq 0, \ \sum_{i=1}^{N} \xi_i(k) = 1 \tag{16}$$

Details of the conversion can be found in [28]; finally $\boldsymbol{A_d^*}$ is converted into (15), with

$$\begin{aligned}
\boldsymbol{A_1} &= \boldsymbol{A_1'} - \frac{\overline{\delta t_l}}{2}\boldsymbol{A_2'} - \frac{\overline{\delta t_{lf}}}{2}\boldsymbol{A_4'}, \\
&\quad \xi_1(k) = 1 - \xi_2(k) - \xi_3(k) - \xi_4(k) \\
\boldsymbol{A_2} &= \boldsymbol{A_1} + 3\overline{\delta t_l}\boldsymbol{A_2'}, \ \xi_2(k) = \frac{\delta t_k^l + \overline{\delta t_l}/2}{3\overline{\delta t_l}} \\
\boldsymbol{A_3} &= \boldsymbol{A_1} + 3\overline{\delta t_f}\boldsymbol{A_3'}, \ \xi_3(k) = \frac{\delta t_k^f}{3\overline{\delta t_f}} \\
\boldsymbol{A_4} &= \boldsymbol{A_1} + 3\overline{\delta t_{lf}}\boldsymbol{A_4'}, \ \xi_4(k) = \frac{\delta t_k^l \delta t_k^f + \overline{\delta t_{lf}}/2}{3\overline{\delta t_{lf}}}
\end{aligned} \tag{17}$$

where

$$\begin{aligned}
\boldsymbol{A_1'} &= \boldsymbol{H_f H_l} e^{\boldsymbol{A}T_p} \\
\boldsymbol{A_2'} &= \boldsymbol{H_f H_l} e^{\boldsymbol{A}T_p} \boldsymbol{A} \\
\boldsymbol{A_3'} &= \boldsymbol{H_f A H_l} e^{\boldsymbol{A}T_p} \\
\boldsymbol{A_4'} &= \boldsymbol{H_f A H_l} e^{\boldsymbol{A}T_p} \boldsymbol{A}
\end{aligned} \tag{18}$$

The above system is poly-quadratically stable, if and only if there exist four symmetric positive definite matrices $\boldsymbol{S_1} \ldots \boldsymbol{S_4} > 0$, and four regular matrices $\boldsymbol{G_1} \ldots \boldsymbol{G_4}$, which satisfy the following linear matrix inequality (LMI):

$$\begin{pmatrix} \boldsymbol{G_i} + \boldsymbol{G_i}^T - \boldsymbol{S_i} & \boldsymbol{G_i}^T \boldsymbol{A_i}^T \\ \boldsymbol{A_i G_i} & \boldsymbol{S_j} \end{pmatrix} > 0 \tag{19}$$

for all $i = 1, \ldots, 4$ and $j = 1, \ldots, 4$. In another word, testing stability of the two-LIPM system is equivalent to examining the feasibility of (19).

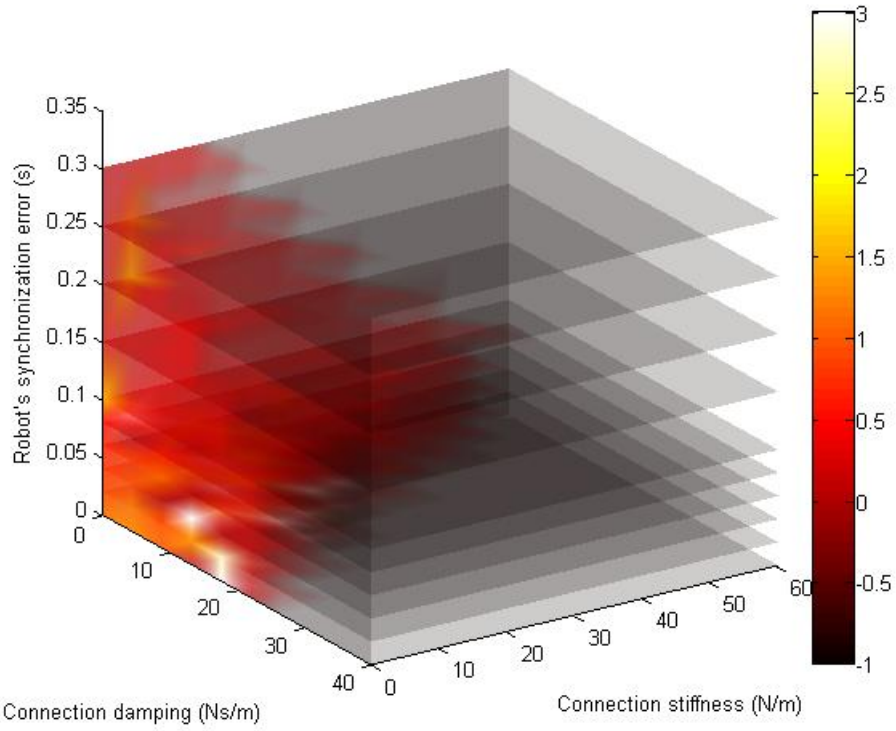

Figure 7: Poly-quadratic stability with respect to $\overline{\delta t_f}$ (z-axis), k_c (y-axis), and d_c (x-axis); regions that have "temperature" greater than 0 correspond to the stable combinations of $\overline{\delta t_f}$, k_c and d_c

2.2.3 Numerical results

Because the stability test involves the process of numerically solving the LMI problems, it is extremely difficult to find a closed-form expression which describes the relationship between stability and synchronization error's upper bound ($\overline{\delta t_l}$ and $\overline{\delta t_f}$). Therefore, we numerically analyze system stability under different conditions.

As system stability involves 4 factors ($\overline{\delta t_l}$, $\overline{\delta t_f}$, k_c, and d_c) which are difficult to be visualized in a 3-D Cartesian space, we assume $\overline{\delta t_l} = 0.1\,\text{s}$ (i.e., the human leader's period error is smaller than 0.1 s, which is a reasonable assumption) and visualize the other 3 factors in Fig. 7.

Three contours with different $\overline{\delta t_f}$ are shown in Fig. 8.

According to Fig. 7 and Fig. 8, smaller $\overline{\delta t_f}$ leads to larger stable region of k_c and d_c, which is in line with our intuition [28].

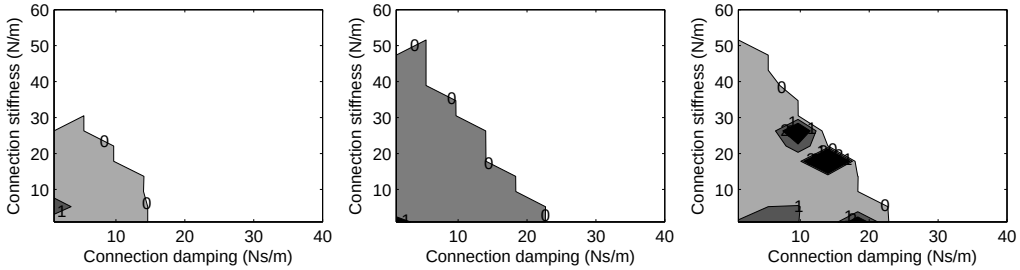

(a) $\overline{\delta t_l} = 0.1\,\mathrm{s}$, $\overline{\delta t_f} = 0.2\,\mathrm{s}$ (b) $\overline{\delta t_l} = 0.1\,\mathrm{s}$, $\overline{\delta t_f} = 0.1\,\mathrm{s}$ (c) $\overline{\delta t_l} = 0.1\,\mathrm{s}$, $\overline{\delta t_f} = 0\,\mathrm{s}$

Figure 8: Contours of poly-quadratic stability with respect to k_c and d_c; dark-colored area inside the 0 border corresponds to poly-quadratically stable combinations of k_c and d_c

2.3 Sensing Human

Besides interaction force in pHRI, the robot also needs extra information to cooperate with the human dancer. The information can be divided into two categories:

1. Timing of dance: The robot needs to know the timing of dance to reset its CoP;

2. State of human dancer: The robot needs to know the human dancer's state, e.g., CoM velocity and position.

Additional sensors are needed to measure those information. In the subsequent part we will introduce how to sense the timing of dance

2.3.1 Sensing timing of dance

Two laser range finders (LRF, Hokuyo UBG-04LX-F01, [32]) are installed on the robot, as shown in Fig. 9. One LRF is installed (at human's waist height) for measuring human's waist position, while the other LRF is installed (at human's ankle height) for measuring ankles' positions.

With the two LRFs, human's waist and ankles can be identified; their centroids are computed to represent their positions, as shown in Fig. 10.

When human is walking, the CoP reset corresponds to the landing of the swing foot, while the landing of the swing foot can be detected by analyzing the spatial information of human's ankles. Actually, by observing the trajectories of the two ankles with LRFs, the robot can sense much human

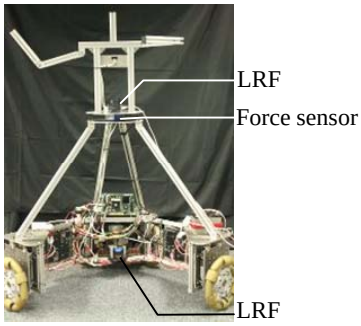

Figure 9: The robot has implemented one force/torque sensor in waist, and two LRFs at ankle and waist height

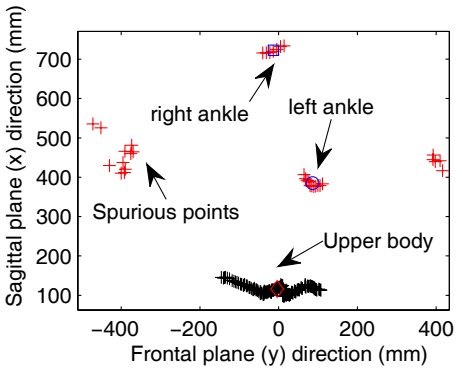

Figure 10: A combined range image. Image of two ankles are obtained from the LRF on the ankle height, while the upper body image is from another LRF installed at the waist height. The markers are the respectively computed centroids of the waist and the ankles

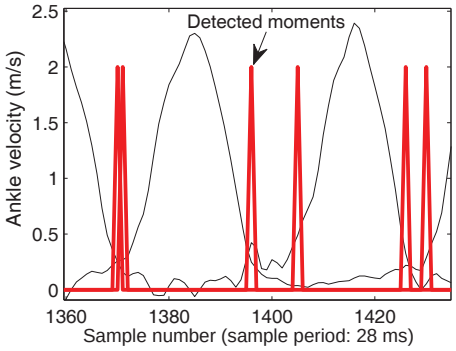

Figure 11: Detecting foot landing/swinging moments from ankle velocities. Black curves: ankle velocities. Red impulses: detected landing/swinging moments, moments between the paired impulses are double-support phases

dancer's information. Besides CoP reset moments, we are also interested in inferring human's single-support phase and double-support phase.

The beginning of double-support phase is represented by the landing moment of the swing foot; similarly, the ending of this phase is related with the initiated motion of the (previous) support foot. Therefore, the two ankles' velocity curves are used to estimate the beginning and ending moments of double-support phase. Using the two ankles' velocity information, we can infer human's timing (i.e., the beginning and ending of double-support phase) with a simple threshold-based method. The idea of this method is to find the "falling edge" and "rising edge" on the velocity curves of the swing foot and the support foot, respectively. The detected moments are shown in Fig. 11.

2.3.2 Sensing state of human

With the two LRFs, we can get positions and velocities of the centroids of human's waist and ankles. Let p_{wst} and $\dot{p}_{\text{wst}}$ be the position and velocity of the waist centroid (in sagittal plane); let p_{spt} be the centroid position of the support foot. To get human's state as an LIPM (including x and $\dot{x}$), one straightforward method is to use

$$[x, \dot{x}]^T = [p_{\text{wst}} - p_{\text{spt}} - d_{\text{LRF}}, \dot{p}_{\text{wst}}]^T \tag{20}$$

where d_{LRF} is the two LRFs' installation offset, which can easily be measured or calibrated.

However, the method given in (20) is not practical due to the following problems:

1. p_{wst} is not the real CoM position. The real CoM position cannot be directly measured by LRF, instead, LRF can only measure the surface points on human body; there is a bias between their centroid and the real CoM position; this bias could be time-varying. We denote this bias with $d_{\text{srf}} + \delta_{\text{srf}}$, where d_{srf} is its static component, and δ_{srf} is the time-varying compoment;

2. p_{spt} is not the real CoP position. During walking, human CoP is "traveling" in the contact surface between the foot and the floor. This error is denoted by δ_{CoP}

3. p_{wst}, $\dot{p}_{\text{wst}}$, and p_{spt} contain large noises.

The listed problems can be formulated in the following way. Firstly, we define the sensors' observation as

$$\boldsymbol{y}_{\text{out}} = \begin{pmatrix} p_{\text{wst}} - p_{\text{spt}} - d_{\text{LRF}} - d_{\text{srf}} \\ \dot{p}_{\text{wst}} \end{pmatrix} \tag{21}$$

Assuming the sensors' measurement noise is $[v_1, v_2]^T$, then

$$\boldsymbol{y}_{\text{out}} = \begin{pmatrix} p_{\text{wst}} - p_{\text{spt}} - d_{\text{LRF}} - d_{\text{srf}} \\ \dot{p}_{\text{wst}} \end{pmatrix} = \begin{pmatrix} x + \delta_{\text{srf}} + \delta_{\text{CoP}} \\ \dot{x} \end{pmatrix} + \begin{pmatrix} v_1 \\ v_2 \end{pmatrix} \tag{22}$$

LIPM's state is $\boldsymbol{x} = [x, \dot{x}]^T$. Define $\delta_o = \delta_{\text{srf}} + \delta_{\text{CoP}}$, the LIPM's dynamics in single-support phase are

$$\begin{aligned} \dot{\boldsymbol{x}} &= \begin{pmatrix} 0 & 1 \\ g/z & 0 \end{pmatrix} \boldsymbol{x} + [0, 1/m]^T f + [w_1, w_2]^T \\ \boldsymbol{y}_{\text{out}} &= [x + \delta_o, \dot{x}]^T + [v_1, v_2]^T \end{aligned} \tag{23}$$

where w_1, w_2 are process noises, representing the unmodeled dynamics of human dancer.

According to (23), inferring human's state is equivalent to observing $\boldsymbol{x}$ from $\boldsymbol{y}_{\text{out}}$, which contains unknown, time-varying offset δ_o and measurement noise v_1, v_2. $\boldsymbol{x}$ can be observed by combining the model knowledge and the sensor measurements; this is realized by implementing a Kalman filter. At the same time, the Kalman-filter-based estimation are only valid when human is in single-support phase; when the human leader is in double-support phase, the Kalman filter is paused.

To evaluate whether the Kalman filter can be used for estimating the human leader's state, two experiments are directed. In both experiments, human's body configurations are measured and recorded by a motion capture system (8 Raptor-E cameras from Motion Analysis Corp.) at the rate of 100 Hz. The difference between the two experiments are:

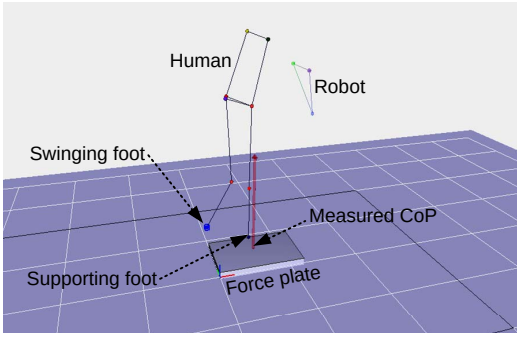

Figure 12: Motion capture system is used to measure human's body configuration; a force plate is used to measure the accurate CoP position of the human

1. In the first experiment, a force plate (Kistler 9286A) is used to measure the traveling of human's CoP; due to the limited size of the force plate, the human stays on the force plate, with the left foot supporting the body and the right foot swinging back and forth for a couple of times (Fig. 12). This experiment tests the performance of the Kalman filter on observing $\dot{x}$ and δ_o.

2. In the second experiment, the robot moves passively in admittance control mode (which will be discussed later in Section 2.4.1). Human's motions are not restricted by specific patterns: he can arbitrarily choose his stride length and walking speed. This experiment tests whether the Kalman filter can properly work when being intermittently disturbed by human's double-support phase.

Results of the first experiment are shown in Fig. 13. We can see that the CoM velocity $\dot{x}$ has been accurately estimated, while the variation of offset δ_o has also been estimated with approximately 0.2 s phase delay.

Result of the second experiment is shown in Fig. 14. This result shows that, although the Kalman filter is intermittently disturbed by human's double-support phase, the proposed method can still keep estimating human's state in single-support phase.

According to the validation results, the proposed filter-based method can be used in state estimation of the human dancer.

2.4 Control

A schematic diagram of the coupled dynamics in waltz is illustrated in Fig. 15. The system involves three components: the human body, the human

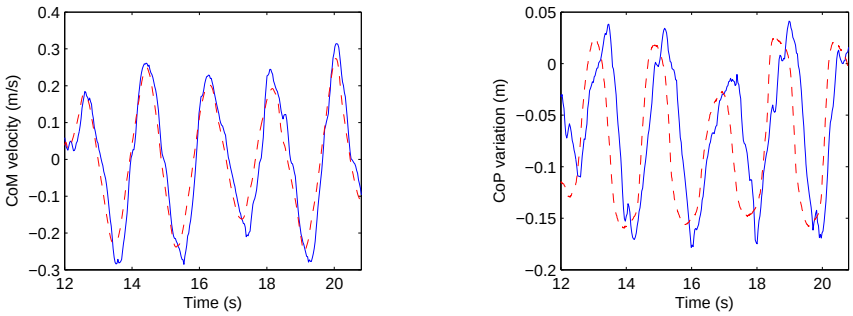

(a) Real and estimated CoM velocities $\dot{x}$ (b) Real and estimated offsets δ_o

Figure 13: Experiment results on testing the filter's performance on observing $\dot{x}$ and δ_o; red dashed curves: accurate human data measured by motion capture system and force plate; blue solid curves: estimated human data given by the Kalman filter

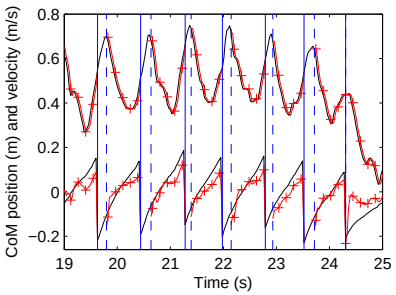

Figure 14: Results of evaluating the proposed Kalman filter. Curves in the bottom are the measured (plain curve) and estimated (curve with "+" markers) CoM positions, curves in the top are CoM velocities (plain: measured; "+" marker: estimated). Vertical blue lines are human's timings; solid: beginning of double-support phase; dashed: ending of double-support phase

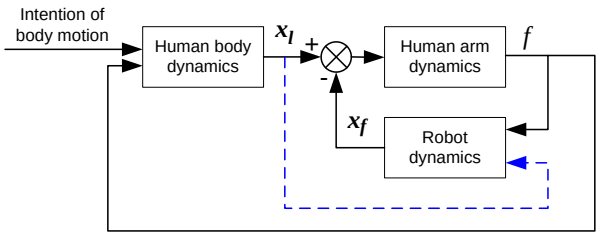

Figure 15: Block diagram of the human-robot system in waltz. $\boldsymbol{x_l}$ and $\boldsymbol{x_f}$ are human's and robot's spatial states (e.g., position, velocity, etc). f is the interaction force.

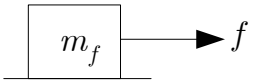

Figure 16: Illustration of the admittance controller

arm, and the robot follower. Among the three components, robot is the only component that can be "manipulated" by a designer. Therefore, to enhance the pHRI of waltz, a robot controller is to be implemented. Depending on how the inputs are used to generate the output, there are infinite candidate controllers, while in this section several of them are introduced.

2.4.1 Admittance controller

Admittance controller is a widely adopted in pHRI [34]. This controller only uses interaction force as the input; the idea of the implemented admittance controller is that the robot is emulating a mass driven by interaction force and dragged by virtual ground friction, as illustrated in Fig. 16.

Suppose the emulated mass is m_f and the emulated viscosity coefficient is d_f; dynamics of the admittance controller are:

$$\ddot{x}_f^g = -\frac{d_f}{m_f}\dot{x}_f^g + \frac{f}{m_f} \tag{24}$$

where x_f^g, $\dot{x}_f^g$, and $\ddot{x}_f^g$ are the robot's position, velocity, and acceleration with respect to the global coordinate frame.

When the admittance controller is implemented, human's estimated state is not utilized (i.e., consider the blue dash in Fig. 15 does not exist), the interconnected human arm and robot dynamics form a closed "loop", as shown in

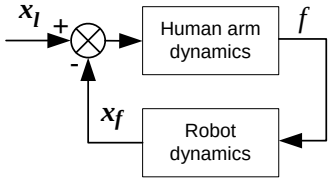

Figure 17: Human arm and robot form a closed-loop system

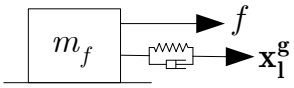

Figure 18: Illustration of the admittance controller with a virtual coupling

Fig. 17. Because the human arm model has large uncertainty, conservative stability conditions (e.g., small gain theorem) are usually introduced in designing the robot controller [16]. Because of the conservativeness in stability, performance is sacrificed.

2.4.2 Admittance controller with virtual coupling

The compromise between stability and performance can be improved by introducing human's spatial information into the robot controller [35] as in Fig. 15. Based on the admittance controller, we can further implement a virtual coupling, which is illustrated in Fig. 18.

The robot dynamics are defined by

$$\ddot{x}_f^g = -\frac{d_f}{m_f}\dot{x}_f^g + \frac{k_v}{m_f}(\hat{x}_l^g - x_f^g) + \frac{d_v}{m_f}(\dot{\hat{x}}_l^g - \dot{x}_f^g) + \frac{f}{m_f} \tag{25}$$

where k_v and d_v are the stiffness and damping coefficient of the virtual coupling; $\hat{x}_l^g$ and $\dot{\hat{x}}_l^g$ are estimated human CoM position and velocity. The transfer function from $\hat{x}_l^g$ to x_f^g is

$$\frac{X_f^g(s)}{\hat{X}_l^g(s)} = \frac{d_v s + k_v}{m_f s^2 + (d_f + d_v)s + k_v} \tag{26}$$

This controller is in essence a low-pass filter. It is intuitive as it tries to implement a virtual force to decrease the real interaction force (f); however,

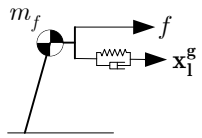

Figure 19: Illustration of the inverted pendulum controller with a virtual coupling

the performance of this controller is also intrinsically restricted by its structure. Define the robot's following error as $E(s) = 1 - X_f^g(s)/\hat{X}_l^g(s)$, i.e., the complement of (26). We can observe that the parameter tuning of the frequency response of $E(s)$ is highly restricted; quantitative analysis of those restrictions can be found in [36].

2.4.3 LIPM with virtual coupling

To better understand the pHHI between two human dancers, we use the inverted pendulum presented in Section 2.1.1 as the robot model. At the same time, the measurement of human's state is continuously rectified by a Kalman filter and used as the input to the robot controller. Diagram of this controller is illustrated in Fig. 19.

Walking can be temporally divided into single-support phase and double-support phase which have different dynamics, therefore, the robot controller also has two phases:

1. When the robot detects that human is in single-support phase, the robot emulates an LIPM with virtual coupling:

$$\ddot{x}_f = \frac{g}{z_f} x_f + \frac{k_v}{m_f}(\hat{x}_l^g - x_f^g) + \frac{d_v}{m_f}(\dot{\hat{x}}_l - \dot{x}_f) \tag{27}$$

2. When human is in double-support phase, the robot switches to admittance control mode (24).

In the following we explain how the virtual coupling appeared in (27) is able to achieve interaction force reduction. Define the objective function as:

$$\begin{aligned} F_{\text{obj}} &= \int_{t_k^{f+}}^{t_k^{f+}+T_p} f^2(t)dt = \int_{t_k^{f+}}^{t_k^{f+}+T_p} \boldsymbol{x}^T(t)\boldsymbol{c}_\boldsymbol{c}^T\boldsymbol{c}_\boldsymbol{c}\boldsymbol{x}(t)dt \\ &= \boldsymbol{x}^T(t_k^{f+})\left(\int_0^{T_p}(e^{\boldsymbol{A}t})^T\boldsymbol{c}_\boldsymbol{c}^T\boldsymbol{c}_\boldsymbol{c}e^{\boldsymbol{A}t}dt\right)\boldsymbol{x}(t_k^{f+}) \\ &= \boldsymbol{x}^T(t_k^{f+})\boldsymbol{W}\boldsymbol{x}(t_k^{f+}) \end{aligned} \tag{28}$$

which means we aim to minimize the interaction force throughout the single-support phase.

The virtual coupling applies a virtual force on the robot. Recall the two-LIPM system in Section 2.1.2, its state matrix $\boldsymbol{A}$ is defined in (6), with the virtual coupling, the state matrix $\boldsymbol{A}$ is replaced by $\boldsymbol{A_v}$, with

$$\boldsymbol{A_v} = \begin{pmatrix} 0 & 1 & 0 & 0 & 0 \\ \frac{g}{z_l} & -\frac{d_c}{m_l} & 0 & \frac{d_c}{m_l} & \frac{k_c}{m_l} \\ 0 & 0 & 0 & 1 & 0 \\ 0 & \frac{d_c+d_v}{m_f} & \frac{g}{z_f} & -\frac{d_c+d_v}{m_f} & -\frac{k_c+k_v}{m_f} \\ 0 & -1 & 0 & 1 & 0 \end{pmatrix} \tag{29}$$

Define

$$\boldsymbol{W_v} = \int_0^{T_p} (e^{\boldsymbol{A_v} t})^T \boldsymbol{c_c}^T \boldsymbol{c_c} e^{\boldsymbol{A_v} t} dt \tag{30}$$

Then the reduction of F_{obj} is

$$\delta F = \boldsymbol{x}^T(t_k^{f+}) \left(\boldsymbol{W} - \boldsymbol{W_v}\right) \boldsymbol{x}(t_k^{f+}) = \boldsymbol{x}^T(t_k^{f+}) \boldsymbol{\Delta_v} \boldsymbol{x}(t_k^{f+}) \tag{31}$$

If $\boldsymbol{\Delta_v}$ is positive definite, then $\delta F > 0$ for all $\boldsymbol{x}(t_k^{f+})$; the interaction force reduction is guaranteed. One may think that a positive definite $\boldsymbol{\Delta_v}$ can be formulated by carefully adjusting parameters (k_v and d_v) of the virtual coupling; unfortunately, this ideal situation is difficult to meet. We illustrate this situation with an numerical example in Fig. 20. According to Fig. 20, it is quite difficult to find these parameters; generally, $\boldsymbol{\Delta_v}$ is indefinite, hence the performance of interaction force reduction also depends on the initial condition $\boldsymbol{x}(t_k^{f+})$.

Therefore, the implementation of the virtual coupling cannot guarantee that F_{obj} is always reduced; instead, the virtual coupling is used to reduce interaction force *in most cases*. Without loss of generality, we assume both dancers are moving along the positive direction of x-axis. Their velocities are assumed to be evenly distributed between $[0, 1.5]$m/s; their relative CoM positions are assumed to be evenly distributed between $[-0.4, 0]$m; their distance variation q is assumed to be evenly distributed between $[-0.2, 0.2]$m. Performance of the proposed controller is evaluated with Monte Carlo method. 10^6 random $\boldsymbol{x}(t_k^{f+})$ are tested.

According to the Monte Carlo test, the proposed controller has reduced F_{obj} in about 95% cases with best performance $\delta F \approx 2\times10^4 \text{N}^2\text{s}$, the controller has failed in about 5% cases with worst performance $\delta F \approx -188\,\text{N}^2\text{s}$. The probability density function of δF is shown in Fig. 21.

This probability density function reveals that the proposed controller can effectively reduce interaction force with 95% probability, while may also

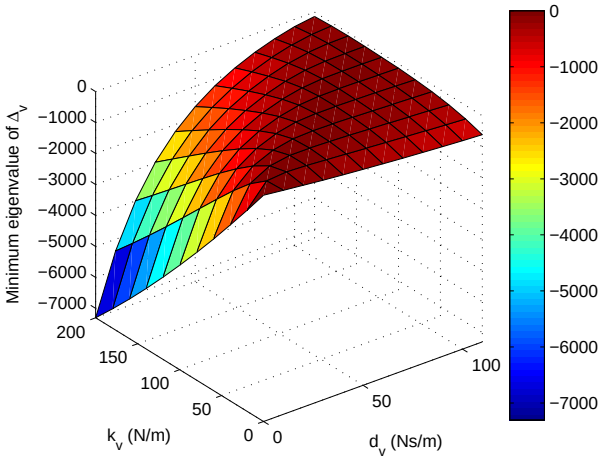

Figure 20: Minimum eigenvalue of $\boldsymbol{\Delta_v}$ with respect to virtual coupling parameters

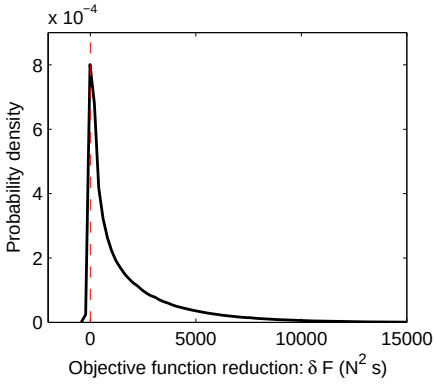

Figure 21: Probability density function of δF; positive part of the horizontal axis represents successful interaction force reduction.

Table 1: Parameters of Controller Used in Experiments

Parameters used in admittance controller	
m_f (kg)	50
d_f (Ns/m)	40
Parameters used in admittance controller with virtual coupling	
m_f (kg)	50
d_f (Ns/m)	40
k_v (N/s)	10
d_v (Ns/m)	150
Parameters used in LIPM controller with virtual coupling	
m_f (kg)	45
z_f (m)	0.9
k_v (N/s)	0
d_v (Ns/m)	225

slightly increase the interaction force with 5% probability. Therefore, the proposed method is worth implementing.

2.4.4 Experiments

In experiments, we evaluate the above three robot controllers. Parameters for controllers are listed in Table 1, which is obtained after a preliminary test.

On the hardware level, the robot controller has two parallel control cycles:

1. Actuation of four omni-wheels are controlled by low-level PD controllers with 1 ms cycle period. In this cycle, few computations are involved.

2. LRF data processing and Kalman filter calculation are handled in high-level cycle; period of this cycle is 28 ms.

For the current hardware, the above computations approximately cost about 6.1 ms (shorter than the 28 ms high-level cycle). The real-time operating system (QNX 6.1) ensures the 1 ms and 28 ms deadlines are satisfied.

Experiment results are shown in Fig. 22.

As discussed in Section 2.4.2, although being intuitively plausible, the "admittance with virtual force" controller has poor performance in force reduction (Fig. 22(c) and Fig. 22(d)).

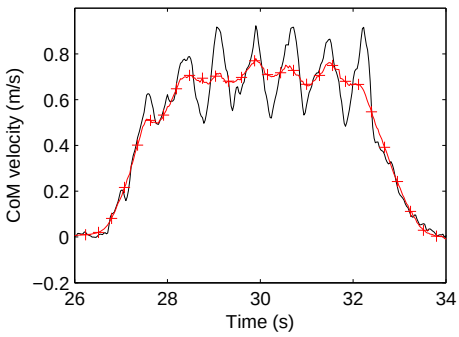

(a) Trajectories, using admittance control

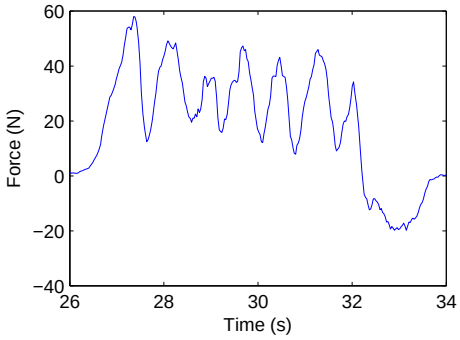

(b) Interaction force, using admittance control

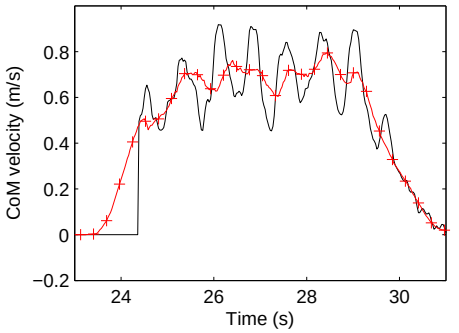

(c) Trajectories, using admittance with virtual coupling

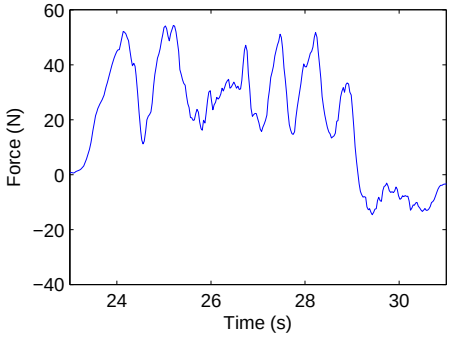

(d) Interaction force, using admittance with virtual coupling

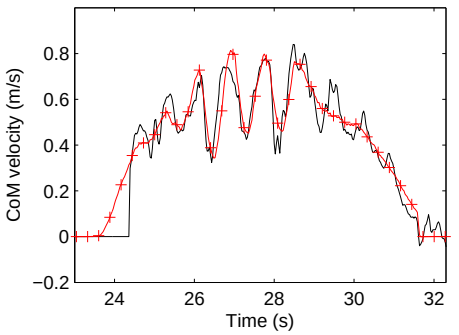

(e) Trajectories, using inverted pendulum with virtual coupling

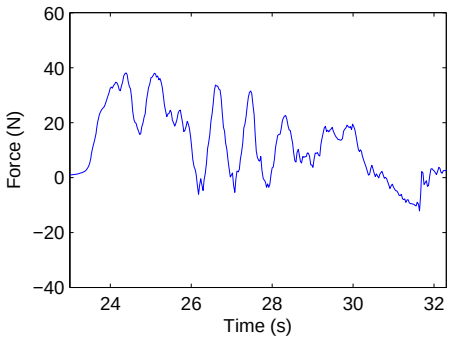

(f) Interaction force, using inverted pendulum with virtual coupling

Figure 22: Experiment results. In (a), (c), and (e), curves with "+" markers show robot's trajectories while plain curves show the human's. For each robot controller, the motion is initiated with admittance control until the end of the first double-support phase. In (e) and (f), the robot switches to admittance mode after six steps.

According to Fig. 22(b) with Fig. 22(f), we can see that the inverted pendulum controller (Section 2.4.3) can reduce interaction force by utilizing the the leader's state estimation, which is being continuously rectified by the Kalman filter. Therefore, the control scheme is supported by the results.

3 Conclusions

To develop a dance partner robot which can dance waltz with human, the physical interaction between the two dancers is studied. In addressing modeling, analysis, and control for enhancing pHRI, we make the following contributions:

1. A model for describing dancers' coupled dynamics in waltz;
2. Implementation of poly-quadratic stability condition in proving the two-LIPM system's stability;
3. A novel method which uses LRF to infer human's timing in pHRI, and a Kalman-filter-based method for estimating the state of human;
4. Analysis and validation of several robot controllers.

However, our study is limited as it only models human's translational motions in sagittal plane; dancers' rotational motions are not studied. As most dance steps in waltz involve body rotations, further studies in understanding and measuring human's rotation are needed.

References

[1] R. Murphy, T. Nomura, A. Billard, and J. Burke, "Human–robot interaction," *Robotics & Automation Magazine, IEEE*, vol. 17, no. 2, pp. 85–89, 2010.

[2] L. Bueno, F. Brunetti, A. Frizera, J. Pons, J. Moreno, E. Rocon, J. Carmena, E. Farella, and L. Benini, "Human–robot cognitive interaction," *Wearable Robots*, pp. 87–125, 2008.

[3] A. De Santis, B. Siciliano, A. De Luca, and A. Bicchi, "An atlas of physical human–robot interaction," *Mechanism and Machine Theory*, vol. 43, no. 3, pp. 253–270, 2008.

[4] K. B. Reed, J. Patton, and M. Peshkin, "Replicating Human-Human Physical Interaction," *Proceedings of the 2007 IEEE International Conference on Robotics and Automation (ICRA)*, pp. 3615–3620, 2007.

[5] J. Chodorow, *Dance therapy and depth psychology: The moving imagination*. Psychology Press, 1991.

[6] T. Takeda, "Coordination between a Human and a Dance Partner Robot," Ph.D. dissertation, Tohoku University, Japan, 2008.

[7] T. Takeda, Y. Hirata, and K. Kosuge, "Dance step estimation method based on HMM for dance partner robot," *IEEE Transactions on Industrial Electronics*, vol. 54, no. 2, pp. 699–706, 2007.

[8] H. Kimura and G. Kajiura, "Motion recognition based cooperation between human operating robot and autonomous assistant robot," in *Proceedings of the 1997 IEEE International Conference on Robotics and Automation (ICRA)*, vol. 1, 1997, pp. 297–303.

[9] K. Tahboub, "Intelligent human-machine interaction based on dynamic bayesian networks probabilistic intention recognition," *Journal of Intelligent & Robotic Systems*, vol. 45, no. 1, pp. 31–52, 2006.

[10] D. Aarno and D. Kragic, "Motion intention recognition in robot assisted applications," *Robotics and Autonomous Systems*, vol. 56, no. 8, pp. 692–705, 2008.

[11] R. Kelley, A. Tavakkoli, C. King, M. Nicolescu, M. Nicolescu, and G. Bebis, "Understanding human intentions via hidden markov models in autonomous mobile robots," in *Proceedings of the 3rd ACM/IEEE international conference on Human robot interaction*, 2008, pp. 367–374.

[12] O. Khatib, O. Brock, K. Yokoi, and R. Holmberg, "Dancing with juliet 1999," in *IEEE Robotics and Automation Conference Video Proceedings*, 1999.

[13] P. Oudeyer, O. Ly, and P. Rouanet, "Exploring robust, intuitive and emergent physical human-robot interaction with the humanoid robot acroban," in *Proceedings of the 2011 11th IEEE-RAS International Conference on Humanoid Robots (Humanoids)*, 2011, pp. 120–127.

[14] S. Setiawan, J. Yamaguchi, S. Hyon, and A. Takanishi, "Physical interaction between human and a bipedal humanoid robot-realization of human-follow walking," in *Proceedings of the 1999 IEEE International*

Conference on Robotics and Automation (ICRA), vol. 1. IEEE, 1999, pp. 361–367.

[15] J. Colgate and N. Hogan, "Robust control of dynamically interacting systems," *International Journal of Control*, vol. 48, no. 1, pp. 65–88, 1988.

[16] H. Kazerooni, "Human/robot interaction via the transfer of power and information signals," *IEEE Transactions on System, Man, and Cypernetics*, vol. 20, no. 2, pp. 450–463, 1990.

[17] J. Colgate and G. Schenkel, "Passivity of a class of sampled-data systems: Application to haptic interfaces," in *American Control Conference*, vol. 3, 1994, pp. 3236–3240.

[18] H. Kazerooni and T. Snyder, "Case study on haptic devices: Human-induced instability in powered hand controllers," *Journal of Guidance, Control, and Dynamics*, vol. 18, no. 1, pp. 108–113, 1995.

[19] S. Sirouspour, "Robust control design for cooperative teleoperation," *Proceedings of the 2005 IEEE International Conference on Robotics and Automation (ICRA)*, pp. 1133–1138, 2005.

[20] A. Haddadi and K. Hashtrudi-Zaad, "Bounded-impedance absolute stability of bilateral teleoperation control systems," *IEEE Transactions on Haptics*, vol. 3, no. 1, pp. 15–27, 2010.

[21] A. Peer and M. Buss, "Robust stability analysis of a bilateral teleoperation system using the parameter space approach," in *Proceedings of the 2008 IEEE/RSJ International Conference on Intelligent Robots and Systems (IROS)*. IEEE, 2008, pp. 2350–2356.

[22] S. Buerger and N. Hogan, "Complementary stability and loop shaping for improved human-robot interaction," *IEEE Transactions on Robotics*, vol. 23, no. 2, pp. 232 –244, 2007.

[23] V. Duchaine and C. Gosselin, "Safe, stable and intuitive control for physical human-robot interaction," *Proceedings of the 2009 IEEE International Conference on Robotics and Automation (ICRA)*, pp. 3383–3388, 2009.

[24] S. Sirouspour, "Modeling and control of cooperative teleoperation systems," *IEEE Transactions on Robotics*, vol. 21, no. 6, pp. 1220–1225, 2005.

[25] J. Holldampf, A. Peer, and M. Buss, "Virtual partner for a haptic interaction task," *Human Centered Robot Systems: Cognition, Interaction, Technology*, vol. 6, p. 183, 2010.

[26] S. Kajita and K. Tani, "Study of dynamic biped locomotion on rugged terrain—theory and basic experiment," *Advanced Robotics, 1991. 'Robots in Unstructured Environments', 91 ICAR., Fifth International Conference on*, pp. 741–746 vol.1, 1991.

[27] W. Haddad, V. Chellaboina, and S. Nersesov, "Impulsive and hybrid dynamical systems," *IEEE CONTROL SYSTEMS MAGAZINE*, 2006.

[28] H. Wang and K. Kosuge, "Understanding and reproducing waltz dancers' body dynamics in physical human-robot interactio," *Proceedings of the 2012 IEEE International Conference on Robotics and Automation (ICRA)*, pp. 3135–3140, 2012.

[29] ——, "An inverted pendulum model for reproducing human's body dynamics in waltz and its applications in a dance partner robot," *Proceedings of the 2010 IEEE/SICE International Symposium on System Integration*, pp. 182–187, 2010.

[30] ——, "Towards an understanding of dancers' coupled body dynamics for waltz," *Proceedings of the 2011 IEEE/RSJ International Conference on Intelligent Robots and Systems (IROS)*, pp. 2008–2013, 2011.

[31] J. Daafouz and J. Bernussou, "Parameter dependent lyapunov functions for discrete time systems with time varying parametric uncertainties," *Systems & Control Letters*, vol. 43, no. 5, pp. 355–359, 2001.

[32] [Online]. Available: http://www.hokuyo-aut.jp/02sensor/07scanner/ubg_04lx_f01.html

[33] E. Ayyappa, "Normal human locomotion, part 1: Basic concepts and terminology," *Journal of Prosthetics and Orthotics*, vol. 9, no. 1, p. 10, 1997.

[34] G. Zeng and A. Hemami, "An overview of robot force control," *Robotica*, vol. 15, no. 05, pp. 473–482, 1997.

[35] N. Jarrassé, J. Paik, V. Pasqui, and G. Morel, "How can human motion prediction increase transparency?" in *Proceedings of the 2008 IEEE International Conference on Robotics and Automation (ICRA)*, 2008, pp. 2134–2139.

[36] H. Wang and K. Kosuge, "Control of a robot dancer for enhancing haptic human-robot interaction in waltz," *IEEE Transactions on Haptics*, vol. 5, pp. 264–273, 2012.

Publications With AOARD Sponsorship

a) Peer-reviewed Journals

1. Hongbo Wang and Kazuhiro Kosuge, "Control of a Robot Dancer for Enhancing Haptic Human-Robot Interaction in Waltz", *IEEE Transactions on Haptics*, vol. 5, pp. 264–273, 2012

b) Peer-reviewed Conference Proceedings

1. Hongbo Wang and Kazuhiro Kosuge, "Attractor Design and Prediction-based Adaption for a Robot Waltz Dancer in Physical Human-Robot Interaction", *Proceedings of the 2012 World Congress on Intelligent Control and Automation*, pp. 3810-3815, Beijing, China, Jul. 4-8, 2012

2. Hongbo Wang and Kazuhiro Kosuge, "Understanding and Reproducing Waltz Dancers' Body Dynamics in Physical Human-Robot Interaction", *Proceedings of the 2012 IEEE International Conference on Robotics and Automation*, pp. 3135-3140,, Saint Paul, USA, May 14–18, 2012.

3. Hongbo Wang and Kazuhiro Kosuge, "Towards an understanding of dancers' coupled body dynamics for waltz", *Proceedings of the 2011 IEEE/RSJ International Conference on Intelligent Robots and Systems*, pp. 2008–2013, San Francisco, USA, Sept. 25–30, 2011.

4. Hongbo Wang and Kazuhiro Kosuge, "An inverted pendulum model for reproducing human's body dynamics in waltz and its applications in a dance partner robot", *Proceedings of the 2010 IEEE/SICE International Symposium on System Integration,* pp. 182–187, Sendai, Japan, Dec. 21–22, 2010.

Control of a Robot Dancer for Enhancing Haptic Human-Robot Interaction in Waltz

Hongbo Wang, *Student Member*, *IEEE*, and Kazuhiro Kosuge, *Fellow*, *IEEE*

Abstract—Haptic interaction between a human leader and a robot follower in waltz is studied in this paper. An inverted pendulum model is used to approximate the human's body dynamics. With the feedbacks from the force sensor and laser range finders, the robot is able to estimate the human leader's state by using an extended Kalman filter (EKF). To reduce interaction force, two robot controllers, namely, admittance with virtual force controller, and inverted pendulum controller, are proposed and evaluated in experiments. The former controller failed the experiment; reasons for the failure are explained. At the same time, the use of the latter controller is validated by experiment results.

Index Terms—Physical/haptic human-robot interaction, dance, inverted pendulum, extended Kalman filter, laser range finder, admittance control.

1 Introduction

Waltz is not only an entertaining activity, but also a typical example of haptic human-human interaction (HHI) which involves human's abilities in sensing, control, and coordination. In waltz, two dancers are acting as a leader (usually the male dancer) and a follower (usually the female dancer), while the follower can interact with the leader by "reading" the haptic signals passed through their physical connection. Understanding of the follower's ability may help designing robots that can be intuitively controlled through human-robot interaction (HRI). Therefore, the goal of our research is to develop a robot follower that can dance with the human leader by utilizing the haptic information. A developed prototype of the robot follower is shown in Fig. 1.

Generally, to interact with human, a robot may refer to models at two different levels.

1. The higher level model is used to relate observed signals with human's intentions [1], [2], [3], which could be named as "intention estimation." Waltz has a "vocabulary" of various kinds of dance steps, while a waltz dance consists of a sequence of steps. When the leader has selected the next step, he is having an "intention." The follower should be able to estimate this intention, as shown in Fig. 2a.
2. The lower level model is used for controlling the dynamics of the interaction system in which the human and robot are coupled [4], [5], [6], [7], [8], which could be named as "coupled dynamics." In waltz, the follower is not dancing alone, her body dynamics are coupled with the leader's; the follower should be able to dance under the coupled dynamics without significant performance degradation, as shown in Fig. 2b.

In one earlier work [9], the higher level interaction in waltz has been investigated. To estimate the human leader's intentions, each candidate dance step is modeled as a hidden Markov model (HMM); haptic signals are considered as observations generated by one of the HMMs. For each HMM, the likelihood of generating the given observations is calculated; the model with the highest likelihood is then selected as the leader's "most probable" intention. Here, we only summarize this approach in Fig. 3; details can be found in [9].

The focus of this paper is the lower level interaction, i.e., "couple dynamics," which is studied independently of the higher level "intention estimation." In another word, fixed "dance step" is applied on the two dancers', hence the HMM-based step estimator (Fig. 3) is not involved in this paper.

More specifically, we focus on two dancers' coupled body dynamics in sagittal plane (Fig. 4). Therefore, our analysis is limited as it only accounts for human's translational motions in sagittal and frontal planes, leaving rotational motions unstudied; however, in waltz, most dance steps involve body rotations; pure translational motions only correspond to a few steps (e.g., closed changes). Clearly, these simple translational motions are still too elementary compared with a dance partner robot's expected capability; however, those simple cases offer us a good start point to explore the fundamentals of interactions. Similar 1D cases also appeared in studies in coordinated teleoperation [10], haptic human-robot interaction [11], and human-robot-human cooperation [12], etc.

In one previous work [13], we assume that the human model has only one parameter—stride length. The robot is able to learn the human leader's stride length, which is later used to scale the planned dance trajectories. Because human's motion has variability and randomness, the robot is also under admittance control while following the learned trajectory.

• *The authors are with the Department of Bioengineering and Robotics, System Robotics Laboratory, Tohoku University, Aoba 6-6-01, Aramaki, Aoba-ku, Sendai 980-8579, Japan.*
E-mail: {h_wang, kosuge}@irs.mech.tohoku.ac.jp.

Manuscript received 1 Dec. 2011; revised 22 Apr. 2012; accepted 19 June 2012; published online 2 July 2012.
Recommended for acceptance by A. Karniel, A. Peer, O. Donchin, F.A. Mussa-Ivaldi, and G.E. Loeb.
For information on obtaining reprints of this article, please send e-mail to: toh@computer.org, and reference IEEECS Log Number THSI-2011-12-0097.
Digital Object Identifier no. 10.1109/ToH.2012.36.

Fig. 1. One developed robot follower.

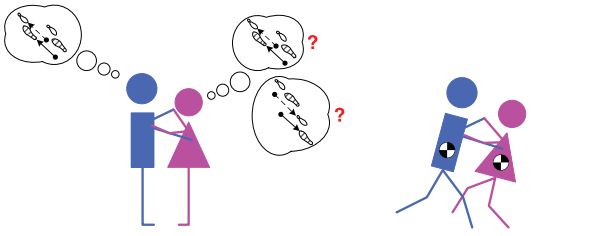

Fig. 2. Two levels of interactions in waltz.

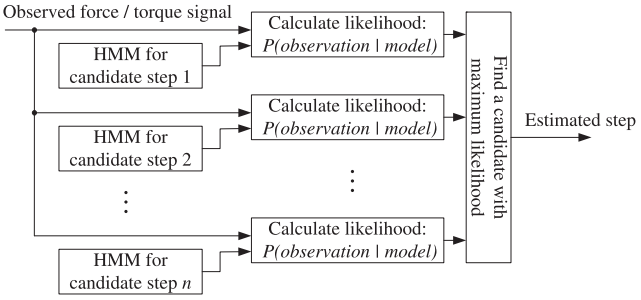

Fig. 3. Estimating leader's intention using HMMs.

Compared with a robot under admittance control, inverted pendulum can better represent a human follower's body dynamics in walking and dancing. Therefore, we employed linear inverted pendulum (LIPM) [14] as the human model; for two dynamically coupled dancers, they are modeled as a pair of connected LIPMs [15]. By assuming the two dancers' feet landing motions are synchronized, we analyzed stability of the system, while interaction force was reduced with gradient descent method [16]. Because the assumption on two dancers' synchronized motions are too strong, this assumption was later replaced by a weaker (bounded timing error) condition and stability was examined [17].

To reduce interaction force, human leader's intended velocity is predicted and used to control the follower's motion [17]. However, because of LIPM's sensitivity to initial position and velocity errors, it is very difficult to accurately estimate the leader's current and future states.

To deal with the above problem and reduce the interaction force (for increased transparency), in this paper, we propose a solution, which includes the following parts:

1. A model of human's body dynamics in sagittal plane;
2. A method for estimating the human model's state;
3. Robot controllers which can be used to reduce interaction force.

In Section 2, the inverted pendulum model is introduced. In Section 3, methods for estimating human leader's state are described. In Section 4, two robot controllers are presented. Simulation and experiment results are shown in Section 5, discussion and conclusions are given in Sections 6 and 7, respectively.

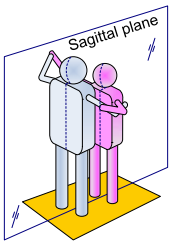

Fig. 4. Dancers' coupled body dynamics in sagittal plane is studied.

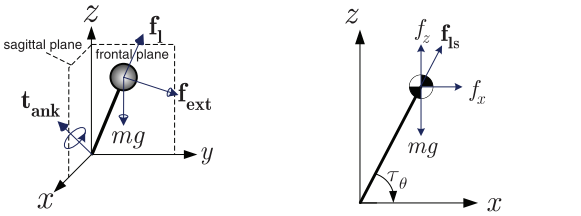

(a) Inverted pendulum with an extendable leg (b) Model in sagittal plane

Fig. 5. Implemented model for single dancer.

2 Model of the Human Dancer's Body Dynamics in Sagittal Plane

To model the human dancer's body dynamics in sagittal plane, an inverted pendulum model is proposed, which has a center of mass (CoM), an extendable leg and an ankle joint actuator (Fig. 5). Fig. 5a shows a 3D inverted pendulum. This 3D inverted pendulum is driven by gravity (mg), leg support ($\boldsymbol{f}_l$), ankle torque ($\boldsymbol{t}_{\text{ank}}$), and external force ($\boldsymbol{f}_{\text{ext}}$). As stated in previous section, we focus on the motions in sagittal plane, hence the 3D pendulum in Fig. 5a is simplified to a 2D model shown in Fig. 5b, where f_x, f_z are components of $\boldsymbol{f}_{\text{ext}}$ in x and z directions; $\boldsymbol{f}_{ls}$, τ_θ are projections of $\boldsymbol{f}_l$ and $\boldsymbol{t}_{\text{ank}}$ in sagittal plane.

In waltz, f_x and f_z correspond to the interaction forces between two dancers, while f_x (and f_y if considering frontal plane motion) is the dominant force; in addition, compared with gravity mg, f_z is much smaller. Thus, we omit f_z and obtain the model dynamics in sagittal plane

$$\ddot{x} = \frac{\ddot{z}+g}{z}x + \frac{\tau_\theta}{mz} + \frac{f}{m}, \tag{1}$$

where $f = f_x$, x is the relative position of CoM with respect to the pivot point (or center of pressure in the supporting foot), z is the height of CoM, m is the mass of the inverted pendulum, g is gravitational acceleration.

Though τ_θ appears as an input in system (1), it is at the same time an internal state of the walking system. We may consider τ_θ as a function of x, $\dot{x}$, and f; when x, $\dot{x}$, and f are all zero, it is reasonable to assume that $\tau_\theta(x, \dot{x}, f) = 0$. A linear approximation of τ_θ is given by

$$\tau_\theta(x, \dot{x}, f) = k_1 x + k_2 \dot{x} + k_3 f. \tag{2}$$

The first two terms in the right-hand side of (2) are the damping/actuation functions of the ankle, making the

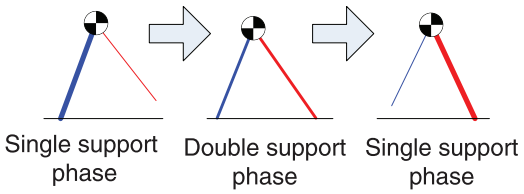

Fig. 6. Switching dynamics in walking.

inverted pendulum less sensitive to initial errors (though still unstable). The last term stands for human's reactions to the external force, with a positive k_3 for cooperating, and a negative k_3 for resisting.

The model described in (1) and (2) only captures human's simplified body dynamics in single-support phase, while in walking or dancing human is switching between single-support phase and double-support phase, as is illustrated in Fig. 6. In double-support phase, human is almost a fully actuated system (except that $\ddot{z}$ cannot be smaller than $-g$); the CoM position and velocity in sagittal plane are fully controlled.

In single-support phase, though human can partly change his trajectory by controlling τ_θ, this trajectory is largely determined by gravity and external force (which can be measured by a force sensor). Further, τ_θ itself may also have some repeatable patterns in walking. The above facts enable us to model human dancer's dynamics in single-support phase.

In double-support phase, the CoM trajectory is fully determined by the human's joint torques, whose patterns are hard to measure or model; therefore, it is quite difficult to model this stage.

For a robot which is haptically interacting with human, it is necessary to deal with human's distinctive dynamics in the two phases. The simplest approach is using a conservative and passive robot model that can work safely in either phase. However, as we have some information about the dynamics in single-support phase, the robot should utilize the information to enhance interaction performance (e.g., transparency), while staying conservative in double-support phase. In this case, the robot should be able to distinguish the two phases. This is discussed in the subsequent part.

3 Estimation of Human Leader's State

3.1 Detecting the Human Leader's Single-Support Phase and Double-Support Phase

In waltz, the switching between single and double support phases is generally synchronized with music beats. Inspired by this fact, a straightforward solution is to extract music beats from audio signals to infer human leader's moments of entering/leaving double-support phase. Also, numerous studies have been directed on beat tracking from MIDI and audio signals [18], [19], [20], [21], as well as their related robotic applications [22]. However, reliable beat tracking from real world sounds in real time is still a great challenge, while for a robot which is designed to be in physical contact with human, reliability is a crucial requirement. Besides reliability, the audio-based method cannot handle situations in which a skilled leader may intentionally and slightly dances "off beat."

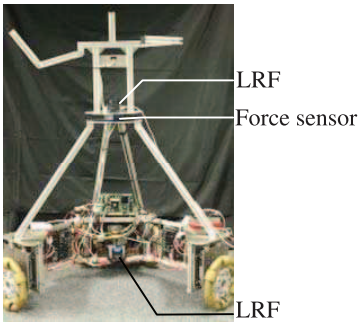

Fig. 7. Robot being used. The robot has implemented one force/torque sensor in waist, and two LRFs at ankle and waist height.

Aside from audio signal, another cue that can be used to infer human's phase is the spatial information of human's feet/ankles. For example, a rapid stop of the left ankle means the left foot has landed on the ground, indicating that human has entered double-support phase; similarly, the acceleration of the right ankle from zero velocity is related with the beginning of single-support phase.

To measure human leader's ankle positions and velocities, one laser range finder (LRF, Hokuyo UBG-04LX-F01) is installed at human's ankle height (Fig. 7). A range image example, which shows what the robot can "see," is shown in Fig. 8. Compared with the usually complicated range images in simultaneous localization and mapping (SLAM) research, the environment in Fig. 8 is rather simple (as in waltz the human leader is close to the robot) and the point sets of two ankles can easily be identified. In the following, we will briefly explain the algorithm.

1. *Preprocessing.* For each frame (i.e., each range image we obtained as shown in Fig. 8), remove the spurious points by searching for line segments shorter than a threshold (e.g., 30 mm). Line segments are extracted by detecting breakpoints [23].
2. *Identification.* For each frame, identify human leader's two ankle centroids by searching for the two nearest clusters from the sagittal plane; calculate leader's waist centroid.
3. *Measuring velocity.* Centroid positions in different frames are used to infer human's ankle and upper body velocities.

Velocities of the two ankles (Fig. 9) are used to detect the beginning and ending moments of double-support phase. Details of the threshold-based detection method can be find

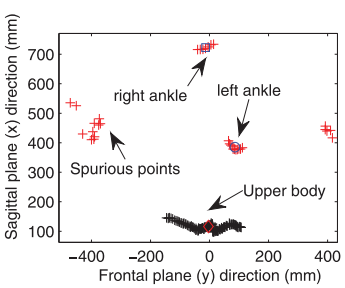

Fig. 8. A captured range image. Image of two ankles are obtained from the LRF on the ankle height, while the upper body image is from another LRF installed at the waist height.

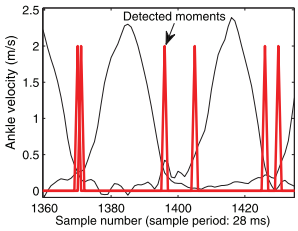

Fig. 9. Detecting human's moments of entering and leaving double-support phase. The impulses are detected moments.

in [17]. Due to the existed noise introduced by the sensor and the algorithm, it is difficult to find the exact moments. As stated at the end of Section 2, because human's patterns in double-support phase are hard to measure or model, the robot is supposed to act conservatively in double-support phase; to ensure a safe HRI, the ambiguous moments should be put into double-support phase. By setting a relatively large threshold on ankles' velocities, the detected moments correspond to an "extended" double-support phase, which is longer than the leader's real double-support phase, as shown in Fig. 9.

3.2 Estimation of Leader's Intended Trajectory in Single-Support Phase

As has been suggested in Section 2, when the human leader is in single-support phase, his CoM trajectory turns to be more patterned; this characteristic can be exploited to improve the performance of HRI. However, there are also several problems that complicate the trajectory tracking task.

1. The real CoM position cannot be directly measured by LRF, instead, what the LRF can measure are some surface points on human body; there is a bias between their mean position and the real CoM position; this bias could be time-varying.
2. Equations (1) and (2) cannot precisely model human's body dynamics in single-support phase.
3. The human leader's model parameters, e.g., m, z in (1) and $k_1 \dots k_3$ in (2), are unknown.
4. The noise contained in the sensor feedback.

The above problems can be interpreted as follows: defining the system state as $\boldsymbol{x} = [x, \dot{x}]^T$, the system described in (1) and (2) are

$$\begin{aligned} \dot{\boldsymbol{x}} &= \begin{pmatrix} 0 & 1 \\ a_1 & a_2 \end{pmatrix} \boldsymbol{x} + [0, b]^T f + [w_1, w_2]^T, \\ \boldsymbol{y} &= [x + \delta, \dot{x}]^T + [v_1, v_2]^T, \end{aligned} \tag{3}$$

where $a_1 = (\ddot{x} + g)/z + k_1/(mz)$, $a_2 = k_2/(mz)$, and $b = k_3/(mz) + 1/m$ are human model's unknown parameters, and δ is the unknown bias of CoM. w_1 and w_2 are the process noises, which stand for the effects of unmodeled dynamics; $\boldsymbol{y}$ is a vector of measured CoM position and velocity; v_1 and v_2 are noises in the measurements.

We can include the unknown parameters in an extended state $\boldsymbol{x}_e$:

$$\boldsymbol{x}_e = [x, \dot{x}, a_1, a_2, b, \delta]^T, \tag{4}$$

then the system defined in (3) turns to be nonlinear, with

$$\begin{aligned} \dot{\boldsymbol{x}}_e &= \boldsymbol{g}_e(\boldsymbol{x}_e, f) + [w_1, w_2]^T, \\ \boldsymbol{y} &= \boldsymbol{h}_e(\boldsymbol{x}_e) + [v_1, v_2]^T. \end{aligned} \tag{5}$$

By discretizing (5), we have

$$\begin{aligned} \boldsymbol{x}_e(k+1) &= \boldsymbol{G}_e(\boldsymbol{x}_e(k), f(k)) \\ &\quad + [w_1(k), w_2(k)]^T, \\ \boldsymbol{y}(k) &= \boldsymbol{H}_e(\boldsymbol{x}_e(k)) + [v_1(k), v_2(k)]^T, \end{aligned} \tag{6}$$

where $\boldsymbol{G}_e$ and $\boldsymbol{H}_e$ are discretized forms of $\boldsymbol{g}_e$ and $\boldsymbol{h}_e$, with the sampling period depending on the LRFs' scanning rates.

The state of the nonlinear system in (6) can be estimated by an extended Kalman filter (EKF). At the beginning of the $k+1$th time step, an estimated state $\tilde{\boldsymbol{x}}_e(k+1)$ and an estimated covariance matrix $\tilde{\boldsymbol{P}}(k+1)$ are predicted

$$\begin{aligned} \tilde{\boldsymbol{x}}_e(k+1) &= \boldsymbol{G}_e(\hat{\boldsymbol{x}}_e(k), f(k)), \\ \tilde{\boldsymbol{P}}(k+1) &= \boldsymbol{\Phi}(k)\hat{\boldsymbol{P}}(k)\boldsymbol{\Phi}^T(k) + \boldsymbol{Q}, \end{aligned} \tag{7}$$

where $\hat{\boldsymbol{x}}_e(k)$ and $\hat{P}(k)$ are estimation results of the kth time step, $\boldsymbol{\Phi}(k)$ is the Jacobian of $\boldsymbol{G}_e$, with $\boldsymbol{\Phi}(k) = (\partial \boldsymbol{G}_e / \partial \boldsymbol{x}_e)|_{(\hat{\boldsymbol{x}}_e(k), f(k))}$; $\boldsymbol{Q}$ is the covariance matrix of process noise w_1 and w_2.

After $\tilde{\boldsymbol{P}}(k+1)$ is obtained, the Kalman gain is given by

$$\begin{aligned} &\boldsymbol{K}(k+1) = \\ &\quad \tilde{\boldsymbol{P}}(k+1)\boldsymbol{\Psi}^T(k)(\boldsymbol{\Psi}(k)\tilde{\boldsymbol{P}}(k+1)\boldsymbol{\Psi}^T(k) + \boldsymbol{R})^{-1}, \end{aligned} \tag{8}$$

where $\boldsymbol{\Psi}(k) = (\partial \boldsymbol{H}_e / \partial \boldsymbol{x}_e)|_{(\tilde{\boldsymbol{x}}_e(k), f(k))}$; $\boldsymbol{R}$ is the covariance matrix of measurement noise v_1 and v_2.

The Kalman gain in (8) is used in building a state observer:

$$\begin{aligned} \hat{\boldsymbol{x}}_e(k+1) &= \tilde{\boldsymbol{x}}_e(k+1) \\ &\quad + \boldsymbol{K}(k+1)(\boldsymbol{y}(k+1) - \boldsymbol{H}_e(\tilde{\boldsymbol{x}}_e(k+1))). \end{aligned} \tag{9}$$

Thus, $\hat{\boldsymbol{x}}_e(k+1)$ is estimated from $\hat{\boldsymbol{x}}_e(k)$ and $\hat{P}(k)$. Finally, the estimation covariance matrix $\hat{\boldsymbol{P}}(k+1)$ is updated by

$$\hat{\boldsymbol{P}}(k+1) = (\boldsymbol{I} - \boldsymbol{K}(k+1)\boldsymbol{\Psi}(k))\tilde{\boldsymbol{P}}(k+1). \tag{10}$$

Hence, $\hat{\boldsymbol{x}}_e(k)$ and $\hat{P}(k)$ can be updated in each time step. At the same time, the implementation of EKF requires the nontrivial task of estimating the covariance matrices $\boldsymbol{Q}$ and $\boldsymbol{R}$, because the Kalman gain is largely determined by $\boldsymbol{Q}$ and $\boldsymbol{R}$ (or more specifically, the "ratio" between $\boldsymbol{Q}$ and $\boldsymbol{R}$). $\boldsymbol{Q}$ and $\boldsymbol{R}$ can be estimated by tuning, or offline analysis of recorded measurements [24].

Generally, precise measurement of human's CoM position in walking is a great challenge [25], [26]. At the same time, as the human dancer's motion is restricted by the requirements of waltz (e.g., the upper body configuration is regulated, the feet should be always in touch with the floor, etc.), the traveling of CoM position is restricted. Hence, large error will not be introduced if we assume the CoM is in a fixed position with respect to the measured body surface. According to this assumption, the CoM is supposed to have a constant bias from the waist centroid, while its velocity is supposed to be the same with the centroid's. The error introduced by this assumption is further reduced by the continuous correction of the EKF.

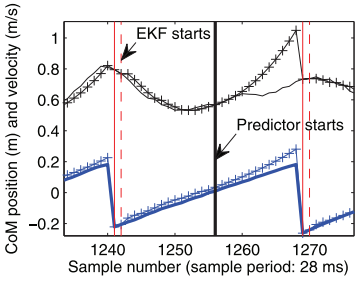

Fig. 10. Predicting leader's trajectory using EKF. Solid curves: leader's real CoM position (bottom, thick) and velocity (top, thin). Curves with markers: estimated/predicted values. Solid/dashed vertical lines: moments of entering/leaving double-support phase.

Because the unknown parameters are also updated, the EKF can be used in predicting human leader's future trajectory. Fig. 10 shows one example of how predictions are made. When human leader leaves double-support phase, the EKF is enabled; after the state and parameter estimations are updated with a specific number of iterations, the predictor (which guesses future states by using the recently updated parameters and state of the LIPM) is started to predict the human leader's future CoM trajectory. Due to unmodeled dynamics and initial estimation error, long-term prediction is less accurate than a short-term one (e.g., the unexpected velocity decrease in Fig. 10). Principally, rather than using EKF as an intermittent predictor (which pauses updating parameters and tries to make long-term predictions, as shown in Fig. 10), EKF should actually be used continuously, hence we can keep updating the parameters and correcting the errors. On the other hand, the intermittent long-term predictor can be used to evaluate the quality of EKF parameters, e.g., an EKF with smaller long-term prediction error should have less unmodeled dynamics and better estimated Q and R.

Note that the above model and the estimation method are only valid when the human leader is in single-support phase; if human is detected to be in double-support phase, EKF is paused.

4 Controlling the Robot

A general representation of the human-robot system in waltz is given in Fig. 11. If we do not consider human body dynamics and the feed-forward path of $\boldsymbol{x}_l$ (blue dash in Fig. 11), the interconnected human arm and robot dynamics form a very typical and frequently encountered "loop" in the research on haptic human-robot interaction. For such systems, there is usually a tradeoff between stability and performance. For example, if the human arm model has large unstructured uncertainty, the designer will tend to use its worst case gain, along with a conservative stability criterion (e.g., small gain theorem) to synthesize the robot controller [4].

The compromise can be improved if the estimated human's motion ($\boldsymbol{x}_l$ in Fig. 11) can be feed-forwarded to the robot controller [27]. In the application of waltz, since human is underactuated in single-support phase, his CoM trajectory can be estimated (as has been discussed in Section 3.2); the estimation can then be sent to the robot

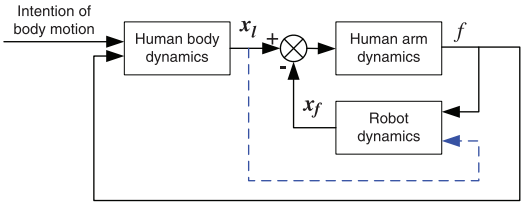

Fig. 11. Block diagram of the human-robot system in waltz. x_l and x_f are leader's and follower's spatial states (e.g., position, velocity, etc.). f is the interaction force.

controller for achieving enhanced performance (e.g., increased transparency with minimized f).

The explicit inclusion of human body dynamics and the feed-forward path of human states yield the model in Fig. 11. In the following, we will discuss two types of robot controllers.

4.1 Admittance Control with Virtual Force

If human's arm has internally stable dynamics with no other unknown inputs, then the amplitude of f is largely determined by $\boldsymbol{x}_l - \boldsymbol{x}_f$; in the ideal case, if the robot can perfectly follow human, i.e., $\boldsymbol{x}_l(t) = \boldsymbol{x}_f(t)$, then $f(t) \to 0$. However, in practice, this simple method has two problems.

1. The state cannot be estimated in human's double-support phase.
2. The estimation (denoted by $\hat{\boldsymbol{x}}_l$) contains (usually high frequency) noise, which cannot be directly used to command the actuators on the robot.

For the first problem, we can have the robot work in admittance mode if the human leader is in double-support phase.

To deal with the second problem in single-support phase, we can implement a low-pass filter, which can be interpreted as a virtual force (for convenience we discuss the continuous case)

$$f_v = k_v(\hat{x}_l - x_f) + d_v(\dot{\hat{x}}_l - \dot{x}_f), \tag{11}$$

where k_v and d_v are designer-specified constants of virtual spring and damper.

The robot is working in admittance control mode, driven by real and virtual forces

$$m_a\ddot{x}_f + d_a\dot{x}_f = f + f_v, \tag{12}$$

where m_a and d_a are virtual mass and damping of the admittance controller. From (11) and (12), the transfer function from $\hat{x}_l$ to x_f is

$$\frac{X_f(s)}{\hat{X}_l(s)} = \frac{d_v s + k_v}{m_a s^2 + (d_a + d_v)s + k_v}, \tag{13}$$

which is a low-pass filter. Intuitively this filter is trying to use a virtual force (f_v) to help decreasing the real interaction force (f), while the robot is working in admittance mode. Because the robot dynamics is stable and linear, this method is easy to understand and implement. In essence, (11) and (12) form an admittance controller with the feed-forward of human's estimated trajectory, this idea has been proposed and validated by Maeda et al. [28] and Corteville et al. [29].

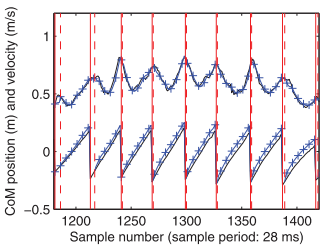

(a) EKF used in estimating leader's state

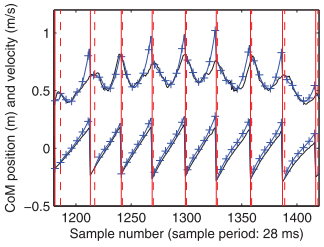

(b) EKF used in predicting state; with 18 iterations in single-support phase, EKF stops and predictor is started; prediction is being made until the next double-support phase comes

Fig. 12. Results of evaluating the proposed EKF. In each figure, curves in the bottom are measured (plain curve) and estimated (curve with "+" markers) CoM position, curves in the top are CoM velocities (plain: measured; "+" marker: estimated).

4.2 A "Human-Like" Approach

For the case of waltz, there is a major difference between HHI and HRI: for HRI, the dynamic model of the robot follower can be artificially created to meet specific requirements. For example, (13) can be replaced with other linear or nonlinear models if the design specifications can be satisfied. In contrast, in HHI, the human follower is subject to her intrinsic dynamics, which can hardly be changed by an external controller.

Therefore, to better understand the haptic interaction between two human dancers, we will use the inverted pendulum presented in Section 2 as an assumed approximation of the follower's body dynamics.

In the single-support phase of the robot follower, its dynamics are similar with (1) and (2), except that the feedforward of $\dot{\hat{x}}_l$ is included in the ankle torque control

$$\tau_\theta = k_1 x + k_2 \dot{x} + k_3 f + k_4(\dot{\hat{x}}_l - \dot{x}_f), \tag{14}$$

which models the follower's effort in catching the leader's varying speed. In addition, to simplify the implementation, $\ddot{z}$ is set to 0 and z is set to a constant value.

At the moment of feet landing, the robot is assumed to follow the leader's stride, i.e., we assume $x_f^+ = \hat{x}_l^+$. In the double-support phase of the robot, we have it work in admittance mode.

It should be noticed that, rather than being a true model of human body dynamics, the above model is an approximation based on the assumed "human-like" behavior. However, compared with the model in Section 4.1, the inverted pendulum better catches human's unstable dynamics in single-support phase, hence this assumed "human-like" model is a better candidate for reproducing the HHI in waltz.

TABLE 1
Parameters of Simulating the Interaction between Two Inverted Pendulums

Parameters	Leader	Follower
m (kg)	70	45
z (m)	$[0.9, 1.1]$	0.9
$\ddot{z}$ (m/s^2)	$[-3, 3]$	0
k_1 (N)	$[-100, 0]$	-40
k_2 (Ns)	$[-100, 0]$	-40
k_3 (m)	$[-50, 50]$	2
k_4 (Ns)	0	5
Connection stiffness k_c (N/m)	$[20, 180]$	
Connection viscosity d_c (Ns/m)	$[0, 0.42k_c]$	

5 Simulations and Experiments

Before HRI experiments, our first concern is that whether our assumed model given in Section 2 and the extended Kalman filter discussed in Section 3.2 can be used for estimating and predicting human leader's state. Therefore, we did experiments in which the robot worked purely in admittance mode, being "pushed" by the human leader while trying to track the leader's states with EKF.

The human leader's motions are not restricted by specific patterns: as long as the velocity does not exceed motors' speed limits, the leader can arbitrarily choose his stride length and walking speed. Five human subjects (age range: 22-30; height range: 1.60-1.85 m; weight range: 50-75 kg) are asked to walk with the robot follower with self-selected speeds and paces. During the above process, surface points on the human leader's waist and ankles are measured by the two LRFs; leader's phase (double/single support) are then inferred and recorded along with the measured interaction force. Then EKF is applied on the recorded data. Covariance matrices $\boldsymbol{Q}$ and $\boldsymbol{R}$ are estimated by offline processing the recorded measurements using ALS package [24]. Results are shown in Fig. 12.

According to the results, the proposed model in (3) and EKF in (7)-(10) can be used in state estimation and short-term prediction. At the same time, the prediction error increases as the look-ahead-time grows larger, which makes long-term predictions less accurate.

The second concern is whether the intrinsically unstable inverted pendulum can be used to interact with human. Although related HRI experiments have demonstrated its feasibility [16], because we have modified the model and included double-support phase, extra validations are necessary. Before experiments, we modeled two dancers as two inverted pendulums (dynamics described in Section 2) connected by a spring and a damper, then simulated the interaction between them. Parameters of the simulation are listed in Table 1.

The leader and the connection are assumed to have uncertain, time-varying, but bounded parameters (varying within the given domain). Values of those parameters are chosen due to the following reasons:

1. The follower is a robot emulating an virtual inverted pendulum; parameters of the virtual pendulum can be arbitrarily specified.

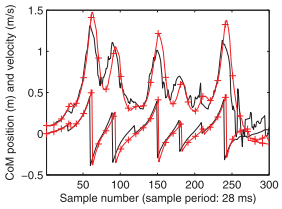

(a) Curves at bottom: CoM positions of leader (plain curve) and follower (curve with "+" marker); curves at top: CoM velocities of leader (plain) and follower (marker)

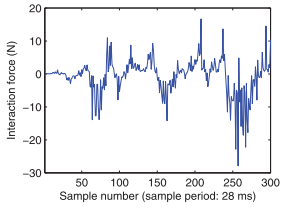

(b) Interaction force

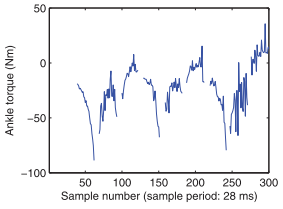

(c) Simulated torque at the follower's ankle

Fig. 13. Simulated interaction between two inverted pendulums.

2. For the human leader, m is the author's mass; z is the 57 percent of the author's height; $\ddot{z}$ is from a dancer's motion capture data in the pelvis. Because $k_1 \dots k_3$ are human dancer's internal control gains that are hard to measure, they are given large uncertain bounds. As human is the leader, k_4 is set to 0.
3. k_c and d_c can be inferred from recorded interaction force and two dancers' distance. A preliminary analysis shows that (perhaps due to different tasks) k_c is smaller than the experiment results given in [30]. The results are used as the upper bound of k_c ($0 \le k_c \le 400$), while d_c's upper bound is $0.42k_c$ ($0 \le d_c \le 0.42k_c$)[31]. With the parameter constraints, k_c and d_c are then identified by minimizing the experiment data fitting error. Because k_c and d_c could be time-varying, the experiment data are partitioned and fitted, respectively. k_c and d_c, in Table 1, are results of the identification.

Besides the time-varying and uncertain parameters, the two dancers also have random but bounded timing errors in entering/leaving double-support phase. Random noise is also included in the measurements.

The robot does not know the leader's trajectory in advance, but tries to follow the leader with the controller proposed in Section 4.2. Simulation results are shown in Fig. 13. We can see that in simulation, the "human-like" controller can drive the robot following the leader's trajectory, regulating the interaction force as well as keeping the ankle torque within a reasonable amplitude.

After the above evaluations, experiments are directed. The control program of the robot follower is running on a single-board computer with 995 MHz (benchmark result) Pentium III CPU and 256 MB memory. The operating system is QNX 6.1.

The program has two parallel control cycles.

1. Four servo motors (which drive four omniwheels) are controlled by PD controllers running on the low-level cycle, with 1ms cycle period. This cycle contains few computations.
2. The high-level cycle contains LRF data processing and EKF calculation, which cost most of the computation time. Period of the high-level cycle is 28 ms.

The EKF needs 213 add operations, 154 subtracts, 391 multiplies, and 4 divides. The LRF data processing needs 252 adds, 504 multiplies, and 504 (worst case) trigonometric function calls, with all operations on double-precision numbers (64 bits in current platform). For the CPU being used, the above computations approximately cost 6.5M clock cycles in the worst case, corresponding to about 6.5 ms, which is shorter than the high-level cycle (28 ms). The operating system (QNX 6.1) guarantees the 1ms and 28 ms deadlines are satisfied in hard real time: if the computation time once exceeds the limit, the program will be stopped with an error report. The program is then tested to ensure that the computation time can satisfy the hard real-time requirement.

Three different robot controllers: pure admittance, admittance with virtual force (Section 4.1) and inverted pendulum (Section 4.2), are examined. The five human subjects are asked to walk with the robot follower with self-selected stride lengths and restrictions on the paces (should be faster than 1 step per second).

Parameters for admittance control are $m_a = 50$ kg, $d_a = 40$ Ns/m; for generating virtual force, $k_v = 10$ N/m and $d_v = 150$ Ns/m. For inverted pendulum, we set $m = 45$ kg, $z = 0.9$ m, $\ddot{z} = 0$, $k_1 = -40$ N, $k_2 = -40$ Ns, $k_3 = 2$ m, and $k_4 = 5$ Ns. The above parameters are selected after a preliminary test before experiments.

Experiment results are given in Fig. 14. Comparing Fig. 14b with Fig. 14f, it can be seen that, when using the inverted pendulum controller (Section 4.2), the interaction force can be reduced by utilizing the feed-forward of the leader's state. Therefore, the control scheme which uses feed-forward (Fig. 11) and a "human-like" controller is supported by the experiment results.

However, despite its intuitive feasibility, the "admittance with virtual force" controller in Section 4.1 demonstrates no evident enhancement in transparency (Figs. 14c and 14d). Originally we attributed the failure to the wrong selections of controller parameters; however, many sets of parameters tested and tuned in experiments still result in no improvement. In the subsequent part, we will give a tentative explanation on the failure of this controller.

6 Discussion

6.1 About the Virtual Force Controller

In developing the virtual force controller in Section 4.1, we used the model in (13), which will drive the robot to follow the human leader's estimated trajectory. Here, we define the robot's following error as $E(s) = 1 - X_f(s)/\hat{X}_l(s)$, i.e., the complement of (13), we have

$$E(s) = \frac{\hat{X}_l(s) - X_f(s)}{\hat{X}_l(s)} = \frac{s(m_a s + d_a)}{m_a s^2 + (d_a + d_v)s + kv} = \frac{s(s+\omega_u)}{(s+\omega_1)(s+\omega_2)}, \tag{15}$$

with $d_a = m_a\omega_u$, $d_v = (\omega_1 + \omega_2 - \omega_u)m_a$, and $k_v = \omega_1\omega_2 m_a$.

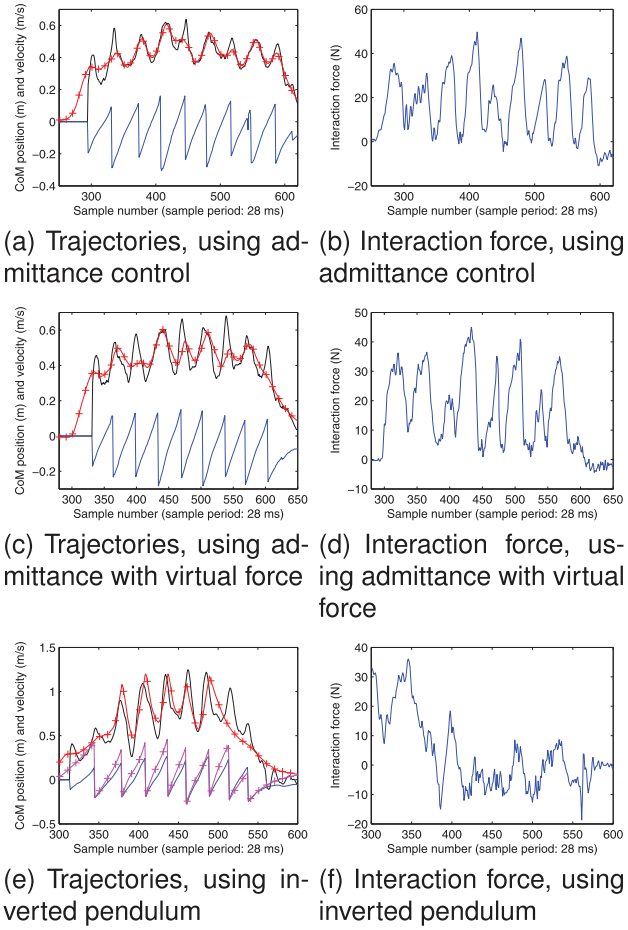

(a) Trajectories, using admittance control

(b) Interaction force, using admittance control

(c) Trajectories, using admittance with virtual force

(d) Interaction force, using admittance with virtual force

(e) Trajectories, using inverted pendulum

(f) Interaction force, using inverted pendulum

Fig. 14. Experiment results. In (a), (c), and (e), curves with "+" markers show robot's trajectories while plain curves show the human's. For each robot controller, the motion is initiated with admittance control until the end of the first double-support phase. In (e) and (f), the robot switches to admittance mode after six steps.

In frequency domain, the behavior of $E(s)$ is fully determined by ω_1, ω_2, and ω_u: on the Bode plot of $|E(s)|$, at frequencies of ω_1 and ω_2, the slope of the magnitude curve decreases by 20 dB per decade, while at ω_u the slope increases by 20 dB per decade. Without loss of generality, we assume $\omega_2 \geq \omega_1$. Depending on the values of ω_1, ω_2, and ω_u, there are three possible Bode plots of $|E(s)|$; we list them in Fig. 15.

In all the three possible cases in Fig. 15, amplitude of the following error, i.e., $|E(s)|$ approaches 0 at low frequencies and 100 percent at high frequencies (because $X_f(s)$ is the low-pass-filtered output of $\hat{X}_l(s)$). At the same time, the case in Fig. 15c is nonoptimal since $|E(s)|$ is amplified at a specific frequency band, therefore the case in Fig. 15c will not be considered.

In the two cases in Figs. 15a and 15b, we have $\omega_2 \geq \max(\omega_1, \omega_u)$. And the slope before ω_2 is 20 dB per decade. To realize effective attenuation of $|E(s)|$ (e.g., $|E(s)| < -20$ dB), we should have ω_2 to be a decade larger than $\max(\omega_1, \omega_u)$, i.e., $\omega_2 \geq 10 \times \max(\omega_1, \omega_u)$, and place $\max(\omega_1, \omega_u)$ around human's walking frequency (approximately 2 Hz, or around 10 rad/s); this arrangement of $\max(\omega_1, \omega_u)$ will give us at least -20 dB attenuation of $|E(s)|$. Therefore, we can consider $\max(\omega_u, \omega_1) \approx 10$ rad/s, and $\omega_2 \approx 100$ rad/s, which yields

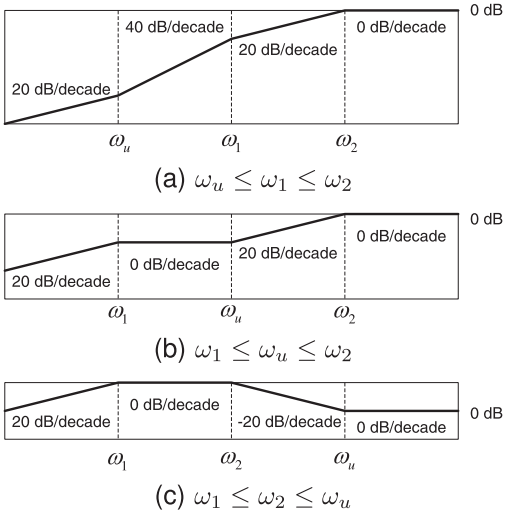

Fig. 15. Possible Bode plots of $|E(s)|$.

$$d_v = (\omega_1 + \omega_2 - \omega_u) m_a \approx 100 m_a, \tag{16}$$

$$\frac{d_a}{m_a} = \omega_u \leq 10. \tag{17}$$

Equations (16) and (17) suggest a dilemma we are facing.

1. If m_a is large, e.g., 50 kg as used in experiment, then $d_v = 5{,}000$, which will greatly amplify the (already large) noise contained in $\dot{\hat{x}}_l$;
2. If m_a is small, then according to (17), d_a must also decrease in proportion; however, values of m_a and d_a are restricted in admittance control: due to the noise introduced by force sensor and the conservativeness of the small gain theorem, m_a and d_a should be sufficiently large.

Generally, because a robot is expected to be safe, insensitive to noise, and easy to analyze/implement, we usually use stable, linear and low-pass-filter type robot models, which can be written as a strictly proper and stable transfer function (e.g., (13)). As the complement of robot model, the following error is not strictly proper and will finally reach 0 dB as frequency increases. It is a nontrivial task to tune the controller's parameters to optimize the frequency response while satisfying the existing restrictions on stability. If the sensors have large signal-to-noise ratio, or if the human model contains small uncertainty, then it is possible to improve system performance with appropriate parameters, e.g., as the case in [28]; in contrast, in our application, the large noise contained in the inferred human CoM, as well as in the interaction force, greatly limited our parameter selection to a narrow range. The parameters used in experiment put much weight on stability and noise attenuation, hence performance was sacrificed, e.g., at frequency of 10 rad/s, the magnitude of $|E(s)|$ is only -0.3 dB.

If the robot model is not constrained to be linear, stable or proper, generally we will have more design space to optimize the interaction. The inverted pendulum model used in Section 4.2 exemplifies the use of an intermittently unstable model. At the same time, compared with the linear and stable case, our knowledge in the broader design space is still quite limited; there are a lot of control methods to be explored in the haptic human-robot interaction.

6.2 Dancers' Body Dynamics in Turning Maneuvers

As stated in Section 1, the planar model in Fig. 5b only describes dancer's translational motions. To fully account for dancers' complete motions in waltz, their body dynamics in turnings (i.e., rotations around the vertical axis) should be modeled and analyzed.

Compared with the "normal" turning maneuvers in walking, the turnings in waltz have several different features.

1. The turnings usually have large rotation angles, e.g., *natural turn* (name of a dance step) consists of two successive turnings, corresponding to two 135 degree clockwise rotations.
2. Turnings mostly happen in single support phase. In addition, for the three-beat waltz music, the rotation usually starts around the second beat and ends around the third beat.
3. The dancer usually keeps a fixed upper body configuration during turning, with the swing foot sliding on the floor.

Human's turning maneuvers during walking have been measured and analyzed [32], [33], [34], suggesting the complicated body dynamics and control in turning maneuvers. At the same time, some simplified models have been introduced to generate turning motions on bipedal robots. A 3D model and its controller proposed by Shih et al. [35] guarantee the input-to-state stability during turning, but the model has point feet and the controller only allows small turn angles. A friction-based method proposed by Miura et al. [36] can generate larger turn angles, but the turnings happen in double-support phases.

A bipedal turning model, which is suitable for modeling dancer's turning maneuvers in waltz, has been recently proposed by Kim and Park [37]. Including upper body moment inertia, swing foot, ankle torque, and ground friction, this model can describe dancer's turnings of large rotation angles in single-support phase. For a waltz dancer, if an additional constraint (zero height of the swing foot) is introduced, this model can be further simplified.

Although we may have a suitable model, there are still two challenges.

1. How turning is controlled by human is unknown; e.g., the way that the rotation is accelerated/decelerated by ankle/hip/friction.
2. It is difficult to measure human leader's angular position with LRFs.

The two challenges are to be addressed to extend the human-robot interaction to more complete motions in waltz.

6.3 Switching of Leader-Follower Role

On the higher level interaction, i.e., "intention estimation" as shown in Fig. 2a, two dancers' roles as the leader and the follower are fixed: the male dancer selects the next step, conveys his intention to the female dancer, who receives, interprets the intention and follows the male dancer's lead. Because of this explicit specialization in the higher level interaction, two dancers in waltz have their names as "leader" and "follower."

However, on the lower level interaction ("coupled dynamics" as shown in Fig. 2b), we cannot rule out the possibility of the dancers' role-switching behavior during dancing. Although it is difficult to quantitatively evaluate one dancer's intention to lead (or to follow) in human-human interaction, to the author's knowledge, a human dancer can hardly keep the role as a pure leader (or follower). For instance, a human leader may give up leading if the interaction force is too large; a human follower also may "override" the lead if she is struggling to keep balance, which should have higher priority than following.

Intuitively, the role-switching can be considered as a continuous process, which has been modeled by a homotopy of maps, with a scalar parameter $\alpha \in [0, 1]$ used to describe the role between leader ($\alpha = 1$) and follower ($\alpha = 0$) [38], [39], [40]. At the same time, the value of α may be a result of task, or interaction force, etc.; modeling the evolution of α is a great challenge. Introducing the role-switching mechanism into HRI of waltz will further complicate the system; however, role-switching has the potential to contribute to a more life-like interaction. Therefore, this feature should be included in the future dance partner robot.

7 Conclusion

To develop a robot follower which can dance waltz with a human leader, the haptic interaction between the two dancers is modeled and studied. The interaction is divided into higher level interaction (step estimation) and lower level interaction (coupled body dynamics).

As the higher level interaction has been modeled with HMMs and reproduced in HRI, the focus of this paper is the lower level interaction. The human leader is modeled as an inverted pendulum. The simplified human model, along with an extended Kalman filter, are used in estimating human leader's state. Feed-forward of the leader's state is utilized by the robot controller to achieve reduced interaction force. Two robot controllers (namely, virtual force and inverted pendulum) are examined. The use of the inverted pendulum controller is supported by experiments; the failure of the virtual force controller is explained.

However, with the large uncertainty contained in the human model, it is still a great challenge to design a robot controller which has guaranteed robustness and optimal performance. In addition, the leader-follower role-switching in the lower level interaction should also be considered. Besides, currently, we have only modeled dancers' motions in sagittal plane, with rotational motions still unstudied. These issues are to be addressed in our future work.

Acknowledgments

This work was supported by the Asian Office of Aerospace Research and Development (AOARD), Air Force Office of Scientific Research (AFOSR) under grant number FA2386-10-1-4126.

References

[1] N. Stefanov, A. Peer, and M. Buss, "Online Intention Recognition for Computer-Assisted Teleoperation," *Proc. IEEE Int'l Conf. Robotics and Automation (ICRA)*, pp. 5334-5339, 2010.

[2] V. Duchaine and C. Gosselin, "Safe, Stable and Intuitive Control for Physical Human-Robot Interaction," *Proc. IEEE Int'l Conf. Robotics and Automation (ICRA)*, pp. 3383-3388, 2009.

[3] Z. Wang, A. Peer, and M. Buss, "An HMM Approach to Realistic Haptic Human-Robot Interaction," *Proc. Third Joint EuroHaptics Conf. and Symp. Haptic Interfaces for Virtual Environment and Teleoperator Systems*, pp. 374-379, 2009.

[4] H. Kazerooni, "Human/Robot Interaction via the Transfer of Power and Information Signals," *IEEE Trans. System, Man, and Cybernetics*, vol. 20, no. 2, pp. 450-463, Mar./Apr. 1990.

[5] B. Miller, J. Colgate, and R. Freeman, "Guaranteed Stability of Haptic Systems with Nonlinear Virtual Environments," *IEEE Trans. Robotics and Automation,* vol. 16, no. 6, pp. 712-719, Dec. 2000.
[6] S. Buerger and N. Hogan, "Complementary Stability and Loop Shaping for Improved Human-Robot Interaction," *IEEE Trans. Robotics,* vol. 23, no. 2, pp. 232-244, Apr. 2007.
[7] S. Sirouspour, "Robust Control Design for Cooperative Teleoperation," *Proc. IEEE Int'l Conf. Robotics and Automation (ICRA),* pp. 1133-1138, 2005.
[8] A. Haddadi and K. Hashtrudi-Zaad, "Bounded-Impedance Absolute Stability of Bilateral Teleoperation Control Systems," *IEEE Trans. Haptics,* vol. 3, no. 1, pp. 15-27, Jan-Mar. 2010.
[9] T. Takeda, Y. Hirata, and K. Kosuge, "Dance Step Estimation Method Based on HMM for Dance Partner Robot," *IEEE Trans. Industrial Electronics,* vol. 54, no. 2, pp. 699-706, Apr. 2007.
[10] S. Sirouspour, "Modeling and Control of Cooperative Teleoperation Systems," *IEEE Trans. Robotics,* vol. 21, no. 6, pp. 1220-1225, Dec. 2005.
[11] J. Holldampf, A. Peer, and M. Buss, "Virtual Partner for a Haptic Interaction Task," *Human Centered Robot Systems: Cognition, Interaction, Technology,* vol. 6, pp. 183-191, 2010.
[12] K.B. Reed, J. Patton, and M. Peshkin, "Replicating Human-Human Physical Interaction," *Proc. IEEE Int'l Conf. Robotics and Automation (ICRA),* pp. 3615-3620, 2007.
[13] T. Takeda, Y. Hirata, and K. Kosuge, "Dance Partner Robot Cooperative Motion Generation with Adjustable Length of Dance Step Stride Based on Physical Interaction," *Proc. IEEE/RSJ Int'l Conf. Intelligent Robots and Systems (IROS),* pp. 3258-3263, 2007.
[14] S. Kajita and K. Tani, "Study of Dynamic Biped Locomotion on Rugged Terrain—Theory and Basic Experiment," *Proc. Fifth Int'l Conf. Advanced Robotics 'Robots in Unstructured Environments' (ICAR' 91),* vol. 1, pp. 741-746, 1991.
[15] H. Wang and K. Kosuge, "An Inverted Pendulum Model for Reproducing Human's Body Dynamics in Waltz and Its Applications in a Dance Partner Robot," *Proc. IEEE/SICE Int'l Symp. System Integration,* pp. 182-187, 2010.
[16] H. Wang and K. Kosuge, "Towards an Understanding of Dancers' Coupled Body Dynamics for Waltz," *Proc. 2011 IEEE/RSJ Int'l Conf. Intelligent Robots and Systems (IROS),* pp. 2008-2013, 2011.
[17] H. Wang and K. Kosuge, "Understanding and Reproducing Waltz Dancers' Body Dynamics in Physical Human-Robot Interaction," *Proc. IEEE Int'l Conf. Robotics and Automation (ICRA),* 2012.
[18] E.W. Large, "Beat Tracking with a Nonlinear Oscillator," *Proc. IJCAI-95 Workshop Artificial Intelligence and Music,* pp. 24-31, 1995.
[19] M. Goto and Y. Muraoka, "Beat Tracking Based on Multiple-Agent Architecture-a Real-Time Beat Tracking System for Audio Signals," *Proc. Second Int'l Conf. Multiagent Systems,* pp. 103-110, 1996.
[20] M. Goto, "An Audio-Based Real-Time Beat Tracking System for Music with or without Drum-Sounds," *J. New Music Research,* vol. 30, no. 2, pp. 159-171, 2001.
[21] Y. Shiu, N. Cho, P.-C. Chang, and C.-C. Kuo, "Robust On-Line Beat Tracking with Kalman Filtering and Probabilistic Data Association (KF-PDA)," *IEEE Trans. Consumer Electronics,* vol. 54, no. 3, pp. 1369-1377, Aug. 2008.
[22] K. Yoshii, K. Nakadai, T. Torii, Y. Hasegawa, H. Tsujino, K. Komatani, T. Ogata, and H.G. Okuno, "A Biped Robot that Keeps Steps in Time with Musical Beats while Listening to Music with Its Own Ears," *Proc. IEEE/RSJ Int'l Conf. Intelligent Robots and Systems (IROS),* pp. 1743-1750, 2007.
[23] G. Borges and M. Aldon, "Line Extraction in 2D Range Images for Mobile Robotics," *J. Intelligent and Robotic Systems,* vol. 40, no. 3, pp. 267-297, 2004.
[24] M. Rajamani and J. Rawlings, "Estimation of the Disturbance Structure from Data Using Semidefinite Programming and Optimal Weighting," *Automatica,* vol. 45, no. 1, pp. 142-148, 2009.
[25] M. Thirunarayan, D. Kerrigan, M. Rabuffetti, U. Croce, and M. Saini, "Comparison of Three Methods for Estimating Vertical Displacement of Center of Mass During Level Walking in Patients," *Gait and Posture,* vol. 4, no. 4, pp. 306-314, 1996.
[26] E. Gutierrez-Farewik, A. Bartonek, and H. Saraste, "Comparison and Evaluation of Two Common Methods to Measure Center of Mass Displacement in Three Dimensions During Gait," *Human Movement Science,* vol. 25, no. 2, pp. 238-256, 2006.
[27] N. Jarrassé, J. Paik, V. Pasqui, and G. Morel, "How can Human Motion Prediction Increase Transparency?" *Proc. IEEE Int'l Conf. Robotics and Automation (ICRA),* pp. 2134-2139, 2008.
[28] Y. Maeda, T. Hara, and T. Arai, "Human-Robot Cooperative Manipulation with Motion Estimation," *Proc. IEEE/RSJ Int'l Conf. Intelligent Robots and Systems (IROS),* vol. 4, pp. 2240-2245, 2001.
[29] B. Corteville, E. Aertbelien, H. Bruyninckx, J. De Schutter, and H. Van Brussel, "Human-Inspired Robot Assistant for Fast Point-to-Point Movements," *Proc. IEEE Int'l Conf. Robotics and Automation (ICRA),* pp. 3639-3644, 2007.
[30] F. Mussa-Ivaldi, N. Hogan, and E. Bizzi, "Neural, Mechanical, and Geometric Factors Subserving Arm Posture in Humans," *The J. Neuroscience,* vol. 5, no. 10, pp. 2732-2743, 1985.
[31] K. Tee, E. Burdet, C. Chew, and T. Milner, "A Model of Force and Impedance in Human Arm Movements," *Biological Cybernetics,* vol. 90, no. 5, pp. 368-375, 2004.
[32] K. Hase and R. Stein, "Turning Strategies during Human Walking," *J. Neurophysiology,* vol. 81, no. 6, pp. 2914-2922, 1999.
[33] B. Glaister, M. Orendurff, J. Schoen, G. Bernatz, and G. Klute, "Ground Reaction Forces and Impulses During a Transient Turning Maneuver," *J. Biomechanics,* vol. 41, no. 14, pp. 3090-3093, 2008.
[34] S. Strike and M. Taylor, "The Temporal-Spatial and Ground Reaction Impulses of Turning Gait: Is Turning Symmetrical?" *Gait and Posture,* vol. 29, no. 4, pp. 597-602, 2009.
[35] C.-L. Shih, J.W. Grizzle, and C. Chevallereau, "From Stable Walking to Steering of a 3D Bipedal Robot with Passive Point Feet," *Robotica,* 2012, doi: 10.1017/S026357471100138X.
[36] K. Miura, S. Nakaoka, M. Morisawa, K. Harada, and S. Kajita, "A Friction Based Twirl for Biped Robots," *Proc. IEEE-RAS Int'l Conf. Humanoid Robots,* pp. 279-284, 2008.
[37] J. Kim and J. Park, "Quick Change of Walking Direction of Biped Robot with Foot Slip in Single-Support Phase," *Proc. IEEE-RAS Int'l Conf. Humanoid Robots,* pp. 339-344, 2011.
[38] P. Evrard and A. Kheddar, "Homotopy Switching Model for Dyad Haptic Interaction in Physical Collaborative Tasks," *Proc. Third Joint EuroHaptics Conf. and Symp. Haptic Interfaces for Virtual Environment and Teleoperator Systems,* pp. 45-50, 2009.
[39] P. Evrard and A. Kheddar, "Homotopy-Based Controller for Physical Human-Robot Interaction," *Proc. IEEE 18th Int'l Symp. Robot and Human Interactive Comm. (RO-MAN),* pp. 1-6, 2009.
[40] A. Kheddar, "Human-Robot Haptic Joint Actions is an Equal Control-Sharing Approach Possible?" *Proc. Fourth Int'l Conf. Human System Interactions (HSI),* pp. 268-273, 2011.

Hongbo Wang received the BS and MS degrees in mechanical engineering from Tsinghua University, Beijing, in 2006 and 2009, respectively. Currently, he is working toward the PhD degree in the Department of Bioengineering and Robotics, Tohoku University, Sendai, Miyagi, Japan. His current research is focused on the controller design for robots that are physically interacting with human in the context of waltz. He is a student member of IEEE.

Kazuhiro Kosuge (M'87-SM'00-F'06) received the BS, MS, and PhD degrees in control engineering from the Tokyo Institute of Technology, in 1978, 1980, and 1988, respectively. From 1980 to 1982, he was a research staff in the Department of Production Engineering, Denso Company, Ltd. From 1982 to 1990, he was a research associate in the Department of Control Engineering, Tokyo Institute of Technology. From 1989 to 1990, he was a visiting scientist, Department of Mechanical Engineering, Massachusetts Institute of Technology. From 1990 to 1995, he was an associate professor at Nagoya University. Since 1995, he has been with Tohoku University, Sendai, Japan, where he is currently a professor in the Department of Bioengineering and Robotics. He was the president of the IEEE Robotics and Automation Society (2011-2012). He was a vice president of the IEEE Robotics and Automation Society (2010-2011). He was the recipient of the JSME Awards for the best papers in 2002 and 2005, the Excellent Paper Award from FANUC FA and Robot Foundation in 2003 and 2006, and the Best Paper Award of IROS97. He is a fellow of the IEEE, SICE, JSME, and RSJ.

Proceedings of the 10th
World Congress on Intelligent Control and Automation
July 6-8, 2012, Beijing, China

Attractor Design and Prediction-based Adaption for a Robot Waltz Dancer in Physical Human-Robot Interaction*

Hongbo Wang and Kazuhiro Kosuge
Department of Bioengineering and Robotics
Tohoku University
6-6-01, Aoba, Aramaki, Aoba-ku, Sendai 980-8579, Japan
{*h_wang, kosuge*}*@irs.mech.tohoku.ac.jp*

***Abstract*— Physical human-robot interaction between a human leader and a robot follower in waltz is studied in this paper. The dancers' body dynamics in single-support phase are modeled as inverted pendulums. On the robot side, an ankle torque control method is proposed and applied. The control law forms a time-dependent vector field, which makes the nominal orbit of the robot to be an attractor. To physically interact with human, the human leader's state is estimated from range image data by using an extended Kalman filter. Parameters of the robot's orbit are then adjusted according to the leader's estimated and predicted state. The proposed method is verified by simulation results.**

***Index Terms*— Physical human-robot interaction, inverted pendulum, attractor, extended Kalman filter.**

I. Introduction

In physical human-robot interaction (pHRI), a robot is expected to interact with a human partner by utilizing the information of the human as well as the physical connection. Usually, the robot is controlled at two levels. At the higher level, human's intention is estimated from some accessible signals (e.g., force/torque, EMG, etc.); the estimated intention then decides the next event of the robot (intention estimation, or intention sensing) [1]–[3]. At the lower level, the coupled dynamics of the human-robot system are modeled, thus the robot is controlled to cooperate with human by utilizing model knowledge (coupled dynamics) [4]–[6].

Waltz is a typical example of physical human-human interaction (pHHI) in which two dancers are acting as a leader (usually the male dancer) and a follower (usually the female dancer). Waltz can also be viewed at higher and lower levels, as shown in Fig. 1. At the higher level, as waltz has a "vocabulary" of various kinds of dance steps, if the leader has selected the next step, the follower should be able to estimate the leader's selection. At the lower level, as the follower's body dynamics are coupled with the leader; she has to dance in the context of coupled dynamics.

To reproduce the pHHI of waltz with pHRI, we developed a mobile robot that plays the role of the female follower.

*This work is supported by the Asian Office of Aerospace Research and Development (AOARD), Air Force Office of Scientific Research (AFOSR) under grant number FA2386-10-1-4126.

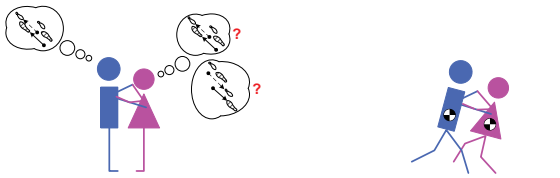

(a) Intention estimation (b) Coupled dynamics

Fig. 1. Two levels of interactions in waltz [7]

The robot is expected to be capable of estimating human leader's next step (higher level) and adapting itself to the coupled body dynamics (lower level). We hope that the knowledge acquired in pHRI may help designing robots that can physically interact with human in more intuitive ways. Because the higher level interaction has been studied in our earlier work [8]; therefore, our focus here is the lower level interaction.

A proper model of the dancers' coupled body dynamics is crucial in achieving good performance in pHRI. In our previous work we modeled dancers as two linear inverted pendulums (LIPM, proposed in [9]) connected by a spring and a damper [10], [11]. However, because of LIPM's unstable orbit, it has large sensitivity to initial condition and disturbance; with the sensitivity problem and measurement noise, it is very difficult to reliably estimate and predict the human leader's state. To deal with the problem, in this paper we propose an approach which makes the orbit to be an attractor and uses extended Kalman filter for human state estimation.

In Section II, models of pHRI, human, and robot are introduced. In Section III, the proposed method for controlling the robot is described. Simulation results are shown in Section IV and conclusions are given in Section V.

II. Models of the Physical Interaction

A. Model of the Physical Interaction

A schematic diagram of the lower level pHRI (i.e., coupled body dynamics) in waltz is illustrated in Fig. 2. This system involves the interaction among three components: the human

body, the human arm, and the robot follower. Principally, the arm should be considered as a subset of the body; however, as the human arm is the "interface" between the coupled systems, the interaction force f is largely affected by arm dynamics. Due to its significant role in the physical interaction, the human arm dynamics are often separately analyzed [12].

As the human body and the human arm can only be commanded by human himself (intention of body motion, and arm actuation), our goal is to design the robot dynamics for achieving some performance requirements, e.g., spatially following human ($\boldsymbol{x_f}$ tracks $\boldsymbol{x_l}$), or reducing the interaction force f. Ideally, if models of the human body and the arm are already known, while accurate measurement of $\boldsymbol{x_l}$ is possible, the robot dynamics can be designed with ease. However, in practice these prerequisites can hardly be satisfied: precisely modeling human and measuring states are still great challenges.

If we ignore the unknown human body dynamics and $\boldsymbol{x_l}$, the robot will be controlled in a simpler context: a feedback loop which consists the inter-connected human arm and robot. This feedback loop is a classic case in pHRI related studies [4]. Usually an assumed arm model with identified parameters are used for robot controller design; however, due to the large structured/unstructured uncertainties in the arm model, the designer will tend to use a worst-case gain, along with a conservative stability criterion (e.g., small gain theorem) to synthesize the robot controller, which leads to the large sacrifice in performance.

This compromise between stability and performance can be alleviated if more information about the human leader is accessible. An extreme case is that if $\boldsymbol{x_l}$ can be accurately observed, we can simply let $\boldsymbol{x_f} = \boldsymbol{x_l}$ to realize human following and f reduction. This extreme case, though impractical, well exemplifies the effectiveness of using the feed-forward of $\boldsymbol{x_l}$ (the dashed arrow in Fig. 2), which has also been experimentally validated in [13].

After introducing the feed-forward of $\boldsymbol{x_l}$, we also need an assumed human body model, which serves two purposes:

1) The measured $\boldsymbol{x_l}$ usually contains large noise/offset. As $\boldsymbol{x_l}$ is the result of human body dynamics; by using an assumed human model, we can design a model-based filter to attenuate the measurement noise;
2) The assumed human body model can also be used for predicting $\boldsymbol{x_l}$ in the future.

Therefore, in the subsequent part we will introduce the human body model which is being used in this paper.

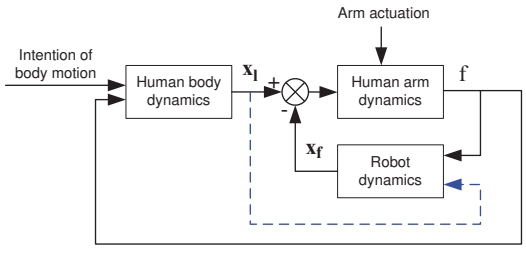

Fig. 2. Diagram of the pHRI model in waltz. $\boldsymbol{x_l}$ and $\boldsymbol{x_f}$ are leader's and follower's spatial states (e.g., position, velocity, etc). f is the interaction force

B. The Human Model

The human leader generally keeps walking throughout the waltz dance, hence a human's body model is firstly a bipedal walking model. A simplified human model which catches the primary features of walking is the inverted pendulum model, as given in Fig. 3. This model consists of a center of mass (CoM), an extendable leg and an ankle joint actuator, with dynamics as

$$\ddot{x}_l = \frac{\ddot{z}_l + g}{z_l} x_l + \frac{u_l}{m_l z_l} + \frac{f}{m_l} \tag{1}$$

where x_l is the horizontal position of CoM with respect to the pivot point, z_l is the height of CoM, m_l is the mass of the inverted pendulum, g is gravitational acceleration, f is external force, and u_l is ankle torque. It is difficult to precisely measure u_l with external sensors, but the repeating patterns of u_l in bipedal walking can be approximated by other known states. Here we assume u_l is a function of x_l, $\dot{x}_l$ and f, while $u_l(x_l, \dot{x}_l, f) = 0$ if x_l, $\dot{x}_l$ and f are all zero. A linear approximation is

$$u_l(x_l, \dot{x}_l, f) = k_1 x_l + k_2 \dot{x}_l + k_3 f \tag{2}$$

where k_1 and k_2 are the damping/actuation coefficients of the ankle, k_3 stands for human's reactions to the external force. With (1) and (2), the human model has only one input f:

$$\dot{\boldsymbol{x}}_{\boldsymbol{l}} = \begin{pmatrix} 0 & 1 \\ a_1 & a_2 \end{pmatrix} \boldsymbol{x_l} + [0, b]^T f \tag{3}$$

where $a_1 = (\ddot{z}_l + g)/z_l + k_1/(m_l z_l)$, $a_2 = k_2/(m_l z_l)$, and $b = k_3/(m_l z_l) + 1/m_l$ are human model's unknown parameters.

The above model can only approximate human's body dynamics in single-support phase, besides which there is another double-support phase. In double-support phase, human is almost a fully actuated system and corresponds to a completely different model instead of (1) and (2).

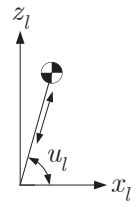

Fig. 3. Simplified human body dynamics with an inverted pendulum model

The transition between the single-support and the double-support phases are foot landings, i.e., when the swing foot lands on ground. At foot landings, x_l is instantaneously reset with a new value, hence the time history of x_l and $\dot{x}_l$ formulates a set of orbits in phase plot. At the same time, since for a human leader in waltz this reset is synchronized with music beats (denoted by $\{t_l\}$), the orbit of x_l and $\dot{x}_l$ is time-dependent, i.e., x_l is reset when $t \in \{t_l\}$, as shown in Fig. 4.

Compared with the gravity-dominated body motions in single-support phase, it is difficult to model human's behavior in double-support phase. However, for a robot which is physically interacting with human, it is necessary to deal with the two phases with distinctive dynamics. A straightforward solution is using one conservative robot model that can work stably in both phases, but this will usually cause degradations in performance. As we have some information about the dynamics in single-support phase, those information should be exploited to enhance interaction performance.

C. The Robot Model

Generally, for the system described in Fig. 2, there are infinite candidate robot models that can be implemented to control the pHRI. Because our purpose is to realize a life-like interaction as in the case of pHHI, a human-like robot model is preferred. The model used here is linear inverted pendulum (LIPM) [9], [14], which has simplified dynamics as

$$\ddot{x}_f = (g/z_f)x_f + u_f/(m_f z_f) + f/m_f \tag{4}$$

where x_f is the robot follower's CoM position with respect to the pivot point, z_f is the height of CoM, m_f is follower's mass, and u_f is the ankle torque.

For simplicity, this model does not contain double-support phase. In addition, values of the reset x_f at k-th foot landing moments (which are also the music beat moments in waltz, denoted by $t_f(k)$) are controlled by a balance controller to guarantee the CoM velocity at moment $t_f(k+1)$. Consider that the period of beat moments has a nominal value T_p, i.e., $T_p = t_f(k+1) - t_f(k)$, the balance controller resets x_f at moment $t_f(k)$ by using the following rule such that $\dot{x}_f(t_f(k+1)) = v_d(t_f(k+1))$ can be achieved (given $u_f(t) = 0$ when $t_f(k) < t \leq t_f(k+1)$) [10],

$$x^+(t_f(k)) = -\frac{\tau C}{S}\dot{x}_f\left(t_f(k)\right) + \frac{\tau}{S}v_d\left(t_f(k+1)\right) \tag{5}$$

where $v_d(t_f(k+1))$ is the desired velocity at $t_f(k+1)$. $\tau = \sqrt{z_f/g}$, $C = \cosh(T_p/\tau)$ and $S = \sinh(T_p/\tau)$.

With the LIPM dynamics described in (4) and the balance controller in (5), the time-dependent orbit of $\boldsymbol{x_f} = [x_f, \dot{x}_f]^T$ is illustrated in Fig. 5. If $u_f = 0$, the trajectory of the single-support phase is a hyperbola with an invariant orbital energy [9].

III. Control of the Robot

A. Orbit Control of the Robot

Although the robot can be balanced by resetting x at beat moments $\{t_f\}$ using (5), the control rule is intermittent and cannot cover the moments throughout the motion; if disturbance is introduced during single-support phase, trajectory will deviate from the nominal orbit; as LIPM is linear and unstable, this deviation will increase exponentially. Therefore, additional control by using the ankle torque u_f is necessary.

Ignoring the interaction force f, system (4) can be written as

$$\dot{\boldsymbol{x}}_{\boldsymbol{f}} = \begin{pmatrix} 0 & 1 \\ g/z_f & 0 \end{pmatrix} \boldsymbol{x_f} + [0, 1/(m_f z_f)]^T u_f \tag{6}$$

As the system is controllable, usually we can use a state-feedback gain to replace the pendulum's original dynamics with an artificial one (with designed poles). However, this requires large ankle torque, which is impossible since human's ankle torque is limited by the size of supporting foot.

For bipedal walking, this control can be realized by turning the nominal orbit into an attractor. For a state-dependent system, a vector field near the nominal orbit can be designed to "attract" neighboring states onto the orbit [15], as shown in Fig. 6(a).

Similarly, it is easy to design an vector field near the robot's nominal orbit according to orbital energy, such that solutions with arbitrary initial conditions can converge to the orbit. However, as our system is time dependent (x is reset only at beat moments $\{t_f\}$) while the LIPM is expected to reach the desired velocity v_d when $t \in \{t_f\}$, convergence to the nominal orbit may lead to the violation of this requirement (the dotted dash curve in Fig. 6(b)). Instead,

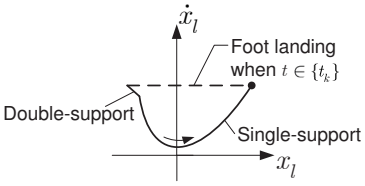

Fig. 4. The orbit in walking

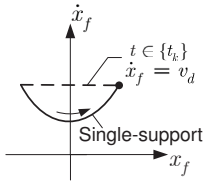

Fig. 5. Orbit of the robot

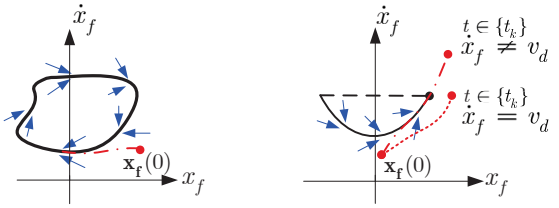

(a) State-dependent orbit (b) Time-dependent orbit

Fig. 6. Designing attractors for two types of orbits. Arrows are vector fields; dotted dashes are solution trajectories for state-dependent orbits; dashed curve in (b) is the solution for time-dependent orbits

a desired solution may deviate from the nominal orbit (the dashed curve in Fig. 6(b)), depending on the current time. In another word, to deal with the time-dependent system, the vector field should also be time-dependent (more specifically, time-state-dependent). Design of the vector field will be introduced in the following part.

The robot is controlled in discrete manner with sampling period t_s, the robot dynamics is

$$\boldsymbol{x_f}(k+1) = \boldsymbol{A_r}\boldsymbol{x_f}(k) + \boldsymbol{B_r}u_f(k) \tag{7}$$

where $\boldsymbol{A_r}$ and $\boldsymbol{B_r}$ are discrete forms of the matrices appeared in (6).

The state at time step N is

$$\boldsymbol{x_f}(N) = \boldsymbol{A_r}^{N-k}\boldsymbol{x_f}(k) + \sum_{i=k}^{N-1}\left(\boldsymbol{A_r}^{N-i-1}\boldsymbol{B_r}u_f(i)\right) \tag{8}$$

Assume there exists a sequence $u_f(k)\dots u_f(N-1)$ which makes $\boldsymbol{x_f}(N) = \boldsymbol{x_f^*}$, where $\boldsymbol{x_f^*}$ is the desired robot state at time step N. Define state error at time step k as

$$\boldsymbol{e}(k) = \boldsymbol{x_f^*} - \boldsymbol{A_r}^{N-k}\boldsymbol{x_f}(k) = \sum_{i=k}^{N-1}\left(\boldsymbol{A_r}^{N-i-1}\boldsymbol{B_r}u_f(i)\right) \tag{9}$$

$\boldsymbol{e}(k)$ is the difference between the desired state and a predicted state, given all future efforts, i.e., $u_f(k)\dots u_f(N-1) = 0$. The evolution of $\boldsymbol{e}(k)$ is

$$\boldsymbol{e}(k+1) = \boldsymbol{e}(k) - \boldsymbol{A_r}^{N-k-1}\boldsymbol{B_r}u_f(k) \tag{10}$$

One may expect to use the feedback of $\boldsymbol{e}(k)$ to build a stable system, in which $\boldsymbol{e}(k)$ asymptotically converges to $\mathbf{0}$ as $k \to N$. Unfortunately, because (10) is uncontrollable, $\boldsymbol{e}(k)$ cannot be eliminated. As we are only concerned about velocity errors, here only $\dot{e}(k)$ is considered. The control law of u_f is

$$u_f(k) = \frac{\dot{x}_r^* - \left[\boldsymbol{A_r}^{N-k}\boldsymbol{x_f}(k)\right]_{(2,1)}}{\gamma\left[\boldsymbol{A_r}^{N-k-1}\boldsymbol{B_r}\right]_{(2,1)}} \tag{11}$$

where $[\boldsymbol{M}]_{(i,j)}$ denotes matrix $\boldsymbol{M}$'s entry on row i and column j. $\gamma > 1$ is a scalar used to control the convergence speed. With u_f being controlled by (11), we have

$$\dot{e}(k+1) = (1 - 1/\gamma)\dot{e}(k) \tag{12}$$

which suggests the exponentially diminishing error of velocity.

The method presented in (11) fully utilizes LIPM's original dynamics and results in an efficient control law. When desired velocity v_d and beat moments $\{t_f\}$ are given, an attractive orbit is defined. At the same time, to physically interact with the human leader, the orbit parameters v_d and $\{t_f\}$ should be adapted to the leader's orbit. Because these parameters are adjusted according to human leader's state (the feed-forward path in Fig. 2), in the following we will introduce the method of estimating and predicting the human leader's state.

B. Estimating and Predicting the Human Leader's State

In single-support phase, human leader's motion is largely determined by gravity, this makes leader's state $\boldsymbol{x_f}$ easier to estimate and predict. To obtain the human leader's state, we installed two laser range finders (LRF) on the robot to detect human's waist and ankle positions, with which the state $\boldsymbol{x_l}$ can be inferred, as shown in Fig. 7.

However, there are also several difficulties in the state estimation/prediction task, namely

1) The human model given in (1) is not the exact model of human's body dynamics;
2) Model parameters are unknown;
3) The noise and offsets contained in the measurements from the LRFs.

With (3), the listed difficulties can be reformulated as a system with uncertainties, process noise, and measurement noise:

$$\begin{aligned}\dot{\boldsymbol{x}}_{\boldsymbol{l}} &= \begin{pmatrix} 0 & 1 \\ a_1 & a_2 \end{pmatrix}\boldsymbol{x_l} + [0, b]^T f + [w_1, w_2]^T \\ \boldsymbol{y} &= [x_l + \delta, \dot{x}_l]^T + [v_1, v_2]^T \end{aligned} \tag{13}$$

where a_1, a_2, and b are unknown model parameters, δ is the unknown offset of measured CoM. w_1, w_2 are the process noises; v_1 and v_2 are measurement noises.

By introducing an extended state $\boldsymbol{x_e}$, which includes the unknown parameters, we have

$$\boldsymbol{x_e} = [x_l, \dot{x}_l, a_1, a_2, b, \delta]^T \tag{14}$$

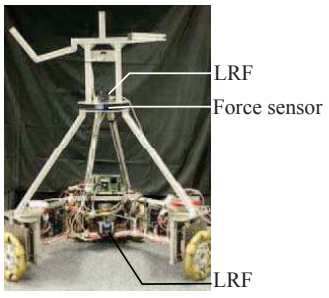

Fig. 7. Two LRFs are installed on the robot for detecting human's waist and ankle positions

then the system defined in (13) turns to be nonlinear, with

$$\begin{aligned} \dot{\boldsymbol{x}}_{\boldsymbol{e}} &= \boldsymbol{g}_{\boldsymbol{e}}(\boldsymbol{x}_{\boldsymbol{e}}, f) + [w_1, w_2]^T \\ \boldsymbol{y} &= \boldsymbol{h}_{\boldsymbol{e}}(\boldsymbol{x}_{\boldsymbol{e}}) + [v_1, v_2]^T \end{aligned} \tag{15}$$

The nonlinear system in (15) is firstly discretized, then its state is estimated by using an discrete extended Kalman filter (EKF). Details of the EKF will not be discussed here. The estimated state and model parameters can also be used to predict the future state.

Since in waltz two dancer's motions are synchronized, the other necessary information is the human leader's beat moments $\{t_l\}$ and support phases (single-support or double-support). These are also inferred from LRF data by detecting foot landing moments, while details can be found in [11].

C. Following the Human Leader

With the feed-forward of the human leader's estimated state, we can adapt the robot's orbit parameters to realize a coupling in which the robot can well follow the human leader in a life-like way.

In single-support phase, if we are at time step k while the next beat moment is on N, we first estimate the human leader's state/parameters $\hat{\boldsymbol{x}}_{\boldsymbol{e}}(k)$ with EKF. From the estimation $\hat{\boldsymbol{x}}_{\boldsymbol{e}}(k)$, human leader's velocity at N can be predicted (we denote this prediction by $\hat{v}_l$(k)). Finally, the predicted velocity $\hat{v}_l(k)$ substitutes $\dot{x}_r^*$ in (11) and $u_f(k)$ is then obtained.

In double-support phase, as the human model is unclear, we have $u_f = 0$. At beat moments $\{t_f\}$, x_f is reset according to (5).

IV. Simulations

A. Control of the Robot

In simulations, parameters of the robot follower are $m_f = 45\,\mathrm{kg}$, $z_f = 0.9\,\mathrm{m}$; period of beat moments is $T_p = 0.75\,\mathrm{s}$.

The ankle torque control in (11) actually generates a time-dependent vector field. To visualize this vector field, the time axis, ranging from 0 to T_p, is included as one dimension, result is shown in Fig. 8. We can see that the solution curves with different initial $\boldsymbol{x_f}$ and t have been attracted by the set defined by $t \in \{t_f\}$ and $\dot{x}_f = v_d$.

Given v_d and $\{t_f\}$, the vector field of (11) and the x-resetting rule of (5) are defined, yielding a stable and periodic orbit of the robot, as shown in Fig. 9.

B. The Physical Interaction

To simulate the interaction between two dancers, we modeled them as two inverted pendulums connected by a spring and a damper. Parameters of the simulation are $m_l = 70\,\mathrm{kg}$, $z_l = 1\,\mathrm{m}$. The connection is assumed to have stiffness of $100\,\mathrm{N/m}$ and damping of $30\,\mathrm{Ns/m}$. Timing errors are considered in two dancer's synchronization with timing error $0.1\,\mathrm{s}$. Measurements of the LRFs are assume to have $\pm 0.05\,\mathrm{m}$ white noise and $-0.05\,\mathrm{m}$ bias in x_l, and $\pm 0.2\,\mathrm{m/s}$ white noise in $\dot{x}_l$. Results of simulation are shown in Fig. 10.

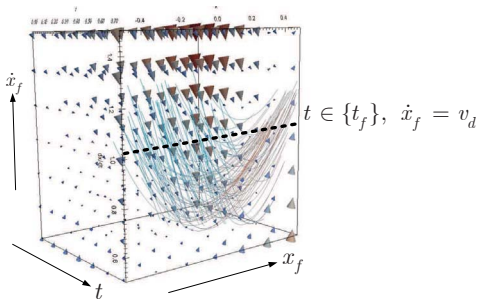

Fig. 8. The time-dependent vector field generated by (11). v_d is set to 1. The cones are vectors of flow directions; the curves are integrated streams of solutions

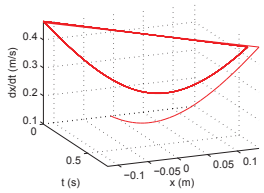

Fig. 9. Solution orbit of the robot

Due to model uncertainties and measurement noise/bias, the predicted $\hat{v}_l$ is quite inaccurate at the beginning; however, the prediction error converges as the time is approaching the next beat moment, as demonstrated in Fig. 10(a). According to Fig. 10(b) and Fig. 10(c), the two dancer's orbits are coupled with reduced interaction force (compared with the results of [10], [11]). The simulated ankle torque u_f is also kept within a reasonable range (Fig. 10(d)). Our proposed method is hence supported by the simulation results in Fig. 10.

V. Conclusion

In this paper, we first introduce a pHRI model, which implies the necessity of designing the robot dynamics model as well as implementing an assumed model of the human leader. We approximate human's body dynamics in single-support phase with an inverted pendulum, while the robot is controlled to emulate the dynamics of an LIPM. In the robot's single-support phase, an ankle torque control method is proposed. The ankle torque control forms a time-dependent vector field, turning the nominal orbit of the robot to be an attractor. To physically interact with human, parameters of the attractor are adjusted according to human leader's state obtained from LRFs. The proposed method is validated by simulations.

However, the current model only considers translational

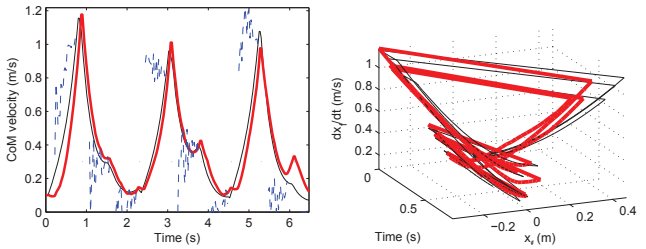

(a) Velocities

(b) Coupled orbits

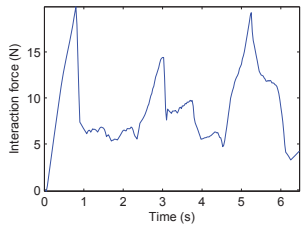

(c) Interaction force

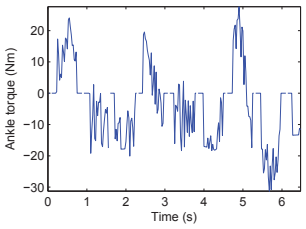

(d) Ankle torque of robot

Fig. 10. Simulated pHRI with the proposed robot controller. The human leader is supposed to have varying v_d with $v_d(t_l(1))\ldots v_d(t_l(9))$ being $\{1, 0.3, 0.1, 1, 0.3, 0.1, 1, 0.3, 0.1\}(\mathrm{m/s})$, respectively. Thin and thick solid curves in (a) and (b) are human and robot's states. Dashed curve in (a) is the predicted velocity $\hat{v}_l$

motions in dancers' sagittal plane, leaving rotational motions (body spins and turns) unstudied. In addition, experimental validations are still to be finished. These issues will be included in our future work.

REFERENCES

[1] N. Stefanov, A. Peer, and M. Buss, "Online intention recognition for computer-assisted teleoperation," *Proceedings of the 2010 IEEE International Conference on Robotics and Automation (ICRA)*, pp. 5334–5339, 2010.

[2] V. Duchaine and C. Gosselin, "Safe, stable and intuitive control for physical human-robot interaction," *Proceedings of the 2009 IEEE International Conference on Robotics and Automation (ICRA)*, pp. 3383–3388, 2009.

[3] Z. Wang, A. Peer, and M. Buss, "An HMM approach to realistic haptic human-robot interaction," *EuroHaptics conference, 2009 and Symposium on Haptic Interfaces for Virtual Environment and Teleoperator Systems. World Haptics 2009. Third Joint*, pp. 374–379, 2009.

[4] H. Kazerooni, "Human/robot interaction via the transfer of power and information signals," *IEEE Transactions on System, Man, and Cypernetics*, vol. 20, no. 2, pp. 450–463, 1990.

[5] S. Buerger and N. Hogan, "Complementary stability and loop shaping for improved human-robot interaction," *IEEE Transactions on Robotics*, vol. 23, no. 2, pp. 232 –244, 2007.

[6] S. Sirouspour, "Robust control design for cooperative teleoperation," *Proceedings of the 2005 IEEE International Conference on Robotics and Automation (ICRA)*, pp. 1133–1138, 2005.

[7] H. Wang and K. Kosuge, "Control of a robot dancer for enhancing haptic human-robot interaction in waltz," *IEEE Transactions on Haptics*, submitted.

[8] T. Takeda, Y. Hirata, and K. Kosuge, "Dance step estimation method based on HMM for dance partner robot," *IEEE Transactions on Industrial Electronics*, vol. 54, no. 2, pp. 699–706, 2007.

[9] S. Kajita and K. Tani, "Study of dynamic biped locomotion on rugged terrain—theory and basic experiment," *Advanced Robotics, 1991. 'Robots in Unstructured Environments', 91 ICAR., Fifth International Conference on*, pp. 741–746 vol.1, 1991.

[10] H. Wang and K. Kosuge, "Towards an understanding of dancers' coupled body dynamics for waltz," *Proceedings of the 2011 IEEE/RSJ International Conference on Intelligent Robots and Systems (IROS)*, pp. 2008–2013, 2011.

[11] ——, "Understanding and reproducing waltz dancers' body dynamics in physical human-robot interactio," *Proceedings of the 2012 IEEE International Conference on Robotics and Automation (ICRA)*, to appear.

[12] F. Mobasser and K. Hashtrudi-Zaad, "A method for online estimation of human arm dynamics," in *Proceedings of the 2006 IEEE International Conference of Engineering in Medicine and Biology Society*, 2006, pp. 2412–2416.

[13] N. Jarrassé, J. Paik, V. Pasqui, and G. Morel, "How can human motion prediction increase transparency?" in *Proceedings of the 2008 IEEE International Conference on Robotics and Automation (ICRA)*, 2008, pp. 2134–2139.

[14] S. Kajita, F. Kanehiro, K. Kaneko, K. Yokoi, and H. Hirukawa, "The 3D linear inverted pendulum mode: a simple modeling for a biped walking pattern generation," *Proceedings of the 2001 IEEE/RSJ International Conference on Intelligent Robots and Systems (IROS)*, no. 4, pp. 239–246, 2001.

[15] M. Okada and K. Murakami, "Robot communication principal by motion synchronization using orbit attractor," in *Proceedings of the 2007 IEEE International Conference on Robotics and Automation (ICRA)*, 2007, pp. 2564–2569.

2012 IEEE International Conference on Robotics and Automation
RiverCentre, Saint Paul, Minnesota, USA
May 14-18, 2012

Understanding and Reproducing Waltz Dancers' Body Dynamics in Physical Human-Robot Interaction

Hongbo Wang and Kazuhiro Kosuge

Abstract— **A pair of spring-damper-connected inverted pendulums are introduced to model two dancers' body dynamics in physical interaction. When timing errors are included in the model, condition for poly-quadratic stability is implemented to examine the system. With two laser ranger finders installed on the robot for measuring human dancer's states, a state-feedback-based method is proposed to minimize the interaction force; because in simulation the theoretically optimal feedback gain is sensitive to measurement noise, another set of empirical gains are used and proved to be effective in experiments.**

Index Terms— **Physical human-robot interaction, dance partner robot, linear inverted pendulum, poly-quadratic stability, laser ranger finder.**

I. Introduction

Physical human-robot interaction (pHRI) involves the coupled system of human and robot. By utilizing the information through the coupling, the robot is able to interact with human in expected ways. To achieve a well-coordinated interaction, the robot usually maintains models at two levels. At the higher level, the correlation between human's intentions and accessible signals (e.g., force/torque, EMG, etc.) is modeled for the purpose of realizing human intention estimation (or intention sensing) [1]–[3]. At the lower level, as pHRI is constrained by the physical laws that govern human's and robot's motions, dynamics of the human-involved system should also be modeled; hence the robot can properly affect the coupled dynamics by utilizing model knowledge [4]–[6].

Waltz is a typical example of demonstrating human's capabilities in physical human-human interaction (pHHI), which can also be viewed at higher and lower levels. Waltz has a "vocabulary" of various types of steps, while a dance consists of a series of temporally concatenated steps. In a social setting, where the male dancer (leader) selects the next step in improvised ways, the female dancer (follower) can estimate the leader's next step by using haptic signals; this is higher level interaction. At the same time, whether the next step is known or unknown to the follower, she is still well-adapted to the coupled body dynamics, as well as keeping her own balance; this is lower level interaction.

The goal of our research is to reproduce the pHHI of waltz with pHRI, in which a mobile robot plays the follower's role, being capable of estimating human leader's next step (higher level) and adapting itself to the coupled body dynamics (lower level). We hope that more knowledge acquired from this pHRI may help designing robots that can physically interact with human in more intuitive ways. In one earlier work, the higher level interaction has been studied [7]; therefore, our current focus is investigating the lower level interaction.

On the lower level interaction, one of our previous work modeled the robot as a free mass following various predefined dance trajectories, whose parameters can be adjusted by learning [8]. In another work we used a pair of connected inverted pendulums as a more accurate system model [9]. By assuming the two dancers' motions are synchronized, we analyzed stability of the system, while interaction force was reduced with gradient descent method [10].

In waltz, two dancers are roughly synchronized with the help of music beats; however, timing errors between the two dancers can frequently occur. Due to the inevitable timing errors, our assumption on the precisely synchronized motion is too strong; therefore, in this paper, we will remove this strong assumption and include timing errors in the model description. In addition, because the gradient descent method we used was slow and often sensitive to step size, in this paper we also propose a method which reduces interaction force by utilizing more human dancer's information from additional sensors (two laser range finders).

Two dancers' motions in sagittal plane are analyzed with the same model proposed in [9], [10]; the limitation of this model is that it only accounts for human's translational motions that can be treated as two independent components in sagittal and frontal plane. Accordingly, for the various dance steps in waltz, only a few steps without body rotation (e.g., closed changes) can be the subjects of our study. Therefore, we are actually modeling two dancers' "coupled walking" instead of the true waltz dancing. Clearly, those very simple cases are still far from the true dances that we expect the robot to do; however, they offer a good start point from which we can explore physical human-robot interaction (pHRI), such as the one-dimensional cases in [6], [11], [12].

In Section II, the system model is introduced. In Section III, stability of the two-dancer system and the method for minimizing interaction force are analyzed. Simulation and experiment results are shown in Section IV and conclusions are given in Section V.

II. System Model

A. Simplified Model for Single Dancer's Body Dynamics

Linear inverted pendulum (LIPM) is a largely simplified model for biped walking systems [13]. If we consider the legs as massless while applying some constraints on CoM's (center of mass) vertical motion, we can simplify a walking system as Fig. 1(a) into an LIPM as in Fig. 1(b) [9]. The

The authors are with the Department of Bioengineering and Robotics, Tohoku University, 6-6-01, Aoba, Aramaki, Aoba-ku, Sendai 980-8579, Japan {h_wang, kosuge}@irs.mech.tohoku.ac.jp

linear dynamics of the LIPM in x direction is [13]:

$$\ddot{x} = (g/z)x + (1/(mz))u_{\text{ank}} \tag{1}$$

where x is the position of CoM with respect to LIPM's pivot point, z is the height of CoM, g is gravity acceleration, m is mass of the body, and u_{ank} is ankle torque. Since u_{ank} is limited in value, it is often used for disturbance rejection rather than as a major source of control input, hence (1) can also be written in homogeneous form without the u_{ank} term.

Due to the instability of LIPM (as can be seen in (1)); to have a working model, we also need a balance controller, which can intermittently set new values for x, i.e., this inverted pendulum can instantaneously relocate pivot point to keep balance. The LIPM along with its controller can be viewed as an impulsive dynamical system:

$$\begin{cases} \ddot{x} &= (g/z)x, \ t \notin \{t_k\} \\ x^+ &= w(x^-, \dot{x}), \ t \in \{t_k\} \end{cases} \tag{2}$$

where $\{t_k\}$ is the set of moments when pivot point instantaneously reaches a new position. Since in waltz $\{t_k\}$ corresponds to the moments of music beat, hereafter we will call $\{t_k\}$ *beat moments*, while x^-, x^+ are x before and after a beat moment.

The function w in (2) is the balance controller. There are many methods to obtain w. In [10] we listed 3 candidates (an energy controller, a velocity controller, and a hybrid version of the former two) and finally selected the hybrid one. However, in this paper we will use the velocity controller. The reason is that when there is no timing error in beat moments (i.e., $t_k - t_{k-1}$ is constant for all k), both the velocity controller and the hybrid one can direct the system to desired velocities; when there is timing error, we can also find an upper bound of errors when using the velocity controller. Below is the explanation:

Consider that the period of beat moments has a nominal value T_p, $t_k - t_{k-1}$ may be different from T_p, but the controller still takes T_p as a constant and known parameter. The velocity controller is

$$x^+ = -(\tau C/S)\dot{x}(t_k) + (\tau/S)v_d(t_{k+1}) \tag{3}$$

where $v_d(t_{k+1})$ is a reference input which represents the desired velocity at t_{k+1}. $\tau = \sqrt{z/g}$. And $C = \cosh(T_p/\tau)$ and $S = \sinh(T_p/\tau)$ are parameters containing the constant T_p.

Let t_{k+1}^- be the instant just before $(k+1)$th beat moment, while $t_{k+1} - t_k = T_p + \delta T_p$ due to the existence of timing error δT_p. Assuming LIPM's velocity is not changed before and after pivot relocation, i.e., $\dot{x}(t_k^-) = \dot{x}(t_k^+) = \dot{x}(t_k)$ for all k, and by solving (2), we have:

$$\dot{x}(t_{k+1}) = -\alpha_1(\delta T_p)\dot{x}(t_k) + \alpha_2(\delta T_p)v_d(t_{k+1}) \tag{4}$$

where $\alpha_1(\delta T_p)$ and $\alpha_2(\delta T_p)$ are two scalar functions of δT_p with $\alpha_1(\delta T_p) = \sinh(\delta T_p/\tau)/\sinh(T_p/\tau)$ and $\alpha_2(\delta T_p) = \sinh\left((T_p + \delta T_p)/\tau\right)/\sinh(T_p/\tau)$. In waltz δT_p should be smaller than T_p (at least smaller than $T_p/2$, otherwise the two dancers would be in opposite phases), thus $|\alpha_1(\delta T_p)| < 1$, and both $\alpha_1(\delta T_p)$ and $\alpha_2(\delta T_p)$ are bounded.

Defining the error of the velocity controller as $e(t_k) = \dot{x}(t_k) - v_d(t_k)$, it yields

$$e(t_{k+1}) = -\alpha_1(\delta T_p)e(t_k) + \gamma(\delta T_p)v_d(t_{k+1}) \tag{5}$$

with $\gamma(\delta T_p) = \alpha_2(\delta T_p) - \alpha_1(\delta T_p) - 1$. This $\gamma(\delta T_p)$ is also bounded. Let $\bar{\alpha}_1 \geq |\alpha_1(\delta T_p)|$, $\bar{\alpha}_1 < 1$ and $\bar{\gamma} \geq |\gamma(\delta T_p)|$ be two upper bounds, then

$$|e(t_{k+1})| \leq \bar{\alpha}_1|e(t_k)| + \bar{\gamma}|v_d(t_{k+1})| \tag{6}$$

If $v_d(t_k)$ has a constant value v_d, the maximum error bound is $|e(t_0)|$ or $\bar{\gamma}|v_d|/(1-\bar{\alpha}_1)$, depending on which is larger.

Based on the above analysis, in the subsequent part we will use LIPM along with the velocity controller as the single dancer's model.

B. Two-LIPM Model for Dancers in Physical Interaction

To model the dynamics of two dancers in physical connection, we use a pair of LIPMs connected by a spring and a damper, as shown in Fig. 2 [10]. Let x_l^g and x_f^g be the CoM positions of the leader and the follower, and p_l^g and p_f^g be their pivot positions, all with respect to the global frame. The state vector $\boldsymbol{x}$ is defined as

$$\boldsymbol{x} = [x_l, \dot{x}_l, x_f, \dot{x}_f, q]^T \tag{7}$$

where $x_l = x_l^g - p_l^g$, $x_f = x_f^g - p_f^g$, which are the leader's and the follower's relative positions of CoM with respect to their own pivot points. $q = x_f^g - x_l^g - d_0$, with d_0 being the spring's natural length. Let k_c and d_c be constants of the spring and the damper, the system dynamics of the two-LIPM system is:

$$\begin{cases} \dot{\boldsymbol{x}} &= \boldsymbol{A}\boldsymbol{x}, \ t \notin \{t_k^l\} \cup \{t_k^f\} \\ \boldsymbol{x}^+ &= \boldsymbol{H_l}\boldsymbol{x}^- + \boldsymbol{B_l}v_d^l, \ t \in \{t_k^l\} \\ \boldsymbol{x}^+ &= \boldsymbol{H_f}\boldsymbol{x}^- + \boldsymbol{B_f}v_d^f, \ t \in \{t_k^f\} \end{cases} \tag{8}$$

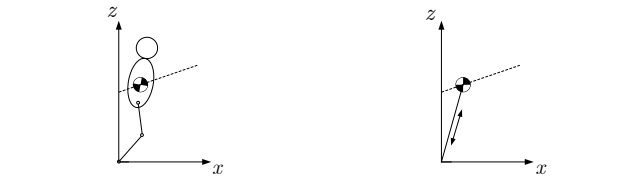

(a) Simplified human walking model (b) Linear inverted pendulum

Fig. 1. LIPM as a simplified model [9]

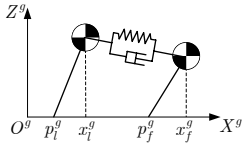

Fig. 2. Two connected LIPMs as two dancers' model [10]

where $\{t_k^l\}$ and $\{t_k^f\}$ are the leader's and the follower's respective beat moments. Matrix $\boldsymbol{A}$ is

$$\boldsymbol{A} = \begin{pmatrix} 0 & 1 & 0 & 0 & 0 \\ \frac{g}{z_l} & -\frac{d_c}{m_l} & 0 & \frac{d_c}{m_l} & \frac{k_c}{m_l} \\ 0 & 0 & 0 & 1 & 0 \\ 0 & \frac{d_c}{m_f} & \frac{g}{z_f} & -\frac{d_c}{m_f} & -\frac{k_c}{m_f} \\ 0 & -1 & 0 & 1 & 0 \end{pmatrix} \tag{9}$$

with z_l, z_f being the leader's and the follower's CoM heights and m_l, m_f being their body masses. $\boldsymbol{H_l}$, $\boldsymbol{H_f}$, $\boldsymbol{B_l}$, and $\boldsymbol{B_f}$ are the matrix forms of (3), with

$$\boldsymbol{H_l} = \left(\begin{array}{cc|c} 0 & -C_l\tau_l/S_l & \boldsymbol{0}_{2\times 3} \\ 0 & 1 & \\ \hline \multicolumn{2}{c|}{\boldsymbol{0}_{3\times 2}} & \boldsymbol{I}_{3\times 3} \end{array}\right) \tag{10}$$

$$\boldsymbol{H_f} = \left(\begin{array}{c|ccc} \boldsymbol{I}_{2\times 2} & \multicolumn{3}{c}{\boldsymbol{0}_{2\times 3}} \\ \hline & 0 & -C_f\tau_f/S_f & 0 \\ \boldsymbol{0}_{3\times 2} & 0 & 1 & 0 \\ & 0 & 0 & 1 \end{array}\right) \tag{11}$$

and $\boldsymbol{B_l} = [\tau_l/S_l, 0, 0, 0, 0]^T$, $\boldsymbol{B_f} = [0, 0, \tau_f/S_f, 0, 0]^T$. $\boldsymbol{H_l}$ and $\boldsymbol{H_f}$ commute: $\boldsymbol{H_l H_f} = \boldsymbol{H_f H_l} = \boldsymbol{H}$. Symbols like $\tau_{l,f}$, $C_{l,f}$ and $S_{l,f}$ are defined similarly as in (3). Also, as a system of two physically interacting LIPMs, their interaction force is denoted by f, with $f = \boldsymbol{cx}$, where $\boldsymbol{c} = [0, d_c, 0, -d_c, -k_c]$.

III. Analysis on Stability and Optimal Interaction

A. Stability of the Two-LIPM System Considering Synchronization Error

A simplified version of system (8) was analyzed in [10]. By assuming two dancers' motions are precisely synchronized, i.e., $t_k^l = t_k^f = t_k$ for all k, system (8) degenerates into an equivalent discrete LTI system:

$$\boldsymbol{x}(t_{k+1}) = \boldsymbol{H A_d x}(t_k) + \boldsymbol{B_l} v_d^l(t_{k+1}) + \boldsymbol{B_f} v_d^f(t_{k+1}) \tag{12}$$

$\boldsymbol{A_d}$ is the discrete form of $\boldsymbol{A}$ with $\boldsymbol{A_d} = e^{\boldsymbol{A}T_p}$. When v_d^l and v_d^f are constant, exponential stability of system (12) can be straightforwardly examined by checking the spectral radius of $\boldsymbol{HA_d}$ (denoted by $\rho(\boldsymbol{HA_d})$): if $\rho(\boldsymbol{HA_d}) < 1$, the system is stable.

The above method relies on the assumed synchronized motion of the two dancers, while in real applications their timing errors (or synchronization error) usually exist. In this part we will consider timing error as a part of the model and analyze the affected stability.

Consider the leader's and the follower's kth beat moment t_k^l and t_k^f, as shown in Figure. 3. Because it is pHRI in which the follower is a robot, without loss of generality, we can have $t_k^f > t_k^l$ for all k. In another word, we assume the robot has some sensors for detecting t_k^l; the detected moment cannot be exactly the real t_k^l, but by adjusting the time delay, we can keep t_k^f always in the "right" neighborhood of t_k^l, i.e.,

$$0 < t_k^f - t_k^l \triangleq \delta t_k^f \le \overline{\delta t_f}, \forall k \tag{13}$$

where the positive δt_k^f is the follower's error in following the leader's timing, and $\overline{\delta t_f}$ is its upper bound.

Unlike the robot follower, the human leader's motions are synchronized with music beats. Ideally, there should be $t_{k+1}^l - t_k^l = T_p$, but again, due to the inevitable timing error of human, along with the robot's following error, we have

$$-\overline{\delta t_l}/2 \le \delta t_{k+1}^l \triangleq t_{k+1}^l - t_k^f - T_p \le \overline{\delta t_l}/2, \forall k \tag{14}$$

Compared with the previous strong assumption of synchronized motion, the new boundedness assumptions, i.e., $0 < \delta t_k^f \le \overline{\delta t_f}$ and $-\overline{\delta t_l}/2 \le \delta t_k^l \le \overline{\delta t_l}/2$ are reasonably weak: if δt_k^f or δt_k^l is large, it would be very difficult to continue the dance even for two human dancers.

Now we can examine one cycle of the system from the moment t_k^{f+} to t_{k+1}^{f+}. In this cycle the system has four times of transitions, namely

1) From t_k^{f+} to t_{k+1}^{l-}, in which there is no beat moment; system dynamics is continuous;
2) From t_{k+1}^{l-} to t_{k+1}^{l+}, the leader's beat moment, impulsive dynamics;
3) From t_{k+1}^{l+} to t_{k+1}^{f-}, a short period of continuous dynamics;
4) From t_{k+1}^{f-} to t_{k+1}^{f+}, the follower's beat moment, impulsive dynamics.

According to the above sequence of transitions and (8), (13), (14), we can write

$$\begin{aligned} \boldsymbol{x}(t_{k+1}^{f+}) \;=\; & \boldsymbol{H_f} e^{\boldsymbol{A}\delta t_{k+1}^f} \boldsymbol{H_l} e^{\boldsymbol{A}(T_p + \delta t_{k+1}^l)} \boldsymbol{x}(t_k^{f+}) \\ & + \boldsymbol{H_f} e^{\boldsymbol{A}\delta t_{k+1}^f} \boldsymbol{B_l} v_d^l + \boldsymbol{B_f} v_d^f \end{aligned} \tag{15}$$

Similar to (12), (15) can also be viewed as a discrete linear system. Consider its homogeneous form in which $v_d^l = v_d^f = 0$:

$$\boldsymbol{x}(t_{k+1}^{f+}) = \boldsymbol{A_d^*}(\delta t_{k+1}^l, \delta t_{k+1}^f) \boldsymbol{x}(t_k^{f+}) \tag{16}$$

where $\boldsymbol{A_d^*}(\delta t_{k+1}^l, \delta t_{k+1}^f)$ is the system matrix in (15) and its entries depend on the time-varying δt_{k+1}^l and δt_{k+1}^f.

System (12) is stable if $\rho(\boldsymbol{HA_d}) < 1$; however, this criterion is not valid for (16) because it is a time-varying system. A sufficient condition for stability of (16) is quadratic stability, i.e., if we can find a matrix $\boldsymbol{P}$ which is time-invariant, symmetric, and positive definite (denoted by $\boldsymbol{P} > 0$) satisfying

$$\boldsymbol{A_d^{*T}}(\delta t_k^l, \delta t_k^f) \boldsymbol{P} \boldsymbol{A_d^*}(\delta t_k^l, \delta t_k^f) - \boldsymbol{P} < 0$$

for all k, then (16) is quadratically stable. However, this condition is quite strong; in many cases systems that are stable cannot satisfy the condition of quadratic stability; hence, it is necessary to implement a weaker condition,

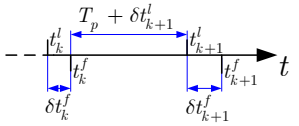

Fig. 3. Timing errors of the leader and the follower

such as one for poly-quadratic stability [14]; to apply the condition, the time-varying matrix $\boldsymbol{A}_{\boldsymbol{d}}^{*}(\delta t_k^l, \delta t_k^f)$ must be converted into a linear matrix polytope form:

$$\boldsymbol{A}_{\boldsymbol{d}}^{*}(\delta t_k^l, \delta t_k^f) = \sum_{i=1}^{N} \xi_i(k) \boldsymbol{A_i} \tag{17}$$

$$\xi_i(k) \geq 0,\ \sum_{i=1}^{N} \xi_i(k) = 1 \tag{18}$$

where in right hand side of (17), the time-varying errors δt_k^l and δt_k^f are only contained in the scalar coefficients $\xi_i(k)$, leaving $\boldsymbol{A_1} \ldots \boldsymbol{A_N}$ a set of constant matrices. Generally, $\boldsymbol{A}_{\boldsymbol{d}}^{*}(\delta t_k^l, \delta t_k^f)$ can hardly be converted into the form like (17) since δt_k^l and δt_k^f both appear in $\boldsymbol{A}_{\boldsymbol{d}}^{*}(\delta t_k^l, \delta t_k^f)$ in nonlinear forms. However, due to the fact that δt_k^l and δt_k^f are very small, we can use the first-order approximation of $\boldsymbol{A}_{\boldsymbol{d}}^{*}(\delta t_k^l, \delta t_k^f)$, which yields:

$$\begin{aligned} \boldsymbol{A}_{\boldsymbol{d}}^{*}(\delta t_k^l, \delta t_k^f) &= \boldsymbol{H_f} e^{\boldsymbol{A}\delta t_k^f} \boldsymbol{H_l} e^{\boldsymbol{A}(T_p + \delta t_k^l)} \\ &\approx \boldsymbol{H_f}(\boldsymbol{I} + \delta t_k^f \boldsymbol{A}) \boldsymbol{H_l} e^{\boldsymbol{A}T_p} (\boldsymbol{I} + \delta t_k^l \boldsymbol{A}) \\ &= \boldsymbol{A_1'} + \delta t_k^l \boldsymbol{A_2'} + \delta t_k^f \boldsymbol{A_3'} + \delta t_k^l \delta t_k^f \boldsymbol{A_4'} \end{aligned} \tag{19}$$

where $\boldsymbol{A_1'} = \boldsymbol{H_f H_l} e^{\boldsymbol{A}T_p}$, $\boldsymbol{A_2'} = \boldsymbol{H_f H_l} e^{\boldsymbol{A}T_p} \boldsymbol{A}$, $\boldsymbol{A_3'} = \boldsymbol{H_f A H_l} e^{\boldsymbol{A}T_p}$, and $\boldsymbol{A_4'} = \boldsymbol{H_f A H_l} e^{\boldsymbol{A}T_p} \boldsymbol{A}$.

By introducing another upper bound $\overline{\delta t_{lf}} = \overline{\delta t_f} \times \overline{\delta t_f}$, which satisfies $-\overline{\delta t_{lf}}/2 \leq \delta t_k^l \delta t_k^f \leq \overline{\delta t_{lf}}/2$, using (13), (14), (19) can be rearranged as

$$\boldsymbol{A}_{\boldsymbol{d}}^{*}(\delta t_k^l, \delta t_k^f) = \sum_{i=1}^{4} \xi_i(k) \boldsymbol{A_i} \tag{20}$$

where

$$\begin{aligned} \boldsymbol{A_1} &= \boldsymbol{A_1'} - \frac{\overline{\delta t_l}}{2} \boldsymbol{A_2'} - \frac{\overline{\delta t_{lf}}}{2} \boldsymbol{A_4'}, \\ & \quad \xi_1(k) = 1 - \xi_2(k) - \xi_3(k) - \xi_4(k) \\ \boldsymbol{A_2} &= \boldsymbol{A_1} + 3\overline{\delta t_l} \boldsymbol{A_2'},\ \xi_2(k) = \frac{\delta t_k^l + \overline{\delta t_l}/2}{3\overline{\delta t_l}} \\ \boldsymbol{A_3} &= \boldsymbol{A_1} + 3\overline{\delta t_f} \boldsymbol{A_3'},\ \xi_3(k) = \frac{\delta t_k^f}{3\overline{\delta t_f}} \\ \boldsymbol{A_4} &= \boldsymbol{A_1} + 3\overline{\delta t_{lf}} \boldsymbol{A_4'},\ \xi_4(k) = \frac{\delta t_k^l \delta t_k^f + \overline{\delta t_{lf}}/2}{3\overline{\delta t_{lf}}} \end{aligned} \tag{21}$$

Equation (20) and (21) satisfy the required form in (17) and (18), now the internal stability can be examined using the condition proposed in [14]: if there exist four symmetric positive definite matrices $\boldsymbol{S_1} \ldots \boldsymbol{S_4} > 0$, and four regular matrices $\boldsymbol{G_1} \ldots \boldsymbol{G_4}$, which satisfy

$$\begin{pmatrix} \boldsymbol{G_i} + \boldsymbol{G_i}^T - \boldsymbol{S_i} & \boldsymbol{G_i}^T \boldsymbol{A_i}^T \\ \boldsymbol{A_i G_i} & \boldsymbol{S_j} \end{pmatrix} > 0 \tag{22}$$

for all $i = 1, \ldots, 4$ and $j = 1, \ldots, 4$, then the system is poly-quadratically stable. The constraints of $\boldsymbol{S_1} \ldots \boldsymbol{S_4} > 0$, along with (22) form twenty linear matrix inequalities (LMIs), whose feasibility can be checked by a standard LMI solver. When $\boldsymbol{A_1} \ldots \boldsymbol{A_4}$ are given, we can gradually find the upper bounds of $\overline{\delta t_l}$ and $\overline{\delta t_f}$ by iteratively changing their values and examining the LMIs' feasibilities.

B. Optimal Interaction

There are numerous objective functions that can be selected to optimize the physical interaction, but it is difficult to find one which is "human-like". Despite the frequently used functions (e.g., minimum joint torque, minimum jerk, etc.) that explain an individual's behavior, determining the objective function in pHHI is still a challenge. Here we use the minimum interaction force as our goal of optimization. This objective has been adopted in many pHRI applications where it is named as "transparency" [15]. Therefore, from the robot follower's point of view, the task of optimal interaction is as follows:

At moment t_k^{f-}, the robot collects all necessary information (e.g., $x_l(t_k^{f-})$, $\dot{x}_l(t_k^{f-})$, etc.) to generate an optimal $x_f(t_k^{f+})$, with which the accumulated interaction force $\int_{t_k^{f+}}^{t_{k+1}^{l-}} f^2(t)dt$ can be minimized. However, as the robot cannot predict the exact t_{k+1}^l which is up to the human, while $f(t)$ is continuous on t and δt_{k+1}^l is small, finally the objective function to be minimized is

$$\begin{aligned} F &= \int_{t_k^{f+}}^{t_k^{f+}+T_p} f^2(t)dt = \int_{t_k^{f+}}^{t_k^{f+}+T_p} \boldsymbol{x}^T(t) \boldsymbol{c}^T \boldsymbol{c} \boldsymbol{x}(t)dt \\ &= \boldsymbol{x}^T(t_k^{f+}) \left(\int_0^{T_p} (e^{\boldsymbol{A}t})^T \boldsymbol{c}^T \boldsymbol{c} e^{\boldsymbol{A}t} dt \right) \boldsymbol{x}(t_k^{f+}) \\ &= \boldsymbol{x}^T(t_k^{f+}) \boldsymbol{Q} \boldsymbol{x}(t_k^{f+}) \end{aligned} \tag{23}$$

which is the same with the problem given previously [10]. However, in [10], as the robot could not access $\boldsymbol{x}(t_k^{f-})$, we had to used the gradient descent of F and v_d^f. In contrast, now we assume all states in $\boldsymbol{x}(t_k^{f-})$ are accessible, while the goal is to find a $x_f(t_k^{f+})$ that minimizes F.

Function (23) only contains one variable $x_f(t_k^{f+})$ (hereafter x_f is used for short). Let Q_{ij} be $\boldsymbol{Q}$'s entry on row i and column j, x_i be the ith component of $\boldsymbol{x}$ (hence $x_3 = x_f$), (23) can be written as a simple quadratic function of x_f

$$\begin{aligned} F &= a_2 x_f^2 + a_1 x_f + a_0 \\ a_2 &= Q_{33} \\ a_1 &= 2[Q_{31}, Q_{32}, 0, Q_{34}, Q_{35}]\boldsymbol{x} = \boldsymbol{\eta x} \end{aligned} \tag{24}$$

F is minimized if $x_f = -\boldsymbol{\eta x}/(2a_2)$. Since $\boldsymbol{Q}$ is assumed to be time-invariant, a_1 and a_2 can be obtained off-line, making the on-line calculation of x_f quite simple. However, as k_c and d_c in (9) are unknown, as well as the errors $\boldsymbol{\delta x}$ contained in the measured $\boldsymbol{x}$, the calculated x_f is not the real system's optimal value: $x_f^* = -\boldsymbol{\eta}^* \boldsymbol{x}^*/(2a_2^*)$, the error is

$$\begin{aligned} e_{x_f} &= x_f - x_f^* = \left(\frac{\boldsymbol{\eta}^*}{2a_2^*} - \frac{\boldsymbol{\eta}}{2a_2} \right) \boldsymbol{x^*} - \frac{\boldsymbol{\eta}}{2a_2} \boldsymbol{\delta x} \\ &\leq |\frac{\boldsymbol{\eta}^*}{2a_2^*} - \frac{\boldsymbol{\eta}}{2a_2}| |\boldsymbol{x}^*|_{\max} + |\frac{\boldsymbol{\eta}}{2a_2}| |\boldsymbol{\delta x}|_{\max} = \overline{e_{x_f}} \end{aligned} \tag{25}$$

where the absolute value of a vector $\boldsymbol{y}$ is define as $|\boldsymbol{y}| = [|y_1|, \ldots, |y_n|]^T$, and $|\boldsymbol{y}|_{\max} = [|y_1|_{\max}, \ldots, |y_n|_{\max}]^T$. Error of F is

$$e_F = a_2 e_{x_f}^2 \leq a_2 \overline{e_{x_f}}^2 = \overline{e_F} \tag{26}$$

According to (3), x_f and v_d^f are related, which yields

$$v_d^f = \frac{S_f}{\tau_f}\left(x_f + \frac{\tau_f C_f}{S_f}\dot{x}_f\right) = \boldsymbol{g}\boldsymbol{x}$$
$$\boldsymbol{g} = -\frac{S_f}{\tau_f}\left[\frac{Q_{31}}{a_2}, \frac{Q_{32}}{a_2}, 0, \frac{Q_{34}}{a_2} - \frac{\tau_f C_f}{S_f}, \frac{Q_{35}}{a_2}\right] \quad (27)$$

Equation (27) reveals that minimizing the interaction force is equivalent to using state feedback with a proper gain $\boldsymbol{g}$. From (15) and (27) we have

$$\boldsymbol{x}(t_{k+1}^{f+}) = (\boldsymbol{H_f} + \boldsymbol{B_f g})e^{\boldsymbol{A}\delta t_{k+1}^f}\boldsymbol{H_l}e^{\boldsymbol{A}(T_p+\delta t_{k+1}^l)}\boldsymbol{x}(t_k^{f+}) + (\boldsymbol{H_f} + \boldsymbol{B_f g})e^{\boldsymbol{A}\delta t_{k+1}^f}\boldsymbol{B_l}v_d^l \quad (28)$$

With the introduced state feedback, stability of the system will be affected; therefore, the poly-quadratic stability should be re-evaluated by using the LMIs in (22).

IV. Simulation and Experiment

A. Simulation

Parameters of simulation are as follows: for the leader dancer, $m_l = 70\,\mathrm{kg}$, $z_l = 1.1\,\mathrm{m}$; for the follower, $m_f = 45\,\mathrm{kg}$, $z_f = 0.9\,\mathrm{m}$, and the nominal period of beat moments is $T_p = 0.75\,\mathrm{s}$.

On poly-quadratic stability, two sets of dancers' upper bounds of timing errors have been tested for different combinations of k_c and d_c, as shown in Figure. 4. As expected, smaller $\overline{\delta t_l}$ and $\overline{\delta t_f}$ lead to larger stable region of k_c and d_c.

On optimal interaction, $\boldsymbol{Q}$ is obtained by using $k_c = 60\,\mathrm{N/m}$ and $d_c = 25\,\mathrm{Ns/m}$. Here we set $|\boldsymbol{x}^*|_{\max} = [0.5, 1.5, 0, 1.5, 0.3]^T$ and $|\boldsymbol{\delta x}|_{\max} = [0.1, 0.1, 0, 0, 0.05]^T$; the contours of $\overline{e_{x_f}}$ and $\sqrt{\overline{e_F}}$, which are caused by the differences between k_c, d_c's nominal and real values, are given in Figure. 5. Notice that $\overline{e_{x_f}}$ and $\sqrt{\overline{e_F}}$ are non-zero even k_c, d_c are the same with their nominal values, suggesting that both error bounds are somehow loose.

The interactions between two LIPMs are simulated, while the leader is supposed to have time-varying desired velocities $v_d^l(t_k^l)$. The "dance" starts from $t_1^l \approx 0.75\,\mathrm{s}$, while $\{v_d^l(t_k^l)\} = (1.1, 0.3, 0.1, 1.1, 0.3, 0.1, 1.1, 0.3, 0.1)\mathrm{m/s}$ for $k = 2, \ldots, 10$. Non-optimal interactions, in which the follower keeps a constant, predefined $v_d^f = 0.6\,\mathrm{m/s}$, are compared with optimal interactions in which v_d^f is obtained

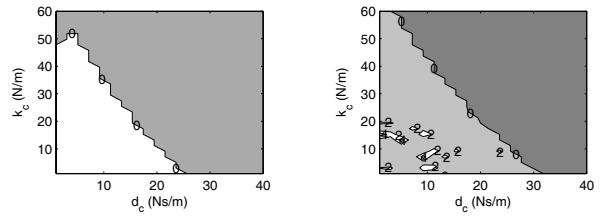

(a) $\overline{\delta t_l} = 0.1\,\mathrm{s}$, $\overline{\delta t_f} = 0.1\,\mathrm{s}$ (b) $\overline{\delta t_l} = 0.08\,\mathrm{s}$, $\overline{\delta t_f} = 0.05\,\mathrm{s}$

Fig. 4. Contours of poly-quadratic stability with respect to k_c and d_c; light-colored area inside the 0 border corresponds to poly-quadratically stable combinations of k_c and d_c

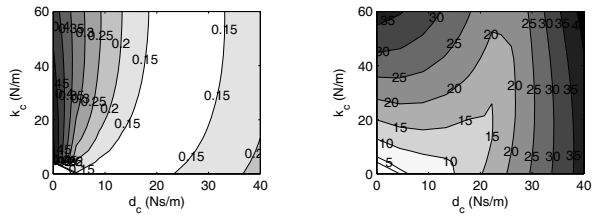

(a) $\overline{e_{x_f}}$ (b) $\sqrt{\overline{e_F}}$

Fig. 5. Contours of $\overline{e_{x_f}}$ and $\sqrt{\overline{e_F}}$ with respect to k_c and d_c, whose nominal values are chosen as $k_c = 60\,\mathrm{N/m}$ and $d_c = 25\,\mathrm{Ns/m}$

by using (27); results are given in Figure. 6; we can see that the optimal interaction with reduced force can be achieved by using (27); this method is also insensitive to timing errors and time-varying k_c, d_c, which were not considered when we analyzed the stability in Section III-A. Since poly-quadratic stability is a subset of stability, it is possible that systems do not satisfy (22) can still be stable. Trajectory generated by LIPM and the real human dancer have been compared in [9].

After introducing the state feedback, the stability of the system is re-evaluated, the contours are shown in Figure. 7. Compared with Figure. 4, it can be observed that proper feedback gains may lead to the increased area of stable region.

For the case of Figure. 6(c), the calculated $\{v_d^f(t_k^f)\}$ are $(0.3, 0.2, 1.1, 0.4, 0.1, 1.2, 0.3, 0.1)\mathrm{m/s}$ for $k = 3, \ldots, 10$, which are very close to $\{v_d^l(t_k^l)\}$. This matches the intuition that in a "good" pHRI, human's and robot's desired velocities should be almost the same. However, when the measurement error $\boldsymbol{\delta x}$ is included in the simulation, the error is amplified, causing $\{v_d^f(t_k^f)\}$ seriously deviate from $\{v_d^l(t_k^l)\}$, and consequently large interaction force, as shown in Figure. 8.

Because the feedback gain $\boldsymbol{g} = [14.3, 4.8, 0, 0.2, -0.1]$, the measurement noise on x_l will be amplified by about fourteen times. At the same time, this error can hardly be decreased as human's pivot point can be located anywhere inside the support polygon. Due to the above facts, the method given in (27) cannot be implemented in experiments. In essence, this large amplification is the result of LIPM's intrinsic instability: very small differences in initial conditions will increase exponentially during one step. In contrast, a human dancer is empirically less sensitive to the initial conditions. Therefore, in pHRI experiment, if we can find another $\boldsymbol{g}$ which can also approximate $\{v_d^l(t_k^l)\}$ while having a small gain on x_l, we will have an alternative solution of optimal interaction.

B. Experiment

To evaluate the analysis in Section III and find alternative feedback gains for optimal interaction, a robot follower is used in pHRI experiment. This robot is the same mobile robot as appeared in [8], [10], except that two LRFs (laser range finders, Hokuyo UBG-04LX-F01) are now installed to detect human dancer's states, as shown in Figure. 9.

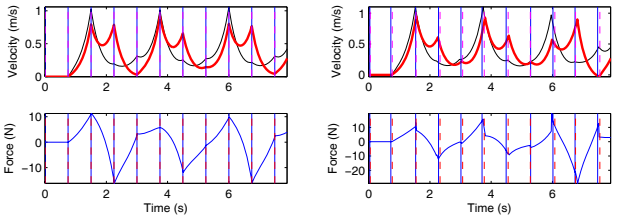

(a) $v_d^f = 0.6\,\mathrm{m/s}$, no timing error, k_c and d_c are known; $F = 35.1$

(b) $v_d^f = 0.6\,\mathrm{m/s}$, with unknown, time-varying k_c and d_c, and timing error; $F = 48.2$

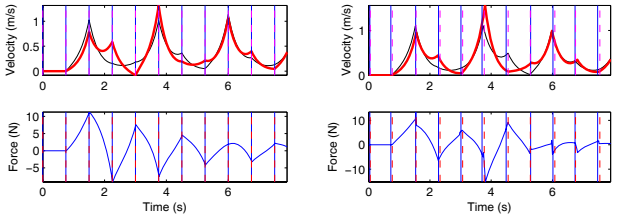

(c) Optimal v_d^f, no timing error, k_c and d_c are known; $F = 12.8$

(d) Optimal v_d^f, with unknown, time-varying k_c and d_c, and timing error; $F = 14.0$

Fig. 6. Results of simulated two-LIPM interaction; thin and thick curves in velocity plots are the leader's and the follower's CoM velocities; vertical solid and dashed lines are the leader's and the follower's beat moments. Timing errors and time-varying k_c and d_c are included in (b) and (d), with $\overline{\delta t_l} = 0.1$, $\overline{\delta t_f} = 0.08$, $20 \le k_c \le 60$, and $10 \le d_c \le 40$

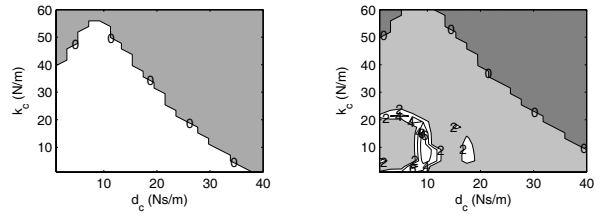

(a) $\overline{\delta t_l} = 0.1\,\mathrm{s}$, $\overline{\delta t_f} = 0.1\,\mathrm{s}$

(b) $\overline{\delta t_l} = 0.08\,\mathrm{s}$, $\overline{\delta t_f} = 0.05\,\mathrm{s}$

Fig. 7. Contours of poly-quadratic stability after state feedback is introduced

One LRF is used to detect human leader's waist and the other is for the ankles. Because the environment is quite simple (human's waist and ankles are the only clusters that appear within the $1.5\,\mathrm{m}$ range), the detection algorithm is straightforward and will not be discussed here. After the three clusters (waist, left ankle and right ankle) are identified, their mean values, which are denoted by l_w (waist), l_l (left ankle) and l_r (right ankle) are used for later stages.

The information needed is human leader's beat moments, x_l, and $\dot{x}_l$ (x_f and $\dot{x}_f$ are robot's states, which can be obtained with ease). The beat moments can be inferred by detecting feet landing using a set of criteria, taking the left foot for example, left foot landings occur at moment t' if:

1) $\max_{(t'-0.6<t<t')} |\dot{l}_l(t)| > 0.5\,\mathrm{m/s}$
2) $|\dot{l}_l(t')| < v_{\text{thres}}$
3) $l_l(t') < 0.5\,\mathrm{m}$
4) $\min_{(t'-0.3<t<t')} |\dot{l}_l(t)| > v_{\text{thres}}$

are all satisfied. v_{thres} is a threshold used for adjusting the

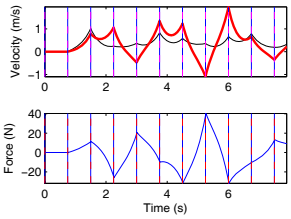

Fig. 8. Introduced measurement error causes large interaction force, $F = 180.0$; $|\boldsymbol{\delta x}|_{\max} = [0.1, 0.1, 0, 0, 0.05]^T$

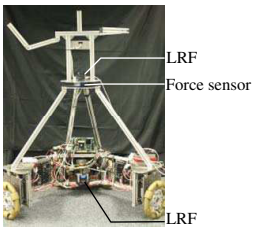

Fig. 9. Robot used in experiment

robot's delay δt_k^f. In experiment $v_{\text{thres}} = 0.3\,\mathrm{m/s}$ and the corresponding delay is about $0.05\,\mathrm{s}$

$\dot{x}_l$ can easily be acquired by using $\dot{x}_l = \dot{x}_f - \dot{l}_w$, while to get x_l, additional procedures are needed. x_l is defined as the human dancer's CoM position with respect to the pivot position; hence firstly we need to know which leg is the support leg. This is done by using the feet landing information, e.g., after left foot landing and before right foot landing, the ankle position of the pivot leg is $l_p = l_l$.

It should be noticed that l_w and l_p are just mean values of clustered points on human's surface; an unknown bias must be considered. x_l is actually $x_l = l_p - l_w - l_{\text{bias}}$. To obtain l_{bias}, the human dancer stands still for several seconds while l_w and l_p are being sampled; assuming $x_l = 0$, l_{bias} is then calculated and averaged over time.

At first, the human leader's independent moves, in which the leader and the robot follower are not in physical contact, are recorded. Assuming the leader's desired velocity at t_{k+1}^l can be estimated by a linear combination of $x_l(t_k^l)$ and $\dot{x}_l(t_k^l)$, i.e., $v_d^l(t_{k+1}^l) = g_1 x_l(t_k^l) + g_2 \dot{x}_l(t_k^l)$, by using least squares for data regression, we have $g_1 \approx 3.65$ and $g_2 \approx 1.90$. Therefore the gain used in experiment is

$$\boldsymbol{g} = [3.65, 1.90, 0, 0, 0] \tag{29}$$

Figure. 10 shows the recorded data in the leader's independent moves. We can see that the predicted v_d^l (danshed curve) can well match the real velocities at beat moments.

Finally, three cases of pHRI, namely damping mode (in which the robot acts as a free mass with ground friction), constant v_d^f mode (where v_d^f is set to $0.6\,\mathrm{m/s}$), and variable v_d^f mode (in which v_d^f is given by (27) and (29)), have been tested and compared. To generate repeatable trials for comparison (rather than restricting human to "fit" the proposed model), a row of markers are attached to the floor; the human leader is asked to land his toe on the markers during walking. To generate time-varying v_d^l, the markers

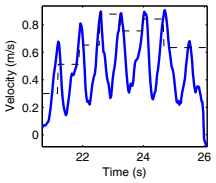

Fig. 10. Human leader's velocity when walking without physical contact with the robot follower; the thick solid curve is $\dot{x}_l$, and the dashed curve is the calculated v_d^l

are not evenly spaced; their positions from the origin are $(0.44, 0.77, 1.05, 1.66, 2.22, 2.54)\mathrm{m}$. The interaction is ended after the sixth step.

Results of the three experiments are shown in Figure. 11. As expected, Figure. 11(a) has largest F since the robot is totally passive. Figure. 11(b) performs well at the beginning but leads to large F at the fourth step. In contrast, in Figure. 11(c), v_d^f can follow v_d^l and hence effectively reduce F; our proposed approach is therefore supported by the comparison. At the same time, although the empirical gains in (29) work well for one subject (the author), as they are the regression result of the many trials on the same human leader, they might be unsuitable for other subjects. This is the limitation of the empirical-gain based method.

V. Conclusions and Future Work

In this paper, we first introduced a spring-damper connected, two-LIPM model for describing two human dancers' body dynamics in sagittal plane. Because timing errors of two dancers are inevitable, we considered the effects of timing errors and analyzed the poly-quadratic stability of the system. A state-feedback-based approach was proposed to minimize the interaction force; because the feedback gain obtained from quadratic optimization can strongly amplify the measurement noise in simulation, an alternative set of gains were used and validated by experiments.

However, the gain obtained in experiments relies much on empirical data rather than a thorough analysis. At the same time, the current model only considers translational motions in one plane, leaving rotational motions (body spins and turns) unstudied. These issues will be included in our future work.

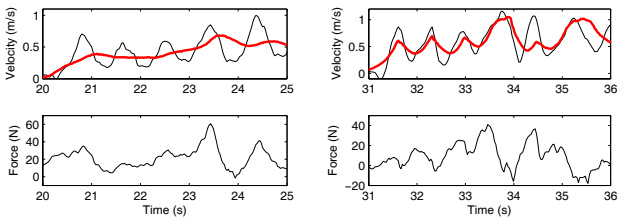

(a) Damping mode, $F \approx 547$ (b) Constant v_d^f mode $(0.6\,\mathrm{m/s})$, $F \approx 217$

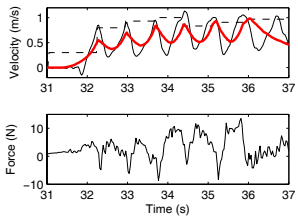

(c) Variable v_d^f mode, $F \approx 29$

Fig. 11. Results of three cases of pHRI; thin and thick solid curves in velocity plots are the leader's and the follower's CoM velocities; dashed curve in (c) is the calculated v_d^f; the pHRI ends after the sixth step

VI. Acknowledgment

This work was supported by the Asian Office of Aerospace Research and Development (AOARD), Air Force Office of Scientific Research (AFOSR) under grant number FA2386-10-1-4126.

References

[1] N. Stefanov, A. Peer, and M. Buss, "Online intention recognition for computer-assisted teleoperation," *Proceedings of the 2010 IEEE International Conference on Robotics and Automation (ICRA)*, pp. 5334–5339, 2010.

[2] V. Duchaine and C. Gosselin, "Safe, stable and intuitive control for physical human-robot interaction," *Proceedings of the 2009 IEEE International Conference on Robotics and Automation (ICRA)*, pp. 3383–3388, 2009.

[3] Z. Wang, A. Peer, and M. Buss, "An HMM approach to realistic haptic human-robot interaction," *EuroHaptics conference, 2009 and Symposium on Haptic Interfaces for Virtual Environment and Teleoperator Systems. World Haptics 2009. Third Joint*, pp. 374–379, 2009.

[4] H. Kazerooni, "Human/robot interaction via the transfer of power and information signals," *IEEE Transactions on System, Man, and Cypernetics*, vol. 20, no. 2, pp. 450–463, 1990.

[5] S. Buerger and N. Hogan, "Complementary stability and loop shaping for improved human-robot interaction," *IEEE Transactions on Robotics*, vol. 23, no. 2, pp. 232 –244, 2007.

[6] S. Sirouspour, "Robust control design for cooperative teleoperation," *Proceedings of the 2005 IEEE International Conference on Robotics and Automation (ICRA)*, pp. 1133–1138, 2005.

[7] T. Takeda, Y. Hirata, and K. Kosuge, "Dance step estimation method based on HMM for dance partner robot," *IEEE Transactions on Industrial Electronics*, vol. 54, no. 2, pp. 699–706, 2007.

[8] ——, "Dance partner robot cooperative motion generation with adjustable length of dance step stride based on physical interaction," *Proceedings of the 2007 IEEE/RSJ International Conference on Intelligent Robots and Systems (IROS)*, pp. 3258–3263, 2007.

[9] H. Wang and K. Kosuge, "An inverted pendulum model for reproducing human's body dynamics in waltz and its applications in a dance partner robot," *Proceedings of the 2010 IEEE/SICE International Symposium on System Integration*, pp. 182–187, 2010.

[10] ——, "Towards an understanding of dancers' coupled body dynamics for waltz," *Proceedings of the 2011 IEEE/RSJ International Conference on Intelligent Robots and Systems (IROS)*, pp. 2008–2013, 2011.

[11] J. Holldampf, A. Peer, and M. Buss, "Virtual partner for a haptic interaction task," *Human Centered Robot Systems: Cognition, Interaction, Technology*, vol. 6, p. 183, 2010.

[12] K. B. Reed, J. Patton, and M. Peshkin, "Replicating Human-Human Physical Interaction," *Proceedings of the 2007 IEEE International Conference on Robotics and Automation (ICRA)*, pp. 3615–3620, 2007.

[13] S. Kajita and K. Tani, "Study of dynamic biped locomotion on rugged terrain—theory and basic experiment," *Advanced Robotics, 1991. 'Robots in Unstructured Environments', 91 ICAR., Fifth International Conference on*, pp. 741–746 vol.1, 1991.

[14] J. Daafouz and J. Bernussou, "Parameter dependent lyapunov functions for discrete time systems with time varying parametric uncertainties," *Systems & Control Letters*, vol. 43, no. 5, pp. 355–359, 2001.

[15] N. Jarrassé, J. Paik, V. Pasqui, and G. Morel, "How can human motion prediction increase transparency?" in *Proceedings of the 2008 IEEE International Conference on Robotics and Automation (ICRA)*, 2008, pp. 2134–2139.

2011 IEEE/RSJ International Conference on
Intelligent Robots and Systems
September 25-30, 2011. San Francisco, CA, USA

Towards an Understanding of Dancers' Coupled Body Dynamics for Waltz

Hongbo Wang and Kazuhiro Kosuge

Abstract— **In this paper, we study two dancers' coupled body dynamics when dancing a waltz. A linear inverted pendulum (LIPM) model for biped locomotion is utilized as each dancer's dynamic model, and a balance controller for each dynamic model is introduced. A pair of dancers are then modeled as two spring-damper-connected LIPMs with their respective controllers. Assuming a perfect rhythmic and synchronized motion, we analyze the stability of the physical interaction. Stable interaction with minimal interaction force is used as the criterion for optimal interaction, which is transformed into a quadratic programming problem and solved by gradient descent. Simulations and experiments show the proposed approach for analysis of the coupled dynamics is reasonable.**

Index Terms— **Physical human-robot interaction, dance partner robot, linear inverted pendulum, optimal physical interaction.**

I. Introduction

In human-involved physical interactions, such as pHHI and pHRI (physical human-human/robot interaction), many human capabilities and characteristics for haptic communication, body coordination, etc., are observed. Understanding the interactions helps designing a robot that physically interacts with a person in more intuitive ways, and many related investigations have been directed. On the one hand, because the interactions involve at least two independent entities, some research concentrates on how intentions are conveyed and how motion coordination is established [1]–[3]; on the other hand, since physical interaction is the result of two (or more) systems' coupled dynamics, another category of investigations focus on studying the human-involved dynamics [4]–[6]. We may categorize the interactions into two levels: intention communication as the higher level, and coupled body dynamics as the lower level. In this paper, we consider the coupled body dynamics during dancing.

Generally we assume that a human's motion has repeatability and predictability under specific circumstances, i.e., there is an assumed human model. An ideal human model would be the exact model of a human's body dynamics; however, due to the complexity of human's body dynamics, the random factors contained in a human's motion, and the unknown control method that human is using, the exact model is still beyond our knowledge. In practice, the human model is usually obtained with some assumptions and simplifications. For instance, a linear mass-spring-damper model could be used to model an operator's arm in interaction with a master [7]; features of the coupled body dynamics in a specific task may be implicitly included in an updated probability density function [6], etc.

The authors are with the Department of Bioengineering and Robotics, Tohoku University, 6-6-01, Aoba, Aramaki, Aoba-ku, Sendai 980-8579, Japan {h_wang, kosuge}@irs.mech.tohoku.ac.jp

Waltz is a typical example of pHHI. The goal of this research is to replicate the pHHI in pHRI by developing a dance partner robot which plays a role of the female dancer. Since the higher level interaction, i.e., the intention communication in waltz has been studied in [8]; our current focus of this paper is the lower level interaction of the two dancer's body dynamics. In one previous work [9], we assume that a human dancer's model contains one parameter—stride length. The robot is able to learn this parameter from trials and use it to scale the robot's pre-recorded trajectories. To deal with variability and randomness in human's motions, the robot was modeled as an inertial mass, trying to follow a predefined trajectory while being affected by external force/torque and ground friction. This approach is effective in experiments, but its core idea relies on more empirical knowledge than a quantitative analysis of the system. And some important characteristics of the lower level interaction may still be hidden. This motivates us to model the two dancers' body dynamics, analyze the physical interaction quantitatively, and implement the acquired knowledge in the dance partner robot.

A simplified model of human's dynamics in walking is the linear inverted pendulum (LIPM) model [10], [11]. Since waltz is different from normal walking and there is no accuracy requirement on the vertical motions of CoM (Center of Mass), the LIPM model is able to reproduce human's motions in some elementary waltz steps [12]. We focus on the elementary steps because they serve as simple cases to start with: elementary steps like closed changes involve no spin or turn, the CoM motions can be decomposed into two independent and one-dimensional motions.

In Section II, we use LIPM as the simplified model for dancer's body dynamics and design a balancing controller for the LIPM. In Section III, the two coupled dancers are modeled as two connected LIPMs and their dynamics are analyzed with some assumptions on motion synchronization. In Section IV, simulation and experiment results are shown. Conclusion is given in Section V.

II. Model of A Single Dancer With Proposed Balance Controller

A. The Simplified Human Body Dynamics Model

Consider a simplified human body model in sagittal plane with a massless leg, as shown in Fig. 1(a). By introducing some constraints, we can obtain an inverted pendulum

978-1-61284-456-5/11/$26.00 ©2011 IEEE

(LIPM) model with linear dynamics and one DOF along x-axis [10].

$$\ddot{x} = (g/z)x + (1/(mz))u_{\text{ank}} \tag{1}$$

where x is the position of CoM with respect to LIPM's pivot point, g is the gravity acceleration, m is the mass of the body, and u_{ank} is the torque input to the ankle.

B. Balance Controllers

LIPM is intrinsically unstable; a balance controller is necessary. The orbital-energy-based controller [10] keeps LIPM on the desired energy level; while another controller [11] tries to have the LIPM reach desired position/velocity at a desired moment by using optimization. The third controller in [12] has LIPM to follow a series of desired velocities. In the following we will briefly introduce the above controllers.

Let $\{t_k\}$ be a set of moments when the pivot position (i.e., position of the LIPM's pivot point) changes. When $t_k < t < t_{k+1}$, and if $u_{\text{ank}}(t) = 0$, the orbital energy [10] is constant throughout the motion. This can be written as:

$$E = -(mg)/(2z)x^2 + (m/2)\dot{x}^2 \tag{2}$$

Assume that $\dot{x}$ does not vary before and after t_k (this is denoted by $\dot{x}^+ = \dot{x}^-$), the controller can have the LIPM stay at a desired energy level by choosing a new pivot position. However, since the relationship between desired trajectory and orbital energy is implicit, this controller is inconvenient for trajectory planning and may cause problems like limping.

In waltz, pivot positions are being changed periodically, synchronized with music beats. Assuming this period is T, an alternative controller can be derived by solving (1):

$$\begin{pmatrix} x(kT+T) \\ \dot{x}(kT+T) \end{pmatrix} = \begin{pmatrix} C & \tau S \\ S/\tau & C \end{pmatrix} \begin{pmatrix} x(kT) \\ \dot{x}(kT) \end{pmatrix} \tag{3}$$

where $\tau = \sqrt{z/g}$, $C = \cosh(T/\tau)$, $S = \sinh(T/\tau)$.

Theoretically, $x(kT)$, which is the CoM's relative position from the pivot point, can easily be calculated when desired $x(kT+T)$ and $\dot{x}(kT+T)$ are given; however, the square matrix in (3) is ill-conditioned. One approach is minimizing a defined error norm [11]; another one is to only guarantee $\dot{x}(kT+T)$:

$$x^+ = -(\tau C/S)\dot{x}(kT) + (\tau/S)v_d(k+1) \tag{4}$$

where $v_d(k+1) = \dot{x}(kT+T)$ and hereafter we will use $v_d(k)$ to denote the desired velocities at $t \in \{t_k\}$. The above two controllers are convenient for use, since the desired position, velocity, and time are explicitly included; however, their stabilities are difficult to prove. In the following we will extend the previously proposed controllers.

(a) Simplified human model (b) Linear inverted pendulum

Fig. 1. Simplification of body dynamics

C. The Proposed Controller

Assume that the pivot position of an LIPM can change instantaneously without a double support phase (where both legs touch the ground), the system can be considered as a hybrid dynamical system with impulsive effects [13]. Let x be the CoM position with respect to the pivot position and $\boldsymbol{x} = [x, \dot{x}]^T$, we have

$$\begin{cases} \dot{\boldsymbol{x}} &= \boldsymbol{A_s}\boldsymbol{x} + \boldsymbol{B_s}u_{\text{ank}},\ t \neq t_k \\ \boldsymbol{x}^+ &= \boldsymbol{h_k}(\boldsymbol{x}^-),\ t = t_k \end{cases} \tag{5}$$

where $\boldsymbol{x}^-$, $\boldsymbol{x}^+$ are the state vectors before and after t_k. Our goal is to find a function $\boldsymbol{h_k}$ which can balance the LIPM while keeping it following desired velocities; u_{ank} is only used for rejecting disturbances.

Given a series of desired velocities $\{v_d(k)\}$ at $\{t_k\}$ and define an orbital energy function $E(q_1, q_2)$ as

$$E_o(q_1, q_2) = -(mg)/(2z)q_1^2 + (m/2)q_2^2 \tag{6}$$

The desired orbital energy at $t = t_k^+$ is

$$E_d = E_o(x_d, v_d(k)) \tag{7}$$

where

$$x_d = -(\tau C/S)v_d(k) + (\tau/S)v_d(k+1) \tag{8}$$

Equation (8) looks like (4). However, $v_d(k)$ is used to approximate $\dot{x}(kT)$, since E_d should be independent of system's states, .

In contrast, the energy corresponding to (4) is

$$E^\star = E_o(x^\star, \dot{x}) \tag{9}$$

where $x^\star$ is obtained from (4).

Energy at $t = t_k^-$ is

$$E^- = E_o(x, \dot{x}) \tag{10}$$

Here we define a scalar α, with

$$\alpha = \text{sat}\left((E_d - E^\star)/(E_d - E^-)\right) \tag{11}$$

where $\text{sat}(q)$ is saturation function: $\text{sat}(q) = q$ if $|q| \leq 1$, $\text{sat}(q) = 1$ if $q > 1$, and $\text{sat}(q) = -1$ if $q < -1$.

In our proposed method, the desired energy at t_k^+ is

$$E^+ = \alpha E^- + (1-\alpha)E_d \tag{12}$$

Therefore, we have

$$x^+ = \text{sign}(x_d)\sqrt{(z/g)\dot{x}^2 - 2z/(mg)E^+} \tag{13}$$

which is the output of $\boldsymbol{h_k}$ in (5).

When $t \notin \{t_k\}$, u_{ank} is controlled to satisfy

$$u_{\text{ank}}(t) = -K_u mz\left(E_o(x, \dot{x}) - E_d\right)\dot{x} \tag{14}$$

where K_u is a positive gain.

Since $\{v_d(k)\}$ explicitly defines the desired trajectory, the controller described in (7)–(14) is easier to use than a pure energy controller. Now we need examine its stability.

Choose a scalar function:

$$V(\boldsymbol{x},t) = \left(E(\boldsymbol{x},t) - E_d\right)^2 \geq 0 \tag{15}$$

When $t = t_k$, we have

$$\begin{aligned} & V(\boldsymbol{x}^+, t_k^+) - V(\boldsymbol{x}^-, t_k^-) \\ = \;& (\alpha^2 - 1)(E^- - E_d)^2 \leq 0 \end{aligned} \tag{16}$$

When $t \neq t_k$,

$$dV/dt = -2K_u m \left(E(\boldsymbol{x},t) - E_d\right)^2 \dot{x}^2 \leq 0 \tag{17}$$

Then the trajectory defined by $E(\boldsymbol{x},t) = E_d$ is an asymptotically stable invariant set. Given constant $v_d(k) = v_d$, if $t_{k+1} - t_k = T$ for any k and if $v_d(m)$ can be reached at t_m, then when $t > t_m$, the intersection of the invariant set and $\dot{x} = v_d$ is a stable equilibrium point of a Poincaré return map (*Theorem 1*, [14]).

The proposed controller can be graphically interpreted by Fig. 2. When $t = t_k^+$, the energy level of E^+ is restricted by $2E_d - E^-$ and E^-, which is the area between the two solid lines in Fig. 2. If $E^\star$ is within this area (as $E_1^\star$), the controller is equivalent to (4); if $E^\star$ lies outside (as $E_2^\star$), then it can be considered as a better energy controller (since $2E_d - E^-$ is closer to $E_2^\star$ than E_d).

III. Model and Analysis of Two Dancers With Physical Connection

A. Two Dancers Having Physical Interaction: Connected LIPMs

In waltz, two dancers are physically connected by the dance frame. We assume that this system can be represented by a pair of LIPMs connected by a spring and a damper, as shown in Fig. 3. Let x_1^g and x_2^g be the CoM positions of the two LIPMs, and p_1 and p_2 be their pivot positions, all with respect to the global frame. Consider the case when $t = 0$, $p_1 - p_2 = d_0$ where $-d_0$ is also the natural length of the spring. The state vector $\boldsymbol{x}$ is defined as

$$\boldsymbol{x} = [x_1, \dot{x}_1, x_2, \dot{x}_2, w]^T \tag{18}$$

where $x_1 = x_1^g - p_1$, $x_2 = x_2^g - p_2$, and $w = p_1 - p_2 - d_0$.

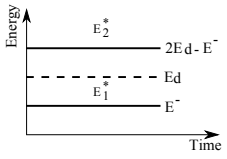

Fig. 2. Illustration of the proposed controller

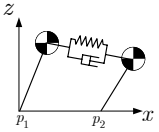

Fig. 3. The dancers' model: two LIPM connected by spring and damper

Suppose $u_{\text{ank}} = 0$ for both dancers, The dynamics of the connected LIPM pair is

$$\dot{\boldsymbol{x}} = \boldsymbol{A}\boldsymbol{x}, t \neq t_k \tag{19}$$

with

$$\boldsymbol{A} = \begin{pmatrix} 0 & 1 & 0 & 0 & 0 \\ \frac{-k_c}{m_1} + \frac{g}{z_1} & \frac{-d_c}{m_1} & \frac{k_c}{m_1} & \frac{d_c}{m_1} & \frac{-k_c}{m_1} \\ 0 & 0 & 0 & 1 & 0 \\ \frac{k_c}{m_2} & \frac{d_c}{m_2} & \frac{-k_c}{m_2} + \frac{g}{z_2} & \frac{-d_c}{m_2} & \frac{k_c}{m_2} \\ 0 & 0 & 0 & 0 & 0 \end{pmatrix} \tag{20}$$

where m_1, m_2, z_1 and z_2 are masses and heights of two LIPMs, g is the gravitational constant, and k_c, d_c are spring and damping constants of the connection.

Two assumptions are made here:

1) For two given LIPMs, $\boldsymbol{A}$ is a constant matrix, i.e., m_1, m_2, z_1, z_2, k_c, and d_c are all constant values.
2) Pivot positions change synchronously, and $t_{k+1} - t_k = T$ for all k.

With an additional assumption that $E^\star$ in (9) is between E^- and $2E_d - E^-$, the proposed controller becomes equivalent to the controller in (4). Although this assumption cannot always hold, later in Section IV we can show that this simplification is reasonable.

With the above assumptions, the system dynamics at $t = t_k$ is

$$\boldsymbol{x}^+ = \boldsymbol{N}\boldsymbol{x}^- + \boldsymbol{u},\ t = t_k \tag{21}$$

$\boldsymbol{N}$ is

$$\boldsymbol{N} = \begin{pmatrix} 0 & -\frac{\tau_1 C_1}{S_1} & 0 & 0 & 0 \\ 0 & 1 & 0 & 0 & 0 \\ 0 & 0 & 0 & -\frac{\tau_2 C_2}{S_2} & 0 \\ 0 & 0 & 0 & 1 & 0 \\ 1 & \frac{\tau_1 C_1}{S_1} & -1 & -\frac{\tau_2 C_2}{S_2} & 1 \end{pmatrix} \tag{22}$$

where τ_1, τ_2, C_1, C_2, S_1 and S_2 are defined similarly as those in (3). And

$$\boldsymbol{u} = [\frac{\tau_1}{S_1} v_{d_1}, 0, \frac{\tau_2}{S_2} v_{d_2}, 0, -\frac{\tau_1}{S_1} v_{d_1} + \frac{\tau_2}{S_2} v_{d_2}]^T \tag{23}$$

B. Stability of Modeled Interaction

Let $\boldsymbol{x}(t_k)$ denote the state at the moment $t = t_k^+$ and $\boldsymbol{x}^-(t_k)$ be the state at $t = t_k^-$. Assume that there is a stable periodic trajectory for $\boldsymbol{x}$ with period T, then the following conditions should be satisfied:

1) $\dot{x}_1(t_k) = \dot{x}_1^-(t_{k+1})$, $\dot{x}_2(t_k) = \dot{x}_2^-(t_{k+1})$
2) $x_1^-(t_{k+1}) - x_1(t_k) = x_2^-(t_{k+1}) - x_2(t_k) = r$, where r is CoM's displacement from t_k to t_{k+1}.

To maintain an invariant periodic trajectory, the above conditions must be satisfied, which could be rearranged as

$$[\boldsymbol{x}^-(t_{k+1})^T, r]^T = \boldsymbol{M}[\boldsymbol{x}(t_k)^T, r]^T \tag{24}$$

with $\boldsymbol{M}$ is similar to an $\mathbb{R}^{6\times 6}$ identity matrix except $\boldsymbol{M}_{1,6} = \boldsymbol{M}_{3,6} = 1$.

From (19), we have

$$\boldsymbol{x}^-(t_{k+1}) = \boldsymbol{A_d}\boldsymbol{x}(t_k) \tag{25}$$

where $\boldsymbol{A_d} = e^{\boldsymbol{A}T}$, which is a constant matrix if T is constant. Equation (24) and (25) yield

$$\left(\tilde{\boldsymbol{A}}_{\boldsymbol{d}} - \boldsymbol{M}\right)[\boldsymbol{x}(t_k)^T, r]^T = \boldsymbol{0} \tag{26}$$

where

$$\tilde{\boldsymbol{A}}_{\boldsymbol{d}} = \begin{pmatrix} \boldsymbol{A_d} & \boldsymbol{0} \\ \boldsymbol{0} & 1 \end{pmatrix}$$

If a non-zero $\boldsymbol{x}(t)$ exists, $[\boldsymbol{x}(t_k)^T, r]^T$ should be in the null space of $\tilde{\boldsymbol{A}}_{\boldsymbol{d}} - \boldsymbol{M}$. Since two rows at the bottom of $\tilde{\boldsymbol{A}}_{\boldsymbol{d}} - \boldsymbol{M}$ are $\boldsymbol{0}$, the non-zero solutions $[\boldsymbol{x}(t_k)^T, r]^T$ exist.

When $t = t_{k+1}$, from (21) and (25)

$$\boldsymbol{x}(t_{k+1}) = \boldsymbol{N}\boldsymbol{x}^-(t_{k+1}) + \boldsymbol{u} = \boldsymbol{N}\boldsymbol{A_d}\boldsymbol{x}(t_k) + \boldsymbol{u} \tag{27}$$

If this discrete system is asymptotically stable, all the eigenvalues of $\boldsymbol{N}\boldsymbol{A_d}$ should be inside the unit circle. Because the analytical form of $\boldsymbol{A_d}$ is usually formidable, the stability is numerically determined. Fig. 4 shows the relationship between $\|\lambda(\boldsymbol{N}\boldsymbol{A_d})\|_{\max}$ and k_c, d_c. It can be shown that even m, z, and T are all given, the pattern of $\|\lambda(\boldsymbol{N}\boldsymbol{A_d})\|_{\max}$ is still quite complicated.

If $\|\lambda(\boldsymbol{N}\boldsymbol{A_d})\|_{\max} < 1$, the system in (27) is stable, and

$$\boldsymbol{x}(t_k) = (\boldsymbol{I} - \boldsymbol{N}\boldsymbol{A_d})^{-1}\boldsymbol{u},\ k \to \infty \tag{28}$$

C. Optimal Physical Interaction

The optimal interaction is defined as follows: if the system is stable, given the leader dancer's desired velocities $\{v_{d_1}(k)\}$, try to find $\{v_{d_2}(k)\}$ for the follower to minimize the interaction force. Without loss of generality, we assume $v_{d_1}(k) = v_{d_1}$, $v_{d_2}(k) = v_{d_2}$ and the two LIPMs have a stable periodic motion, then our goal is

$$\begin{aligned} \text{minimize:} \quad & F = \int_0^T f^2(t)dt \\ \dot{\boldsymbol{x}} &= \boldsymbol{A}\boldsymbol{x} \\ f &= \boldsymbol{c}^T\boldsymbol{x} \end{aligned}$$

where $\boldsymbol{c} = [k_c, d_c, -k_c, -d_c, k_c]^T$.

Using the analytical solution of $\dot{\boldsymbol{x}} = \boldsymbol{A}\boldsymbol{x}$ and (28), we have

$$\begin{aligned} F &= \int_0^T f^2(t)dt = \int_0^T \boldsymbol{x}^T\boldsymbol{c}\boldsymbol{c}^T\boldsymbol{x}dt \\ &= \boldsymbol{x}(0)^T\left(\int_0^T e^{\boldsymbol{A}^T t}\boldsymbol{c}\boldsymbol{c}^T e^{\boldsymbol{A}t}dt\right)\boldsymbol{x}(0) \\ &= \boldsymbol{u}^T\boldsymbol{Q}\boldsymbol{u} \end{aligned}$$

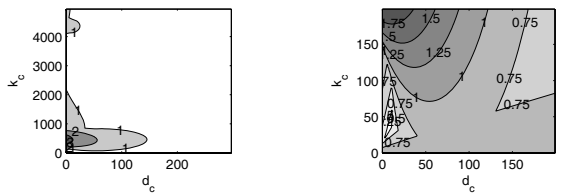

(a) $k_c \le 5000$, $d_c \le 300$ (b) $k_c \le 200$, $d_c \le 200$

Fig. 4. Contour of $\|\lambda(\boldsymbol{N}\boldsymbol{A_d})\|_{\max}$, given $m_1 = 70\,\text{kg}$, $z_1 = 1.1\,\text{m}$, $m_2 = 45\,\text{kg}$, $z_2 = 0.9\,\text{m}$, and $T = 0.75\,\text{s}$

where

$$\boldsymbol{Q} = (\boldsymbol{I} - \boldsymbol{N}\boldsymbol{A_d})^{-T}\int_0^T e^{\boldsymbol{A}^T t}\boldsymbol{c}\boldsymbol{c}^T e^{\boldsymbol{A}t}dt\ (\boldsymbol{I} - \boldsymbol{N}\boldsymbol{A_d})^{-1}$$

is a constant matrix, if m, z, T, k_c and d_c are given.

Our problem can be reformulated as:

$$\begin{aligned} \text{minimize:} \quad & F = \boldsymbol{u}^T\boldsymbol{Q}\boldsymbol{u} \\ \text{subject to:} \quad & \boldsymbol{H}\boldsymbol{u} = \boldsymbol{b} \end{aligned} \tag{29}$$

where

$$\begin{aligned} \boldsymbol{H} &= \begin{pmatrix} 1 & 0 & 0 & 0 & 0 \\ 0 & 1 & 0 & 0 & 0 \\ 0 & 0 & 0 & 1 & 0 \\ 1 & 0 & -1 & 0 & 1 \end{pmatrix} \\ \boldsymbol{b} &= [(\tau_1/S_1)v_{d_1}, 0, 0, 0]^T \end{aligned}$$

The problem described in (29) is a typical quadratic programming problem and can be easily solved. However, $\boldsymbol{Q}$ needs to be numerically integrated and the calculation is often time consuming.

Optimal result can be expected if the dance partner robot, i.e., the follower, can get access to all the state variables and parameters of the human dancer. However, this is usually not possible; for physical interaction, only $f(t)$ is available. Since F is a quadratic, differentiable function of v_{d_2}, if a specific v_{d_1} exists, we can use gradient descent to update v_{d_2} at the beginning of each period:

$$v_{d_2}^{(k+1)} = v_{d_2}^{(k)} - \gamma\left(\frac{F^{(k)} - F^{(k-1)}}{v_{d_2}^{(k)} - v_{d_2}^{(k-1)}}\right) \tag{30}$$

where γ is the step size.

IV. Simulation and Experiment

A. Simulation

For simulation, we use $m_1 = 70\,\text{kg}$, $z_1 = 1.1\,\text{m}$, $m_2 = 45\,\text{kg}$, $z_2 = 0.9\,\text{m}$, $T = 0.75\,\text{s}$, and $v_{d_1}(0) = v_{d_2}(0) = 0$.

The three controllers discussed in Section II are compared in simulations, let $v_d(0) = 0$ and $v_d(k) = 1$ for all $k > 0$. $m = 45$ and $z = 0.8$. We disturb t_3 by $-T/4$ and continuously apply a $2\,\text{N}$ external force on the single LIPM, simulation results are shown in Fig. 5.

Due to the external force, the energy error (the distance between current energy and desired energy levels) keeps increasing, except at $\{t_k\}$ when the controller is supposed to work. Although the energy controller reduces energy error to 0 at $\{t_k\}$ (Fig. 5(b)), the velocity is poorly controlled (Fig. 5(a)) with the obvious problem of limping (i.e., LIPM moves faster when k is even and slower when k is odd).

The latter two controllers both yield acceptable results in velocity control (Fig. 5(c) and Fig. 5(e)). However, for the velocity controller, its energy error is not always decreasing at $\{t_k\}$, e.g., when $k = 3$ and $k = 5$, the energy errors increase by $0.72\,\text{J}$ and $0.87\,\text{J}$, which violates the requirement in (16). In contrast, the proposed controller can satisfy both requirements on velocity and energy error control (Fig. 5(e)

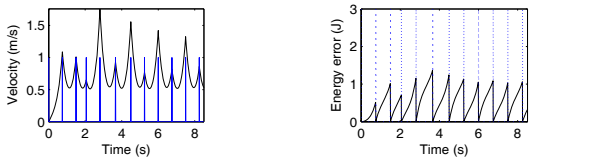

(a) Energy controller: velocity (b) Energy controller: energy error

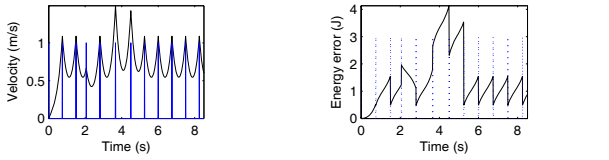

(c) Velocity controller: velocity (d) Velocity controller: energy error

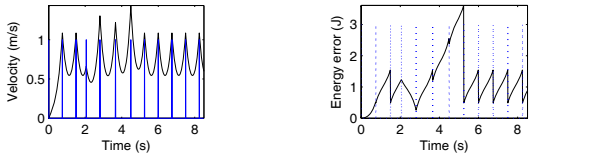

(e) Proposed controller: velocity (f) Proposed controller: energy error

Fig. 5. Single LIPM simulation results. Impulses denote moments of pivot changes (t_k). Energy error is defined as $|E_{\text{desired}} - E(t)|$

and Fig. 5(f)); the advantage of the proposed controller is supported by simulation.

The k_c–d_c–stability contours have been shown in Fig. 4. Here we choose a stable combination as $k_c = 100$ and $d_c = 200$. Set $v_{d_1}(k) = 1$ for all $k > 0$. Two interactions with different $v_{d_2}(k)$ are simulated and shown in Fig. 6. We can see that even v_{d_1} and v_{d_2} are very different, the interaction is still stable since k_c, d_c have been properly selected. However, the quality of the physical interaction is affected by v_{d_2}: if it is poorly chosen, the interaction force would be very large (Fig. 6(a)). In contrast, if v_{d_2} is the solution to the optimization problem given in (29), the interaction force can be minimized, as shown in Fig. 6(b). To quantitatively evaluate the interaction forces throughout the interactions, we can implement a value $\tilde{F}$, which is defined as $\tilde{F} = \int_{t_{\text{start}}}^{t_{\text{end}}} f^2(t)dt/(t_{\text{end}} - t_{\text{start}})$, where t_{start} and t_{end} are the start and end moments of simulation. Then we have $\tilde{F} \approx 225\,\text{N}^2$ in Fig. 6(a) and $\tilde{F} \approx 10\,\text{N}^2$ in Fig. 6(b).

Simulation of the v_{d_2} updating based on the gradient descent method is shown in Fig. 7. The original v_{d_2} is set

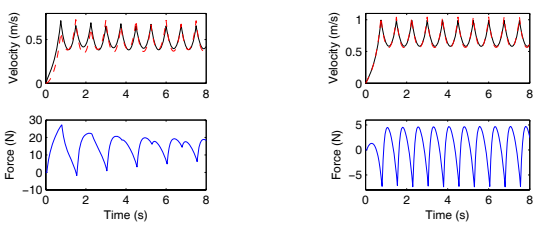

(a) $v_{d_2} = 0.1$ (b) $v_{d_2} = v_{d_2}^{\star} \approx 1.0309$

Fig. 6. Simulated interaction of two connected LIPM

to 0.3 and $\gamma = 2 \times 10^{-4}$. The simulation results suggest that v_{d_2} is able to be adjusted so as to minimize F by using (30). From Fig. 7(c) we can see that α stays between 0 and 0.5, which implies the controller has lead to the velocity controller given in (4). Actually, interaction forces usually drive a single LIPM away from its desired E_d, this makes the assumptions about $\boldsymbol{N}$ in Section III-A reasonable.

B. Experiment

Experiments have been conducted to test our analysis and the method for human-robot coordination. The robot used in the experiment, shown in Fig. 8, is the same mobile robot as appeared in [9]. The robot emulates LIPM's dynamics by implementing a virtual internal model in its controller. Parameters of this virtual LIPM are set as $m_2 = 45\,\text{kg}$ and $z_2 = 0.9\,\text{m}$. When no external force is applied, the velocity curve of robot is shown in Fig. 9(a), which supports the validity of the proposed controller in Section II. Since the virtual dynamics of the robot have no unmodeled factors, the robot's real motion is only affected by disturbances and well matches the simulation results as given in Fig. 5(e).

To minimize the variability contained in human's motions and generate relatively repeatable trials, a row of markers, with $0.4\,\text{m}$ separation, are attached to the floor; the human dancer is asked to keep his toes landing on the marker during walking, while his motion is synchronized by audio cues with 0.75s period. Parameters of the subject are $m_1 \approx 70\,\text{kg}$ and $z_1 \approx 1.1\,\text{m}$. The single subject's velocity curve is obtained by a motion capture system (VICON 460) and given in Fig. 9(b).

When v_{d_2} is fixed at $0.3\,\text{m/s}$, results of the pHRI experiment are shown in Fig. 10(a). We can see that although there is a large difference between v_{d_1} and v_{d_2}, the human's and robot's motions are still coupled together; however, the interaction force is quite large ($\tilde{F} \approx 814\,\text{N}^2$).,

When v_{d_2} can be adjusted by (30), with $\gamma = 1 \times 10^{-5}$,

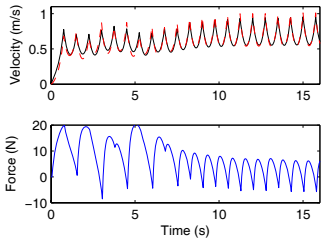

(a) Coupled velocities and interaction force

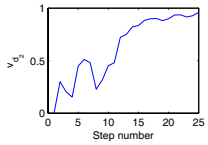

(b) v_{d_2}

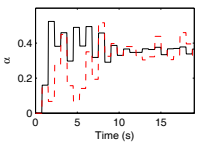

(c) α

Fig. 7. Simulated v_{d_2} adaptation. Solid and dashed line in (a) are leader's and follower's respective velocities; solid and dashed line in (c) are leader's and follower's α given in (11).

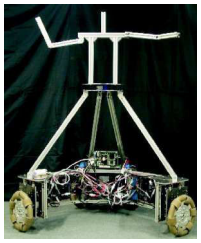

Fig. 8. Robot used in experiment

(a) Robot (b) Human

Fig. 9. Velocity curves of human's and robot's independent motions

results are given in Fig. 10(b). The interaction force can be decreased to $\tilde{F} \approx 414\,\mathrm{N}^2$, hence the validity of gradient descent method is supported.

However, since interaction force is the only feedback for v_{d_2} updating and usually affected by noises and unmodeled errors (e.g. k_c and d_c of human's arms may keep changing according to some adaptation rules). Those unmodeled errors cause large difference between simulation (Fig. 7) and experiment (Fig. 10(b)). It can also be observed that v_{d_2} converges rather slowly and does not converge to the optimal value (which should be around $0.7\,\mathrm{m/s}$–$0.8\,\mathrm{m/s}$).

V. Conclusions and Future Work

In this paper, we first proposed a balance controller for a simplified human model, LIPM. A pair of dancers are modeled by two spring-damper-connected LIPMs with balance controllers. Assuming the perfectly rhythmic and synchronized motion, the physical interaction is analyzed. The proposed approach for realizing optimal interaction has also been supported by simulation and experiment. However, currently our analysis relies on the assumption that two dancers' pivot positions change in synchrony, while in reality the synchronization error usually exists and may significantly affect the coupled dynamics. In addition, the gradient descent method is slow and sensitive to step size. If we can have more information about the system, either by using additional sensors or by estimating $\boldsymbol{Q}$ in (29), more options might become available. Another limitation is that our current model does not include the dynamics of spins and turns, which are essential elements of waltz. The above issues will be addressed in our future work.

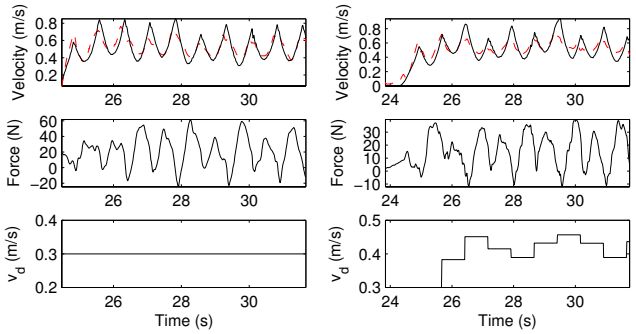

(a) pHRI with fixed v_{d_2} (b) pHRI with v_{d_2} being updated

Fig. 10. Results of the coupled dynamics of human and robot. Solid curves in the first row are velocities of the robot; dashed curves are velocities of the human. $\tilde{F} \approx 814\,\mathrm{N}^2$ in (a) and $\tilde{F} \approx 414\,\mathrm{N}^2$ in (b).

VI. Acknowledgments

This work was supported by the Asian Office of Aerospace Research and Development (AOARD), Air Force Office of Scientific Research (AFOSR) under grant number FA2386-10-1-4126.

References

[1] K. B. Reed, J. Patton, and M. Peshkin, "Replicating Human-Human Physical Interaction," *Proceedings of 2007 IEEE International Conference on Robotics and Automation (ICRA)*, pp. 3615–3620, 2007.

[2] S. Gentry, "Dancing cheek to cheek: Haptic communication between partner dancers and swing as a finite state machine," Ph.D. dissertation, Massachusetts Institute of Technology, 2005.

[3] Z. Wang, A. Peer, and M. Buss, "An HMM approach to realistic haptic human-robot interaction," *EuroHaptics conference, 2009 and Symposium on Haptic Interfaces for Virtual Environment and Teleoperator Systems.*, pp. 374–379, 2009.

[4] H. Kazerooni, "Human/robot interaction via the transfer of power and informationsignals," *IEEE Transactions on System, Man, and Cypernetics*, vol. 20, no. 2, pp. 450–463, 1990.

[5] D. Feth, A. Peer, and M. Buss, "Incorporating human haptic interaction models into teleoperation systems," *Proceedings of 2010 IEEE/RSJ International Conference on Intelligent Robots and Systems (IROS)*, pp. 4257–4262, 2010.

[6] S. Ikemoto, H. B. Amor, T. Minato, H. Ishiguro, and B. Jung, "Physical interaction learning: Behavior adaptation in cooperative human-robot tasks involving physical contact," *RO-MAN 2009 - The 18th IEEE International Symposium on Robot and Human Interactive Communication*, pp. 504–509, 2009.

[7] S. Sirouspour, "Robust control design for cooperative teleoperation," *Proceedings of 2005 IEEE International Conference on Robotics and Automation (ICRA)*, pp. 1133–1138, 2005.

[8] T. Takeda, Y. Hirata, and K. Kosuge, "Dance step estimation method based on HMM for dance partner robot," *IEEE Transactions on Industrial Electronics*, vol. 54, no. 2, pp. 699–706, 2007.

[9] ——, "Dance partner robot cooperative motion generation with adjustable length of dance step stride based on physical interaction," *Proceedings of 2007 IEEE/RSJ International Conference on Intelligent Robots and Systems (IROS)*, pp. 3258–3263, 2007.

[10] S. Kajita and K. Tani, "Study of dynamic biped locomotion on rugged terrain—theory and basic experiment," *Advanced Robotics, 1991. 'Robots in Unstructured Environments', 91 ICAR., Fifth International Conference on*, pp. 741–746 vol.1, 1991.

[11] S. Kajita, F. Kanehiro, K. Kaneko, K. Yokoi, and H. Hirukawa, "The 3D linear inverted pendulum mode: a simple modeling for a biped walking pattern generation," *Proceedings of 2001 IEEE/RSJ International Conference on Intelligent Robots and Systems (IROS)*, no. 4, pp. 239–246, 2001.

[12] H. Wang and K. Kosuge, "An Inverted Pendulum Model for Reproducing Humans Body Dynamics in Waltz and Its Applications in a Dance Partner Robot,," *Proceedings of IEEE/SICE International Symposium on System Integration*, pp. 182–187, 2010.

[13] H. Ye, A. Michel, and L. Hou, "Stability theory for hybrid dynamical systems," *IEEE Transactions on Automatic Control*, vol. 43, no. 4, pp. 461–474, 2002.

[14] J. Grizzle, G. Abba, and F. Plestan, "Asymptotically stable walking for biped robots: Analysis via systems with impulse effects," *IEEE Transactions on Automatic Control*, vol. 46, no. 1, pp. 51–64, 2002.

An Inverted Pendulum Model for Reproducing Human's Body Dynamics in Waltz and Its Applications in a Dance Partner Robot

Hongbo Wang and Kazuhiro Kosuge

Abstract— **A linear inverted pendulum (LIPM) is used to model the human dancer's body dynamics in closed changes. Several assumptions are made: a controller is proposed to balance the LIPM; the dance frame is considered as a spring-damper connection; the two dancers are assumed to choose support positions independently. Motions generated by the model are compared with human's real motions. Results of comparisons suggest the model and the assumptions are effective in reproducing human dancers' body dynamics in waltz. Issues in implementing the model on a dance partner robot are discussed.**

I. INTRODUCTION

Physical interactions between humans involve many aspects, including bidirectional flow of force/haptic signals, proactive/reactive responses to the signals, and humans' affected body dynamics, etc. Due to the complexity of human's body and random factors contained in human's motions, many principles and mechanisms underlying physical human-human interaction (pHHI) are still unknown. Since understandings of the pHHI may facilitate designs of robots which can be intuitively controlled through physical human-robot interaction (pHRI), a number of investigations have been directed for studying and reproducing the subtle features in the interaction [1]–[5].

Waltz is a typical case of pHHI. When dancing together, two dancers can communicate with each other through physical interactions. At higher level, the force or haptic signals can be used by the male dancer to suggest his selection of the next dance step, and the female dancer uses the signals to estimate the leader's intentions. At lower level, two dancers' body dynamics are coupled together; both of the dancers' motions are affected by the interaction forces, resulting in modified motion trajectories. To understand mechanisms of pHHI in waltz and apply them to a dance partner robot, we have proposed some methods for realizing intention estimation [6] and cooperative motion generation [7]. A dance partner robot, PBDR (Partner Ballroom Dance Robot) has also been developed in the aim of creating a robot who can dance with human through physical interaction in human-like ways.

Usually, researchers assume that repeatability and predictability exist in human's behaviors, in another word, there exists a human model (which could be deterministic or probabilistic, explicit or implicit), through which the status of interaction can be estimated. Aside from the human model, since interaction involves at least two entities, it is also necessary to implement a robot model which defines the robot's responses to the force/haptic signals.

In the case of the dance partner robot, the human dancer and the robot were also modeled at higher level (step intention suggestion and estimation) and lower level (coupled body dynamics):

1) At the intention suggestion/estimation level, the human dancer is assumed to be capable of producing different time–force/torque patterns for different selected steps. On the robot side, several hidden Markov models (HMM) were implemented to select a step with maximum likelihood [6].
2) At the body dynamics level, the human dancer model contains one parameter—stride length. The robot is able to learn this parameter from trials and use it to scale the robot's pre-recorded trajectories. To define its responses to force/torque inputs, the robot was modeled as an inertial mass affected by external force/torque and ground friction [7].

Although the above models have been proved to be effective as successful cooperated dancing can be generated in experiments, the simple inertial mass model has hidden some important features in the physical interaction. When the robot acts like a mass on the ground, which is quite different from the behavior of a real female dancer, the resultant pHRI will be deviated from real pHHI. Therefore, to make the human-robot cooperated dance more life-like , it is necessary to have the robot behave like a human dancer, i.e., the robot should contain a sufficiently precise model of a female dancer's body dynamics.

Rather than a free mass moving on flat ground, human's body dynamics in walking is often modeled as an inverted pendulum. The linear inverted pendulum mode (LIPM) [8] and its 3-D extension (3D-LIPM) [9] proposed by Kajita et al. are widely used for biped gait planning. The LIPM is considered as simplified model since it assumes the biped as an inverted pendulum with massless legs, while applying some restrictions on its center-of-mass (CoM) trajectories, upper body rotations and ankle input torques.

It is certain that those simplifications and restrictions will introduce some errors, which make LIPM less accurate than a more sophisticated, whole body model (e.g., a 34-DOF humanoid model). However, LIPM is an affordable model for our analysis, especially when two coupled systems are involved. The model's simplicity ensures that we can find some qualitative and (approximate) quantitative rules of the interaction, and make use of these rules to control the dance

The authors are with the Department of Bioengineering and Robotics, Tohoku University, 6-6-01, Aoba, Aramaki, Aoba-ku, Sendai 980-8579, Japan {h_wang, kosuge}@irs.mech.tohoku.ac.jp

partner robot. Therefore, in this paper, we will model a waltz dancer as LIPM and analyze his/her behavior in single and paired dance. We will also discuss the model's accuracy, as well as issues in implementing the model on the current robot.

In Section II, a single female dancer is modeled as an LIPM, comparisons between real motion data and model-predicted data are directed to evaluate the model's goodness. In Section III, the two coupled dancers are modeled as two connected LIPM, dynamics of the coupled systems are analyzed and comparisons with the experiment data are made. In Section IV, issues in using LIPM in a dancer robot are briefly discussed. Conclusion is given in Section V.

II. MODELING A SINGLE DANCER WITH LIPM

A. The Linear Inverted Pendulum Mode

Consider a simplified human body model with a massless leg in sagittal plane, as shown in Fig. 1(a). The origin of the coordinate frame is at the supporting point. By applying the following constraints:

1) The CoM of the whole body moves along a straight line defined by $z = kx + h$, $h \neq 0$;
2) The angular velocity of the upper body is a constant;

we can then consider the system as an inverted pendulum with a massless, extendable leg and a point mass, as shown in Fig. 1(b). Since two constraints exist in the 3-DOF system, the resultant system has one DOF, with linear dynamics defined by the following equation [8]

$$\ddot{x} = \frac{g}{h}x + \frac{1}{mh}u \tag{1}$$

where g is the gravity acceleration, m is the mass of the body, and u is the torque input on the ankle.

When the supporting point is not at the origin, (1) can be rewritten as

$$\ddot{x} = \frac{g}{h}x - \frac{g}{h}p \tag{2}$$

where p is the position of the supporting point. Notice that the term u in (1) does not appear in (2), because changes of u can be substituted by changes of p; this simplification is reasonable, as for real human walking, we can consider the changes of ankle torque as the result of CoP (center of pressure) changes. p is used as the input to stabilize the system.

Although LIPM has been successfully implemented by many biped walking systems, when to model human dancers' body dynamics in waltz, some difficulties exist:

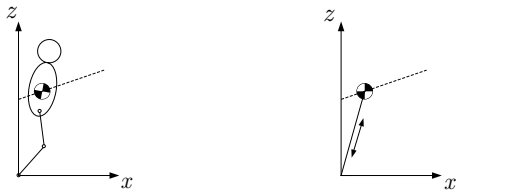

(a) Simplified human body model (b) Linear inverted pendulum

Fig. 1. Simplification of body dynamics

1) Human's motion contains large variability, as human body has too many DOFs and can be affected by too many random factors. This is a common problem that all assumed human models are facing.
2) LIPM is a largely simplified model, it might be unable to include many crucial features in human dancers' body dynamics.
3) LIPM is intrinsically unstable, hence we need assume a controller to stabilize LIPM; however, the difference between the assumed controller and human's real controller would introduce additional errors.

In the following, after modeling waltz sequence with LIPM and comparing the simulation and the experiment results, we will examine and discuss the effects of the above difficulties.

B. Modeling The Dancing Sequence

Closed changes are the elementary steps in waltz as no rotation is involved; closed changes can be analyzed separately in sagittal plane and frontal plane, while in this paper we concentrate on the dynamics in sagittal plane. The step diagram of *left closed change* (CCL) is given in Fig. 2, in which the male dancer initiates the dance with his left foot. Similarly, *right closed change* (CCR) is the mirrored moves of CCL, as in CCR the male dancer begins with his right foot.

In this section we are to analyze a single dancer's body dynamics in sagittal plane. Consider a single dancer's moves in CCL/CCR. If we approximate those moves with the LIPM model, a sequence of motions of an inverted pendulum can be obtained, as illustrated in Fig. 3. The numbers (1,2,3) indicate moments of supporting point changes. In Fig. 3, initiaion–1, 1–2, and 2–3 respectively correspond to Fig. 2(b), Fig. 2(c), and Fig. 2(d). p_1 and p_2 are the landing locations of Fig. 2(b) and Fig. 2(c). In order to use the LIPM model, we assume the CoM follows a series of straight segments, which in Fig. 3 are dashed lines with arrowheads.

C. The Assumed Controller

As mentioned in Section II-A, an assumed controller which guides and balances the LIPM is essential for modeling the dance sequence. One straightforward method is firstly

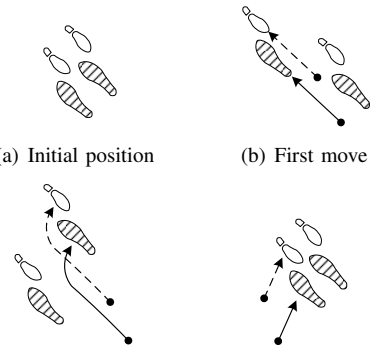

(a) Initial position (b) First move

(c) Second move (d) Third move

Fig. 2. Left closed change (CCL)

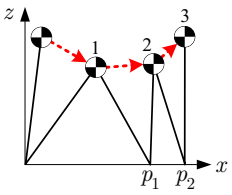

Fig. 3. Approximate motion sequence of CCL

solving the homogeneous form of (2) and using its solution to control p. Assuming that when $t_0 < t < t_1$ support changes do not happen, i.e., $p(t)$ is a constant for $t_0 < t < t_1$. Then we have a homogeneous differential equation

$$\ddot{x}' = (g/h)x' \tag{3}$$

where $x' = x - p$ is the CoM's relative position with the supporting point. And for $t_0 < t < t_1$, $\dot{x}' = \dot{x}$, $\ddot{x}' = \ddot{x}$. The analytical solutions for this equation are a set of linear combinations of $e^{t/\tau}$ and $e^{-t/\tau}$, where $\tau = \sqrt{h/g}$.

In waltz, dancers' support changes are synchronized with music beats. If we consider the constant beat period (denoted by T) between two support changes, the analytical solutions to (3) can be written as

$$\begin{aligned} x'(kT+T) &= Cx'(kT) + \tau S\dot{x}'(kT) \\ \dot{x}'(kT+T) &= (S/\tau)x'(kT) + C\dot{x}'(kT) \end{aligned} \tag{4}$$

where $\tau = \sqrt{h/g}$, $C = \cosh(T/\tau)$, $S = \sinh(T/\tau)$.

From (4), we have

$$x'(kT) = -(\tau C/S)\dot{x}'(kT) + (\tau/S)\dot{x}'(kT+T) \tag{5}$$

The new support position $p(kT) = x(kT) - x'(kT)$, and in single support phase $\dot{x}(kT) = \dot{x}'(kT)$, hence

$$p(kT) = x(kT) + (\tau C/S)\dot{x}(kT) - (\tau/S)\dot{x}(kT+T) \tag{6}$$

Equation (6) is the proposed controller while $\dot{x}(kT+T)$ is a reference velocity we want to achieve.

D. Experiment

To evaluate the effectiveness of the LIPM in modeling a single dancer's body dynamics, a professional female dancer's real motions were used for comparisons. CCL (with period $T = 0.75\,\mathrm{s}$) was performed three times by the same female dancer and her body motions were measured and recorded by a motion capture system (VICON 460) at the rate of 120 frames per second. Since it is difficult to distinguish the moment of initiation, the moments of peak velocities in the three trials were used to align the data along the time axis, as shown in Fig. 5(a).

To approximate the human dancer's motions, the LIPM model needs several parameters, which are listed in Table I. The first set of parameters includes m, h_{t_1}, and h_{t_2} (h_{t_1} and h_{t_2} are respectively the heights of CoM at *fall* and *rise* positions in waltz), which defines the dancer's physical conditions.

An important point to be noticed is that obtaining accurate CoM locations from motion capture data is itself a challenge [10], [11]. For simplicity, here we choose a point on the pelvis as the approximate CoM location. Hence h_{t_1} and h_{t_2} in Table I are two estimations. Although causing inaccuracy, the errors in CoM estimation are partly compensated by the following facts:

1) In waltz, the human's upper body keeps a fixed configuration while the lower body movements are fairly moderate; these avoid the CoM to be deviated too much from the pelvis.
2) On the model side, due to the existence of the controller (Section II-C), the resultant movement is not sensitive to h_{t_1} or h_{t_2}. An example is given in Fig. 4; the variations in h_{t_1} and h_{t_2} does not largely affect the result.

Another set of parameters includes $\dot{x}(T)$, $\dot{x}(2T)$ and $\dot{x}(3T)$, which are velocities measured from motion capture data (as shown in Fig. 5(a)) and represent some features of the female dancer's motions. $\dot{x}(0)$ is assumed to be 0.

Results of the comparisons are given in Fig. 5. The "+" markers represent motions generated by the LIPM model. Aside from CoM positions and velocities, another set of criteria is the comparisons of $p(t)$. LIPM gives the results as $p(T) = 0.77\,\mathrm{m}$ and $p(2T) = 0.80\,\mathrm{m}$, while the experiment results are $p(T) = 0.75\,\mathrm{m}$ and $p(2T) = 0.90\,\mathrm{m}$. The error at $p(2T)$ is not negligible; however, considering the fact that the human dancer's supporting point (or CoP) can be located anywhere within the support polygon, the above error is acceptable. In addition, it should be noticed that only $\dot{x}(T)$ and $\dot{x}(2T)$ were given to the LIPM model, other data ($\dot{x}$ at $t \neq kT$, x, and p) are all generated by the model.

According to the results of comparisons, the LIPM model approximates the female dancer's real motions quite well. Another phenomenon is that the large variability expected in human's motions was not observed. Here we can give a tentative explanation to these results: because waltz has

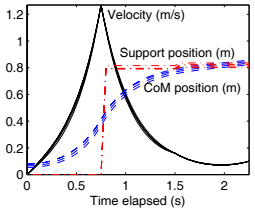

Fig. 4. CoM positions, velocities and support positions generated by LIPM with four sets of height parameters. First set: $h_{t_1} = 0.9$, $h_{t_2} = 1.0$; second set: $h_{t_1} = 1.0$, $h_{t_2} = 0.9$; third set: $h_{t_1} = 0.8$, $h_{t_2} = 1.1$; fourth set: $h_{t_1} = 1.0$, $h_{t_2} = 1.0$.

TABLE I

PARAMETERS FOR LIPM AND ITS CONTROLLER

m	$\approx 45\,\mathrm{kg}$
h_{t_1}	$\approx 0.9\,\mathrm{m} (T < t \leq 2T)$
h_{t_2}	$\approx 1.0\,\mathrm{m} (0 < t \leq T, 2T < t \leq 3T)$
$\dot{x}(0)$	0
$\dot{x}(T)$	$\approx 1.27\,\mathrm{m{\cdot}s^{-1}}$
$\dot{x}(2T)$	$\approx 0.16\,\mathrm{m{\cdot}s^{-1}}$
$\dot{x}(3T)$	$\approx 0.10\,\mathrm{m{\cdot}s^{-1}}$

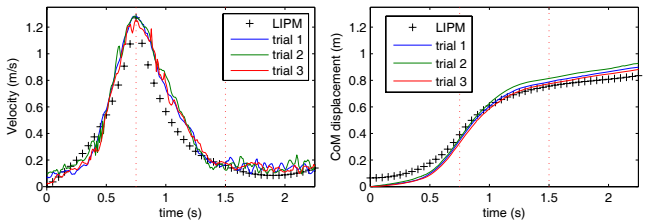

(a) CoM velocities (b) CoM displacements

Fig. 5. Comparison of theoretical and trial data

applied many constraints to human's motions (e.g., constant walking period, CoM trajectories regulated by rise and fall, and straight upper body, etc.), it is possible that these constraints might reinforce the repeatability in different trials and make the human body behave like an inverted pendulum. Though the underlying reasons are still not clear, our proposed approach, which uses a simple inverted pendulum to model human's body dynamics in waltz, is supported by the comparisons.

III. MODELING THE PHYSICAL INTERACTION

A. Modeling The Interaction Between Two LIPM

Waltz involves physical interactions between two dancers, whose body dynamics can be modeled as two LIPM connected by a dance frame, as shown in Fig. 6. The equations describing the dynamics of the two-LIPM system are

$$\ddot{x}_1 = \frac{g}{h_1}(x_1 - p_1) - \frac{f}{m_1} \quad (7)$$

$$\ddot{x}_2 = \frac{g}{h_2}(x_2 - p_2) + \frac{f}{m_2} \quad (8)$$

where f is the compression force between the two dancers.

If we approximately consider the dance frame as a rigid connection as in Fig. 6(a), then we have $x_1 = x_2 - d$, $\dot{x}_1 = \dot{x}_2$, and $\ddot{x}_1 = \ddot{x}_2$. By defining the following error of the female dancer's supporting location as $e = p_2 - p_1 - d$, and letting $x = x_1$ and $p = p_1$, the dynamics of the two-LIPM system are

$$M\ddot{x} = Kx - Kp - k_2 e \quad (9)$$

$$f = \frac{m_1 m_2}{M}\left[(\frac{g}{h_1} - \frac{g}{h_2})(x - p) + \frac{g}{h_2}e\right] \quad (10)$$

where $M = m_1 + m_2$, $k_1 = m_1 g/h_1$, $k_2 = m_2 g/h_2$, and $K = k_1 + k_2$. Some rough characteristics of the interaction can directly be obtained from (9) and (10): according to (9), if the female dancer follows perfectly, i.e., $e(t) = 0$ for all t, then the two-LIPM system will behave like a single LIPM, with time constant $\sqrt{M/K}$. According to (10), as long as $h_1 \neq h_2$, even $e(t) = 0$ for all t, $f(t)$ is still not always 0; on the other hand, (10) also suggests the possibility of eliminating $f(t)$ by controlling $e(t)$.

Alternatively, we can also assume that the two dancers are connected by spring and damper as shown in Fig. 6(b). This spring-damper assumption is more accurate than the rigid one, as distance changes between the two dancers were observed in experiments. According to this assumption, the interaction force f is

$$f = -k_c(x_2 - x_1 - d_k) - D_c(\dot{x}_2 - \dot{x}_1) \quad (11)$$

where k_c is the spring constant, D_c is the damping ratio, and d_k is the natural length of the assumed spring. The two-LIPM system's behavior is hence determined by (11) along with (7) and (8).

B. Analyzing The Interaction

Interaction between two dancers' body dynamics is one of the crucial features we want to investigate and reproduce with robot. Because the interaction is influenced by too many physical and non-physical factors (e.g., empirically, merely the presence of a partner would influence the dancer's expectations about the future moves), it is very difficult to reveal the mechanisms in the interaction. However, with the LIPM model and some additional assumptions, it is possible to analyze the interaction with the approximate model.

From the female dancer's point of view, two assumptions of the interaction can be made. The first one assumes that the female dancer follows the male dancer perfectly (i.e., $p_2 = p_1 + d$ where d is constant), while the second one assumes the female dancer to be completely independent (i.e., p_2 is determined only by and (6), as if she is dancing alone). Then the above two assumptions are examined both with the rigid-connection model (Fig. 6(a)) and the spring-damper-connection model (Fig. 6(b)).

Simulation results based on the second assumption, in which the female dancer chooses p_2 independently, are shown in Fig. 7. The two dancers have different parameters ($m_1 = 70\,\mathrm{kg}$, $h_1 = 1.2\,\mathrm{m}$, $m_2 = 50\,\mathrm{kg}$, $h_2 = 0.8\,\mathrm{m}$) but are given the same desired velocities at $t = kT$, $k = 1, 2, 3$. When $k_c = D_c = 0$, the dancers can be considered as two separated LIPM (Fig. 7(a)). In contrast, when $k_c, D_c \neq 0$,

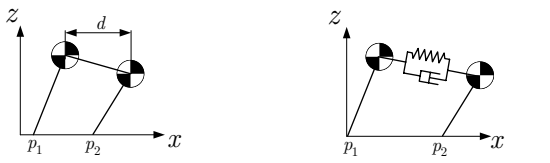

(a) Rigid connection (b) Spring-damper connection

Fig. 6. Dancers' model as two inverted pendulums

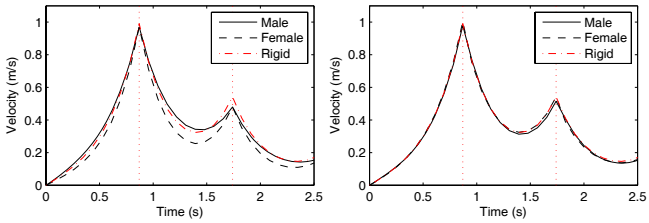

(a) $k_c = D_c = 0$ (b) $k_c = D_c = 1000$

Fig. 7. Simulation results: independent female dancer

a physical connection is established and dynamics of the two dancers are coupled in spite that their controllers are independent. The coupled velocities under the condition $k_c = D_c = 1000$ (which is nearly a rigid connection) are shown in Fig. 7(b).

If the female dancer's support position completely follows $p_1 + d$ (i.e., $e(t) = 0$ for all t), the dance cannot be continued if the connection is too weak (e.g., $k_c = D_c = 140$), since she will rapidly loose balance (Fig. 8(a)). If the connection is strong (or rigid), the system can then be balanced by the male dancer's controller; however, the desired velocities cannot be reached, because the male dancer's controller does not take the female dancer's body dynamics into account (Fig. 8(b)).

Based on the above analysis, it might be reasonable to assume the two dancers' support positions are independently controlled while their body dynamics are coupled through the physical connection—the dance frame.

C. Experiment

A dance sequence which consists of a CCR and a CCL was performed by two dancers. Two LIPM with spring-damper connection are used as the system model. The two LIPM are assumed to have independent controllers. Because it is relatively difficult to determine the desired velocities for the controllers, the two dancers' real velocities at $t = kT$ were used as approximations. Results of comparisons are given in Fig. 9.

According to Fig. 9(a) and Fig. 9(b), the assumed two-LIPM system and their independent controllers are able to model the real dancers' dynamics. The male dancer's simulated and real support positions are compared in Fig. 9(c). The two dashed lines are toe and heel locations of the male dancer; the solid line is the model's simulated support position. If we consider the dashed lines as upper and lower bounds of a support polygon, then the solid line should be located inside or on the edge of the polygon.

IV. DISCUSSION

A. Issues in Implementing LIPM on a Mobile Robot

Instead of focusing on kinesiology, the final goal of our study is developing a robot that can dance waltz with human by emulating a female dancer's behaviors. Because the previous model cannot represent dancers' body dynamics with sufficient closeness, while the LIPM and the assumed

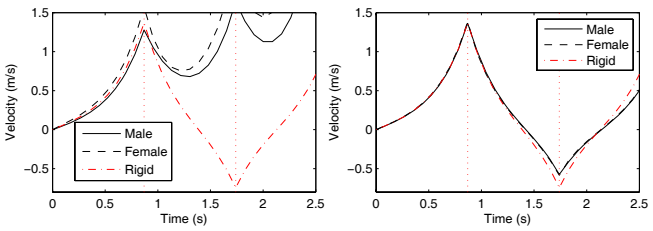

(a) $k_c = D_c = 140$ (b) $k_c = D_c = 2000$

Fig. 8. Simulation results: $e(t) = 0$ for all t

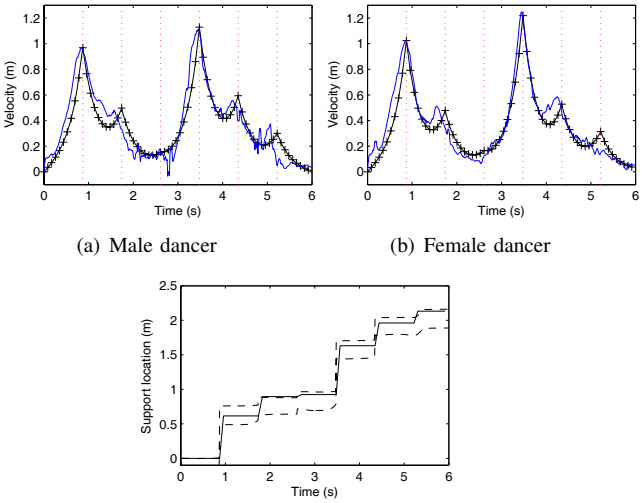

(a) Male dancer (b) Female dancer

(c) support position of the male dancer

Fig. 9. Comparisons of simulation and experiment data

controller gave good approximations, it would be better to have the robot to adopt the LIPM as its dynamics model.

With a motor actuated, omni-directional mobile base and a force/torque sensor in the waist, the developed prototype, PBDR, is able to emulate an LIPM's dynamics (given in (8)), as long as the speed and the acceleration do not exceed the motors' limits. The controller described in (6) can be used to direct and balance the robot at low level, while another high level controller is also needed to feed the low level controller with desired velocities, which could be obtained from experiments or determined by other rules.

In essence, adopting the LIPM model means we are turning an intrinsically stable mobile robot into an unstable inverted pendulum, then applying an extra controller to re-stabilize the system. It may look strange and redundant of doing this, while additional dangers are introduced due to the new system's instability; however, as our goal is the life-like pHRI, there are many advantages in doing this:

1) The robot can react to the interaction force in a more human-like way.
2) Stride length adjustments are more dynamic, i.e., it is not a constant parameter learned in trials, but a compromise between dance trajectories and body balance.
3) During the transition time between two dance steps, the robot is in an unstable equilibrium state; the motion direction can easily be changed by a slight force. This fact has the potential to be utilized to estimate the male dancer's intentions.

The value of the above advantages to the study of pHRI makes it worthy to implement the LIPM model on the dance partner robot.

B. LIPM versus Other Models/Methods

There are many alternatives to LIPM: two typical examples are human-like model and curve fitting. The former one is supposed to be more precise than LIPM, while the

latter one is supposed to be equivalent to LIPM in generating dancing trajectories. Nevertheless, LIPM is still selected over the other two alternatives; the reasons are explained below.

Although a model with fewer simplifications is generally more precise than LIPM in reproducing human-like motions, it is consequently more complicated. The complexity of the model implies many difficulties in analysis and a result which may be hard to simplify and interpret. In addition, a precise and complicated model usually requires more parameters; if those parameters can not be properly defined to reflect human's real motions, the model's fidelity would still be decreased. Due to the above facts, selecting the model is a compromise between accuracy and practicality.

On one hand, limited knowledge of human's dynamics and control in waltz, along with the complexity of analysis, restrict us from implementing an over-complicated model. On the other hand, as a mobile robot, PBDR's vertical motion is independent of its horizontal motion, while LIPM can generate sufficiently accurate motion in horizontal plane (and less accurate in vertical plane); therefore, precise motions can be yielded by using LIPM for horizontal motion and using recorded trajectories for vertical motion. For these reasons we choose LIPM as the compromise point.

Another comparison is between LIPM and curve fitting methods. Similar dancing trajectories, e.g., Fig. 5, Fig. 9(a), and Fig. 9(b), can simply be produced by curve fitting. Indeed, if the robot is supposed to dance on its own, curve fitting is more straightforward than LIPM. However, the robot is expected to physically interact with human dancer; curve fitting can be used to yield a trajectory, but the body dynamics model would still be needed to respond to external forces/torques (e.g., the term f in (7) and (8)) in a human-like way. Compared with curve fitting, LIPM not only fits trajectory but also serves as a dynamics model. The purpose of using LIPM is to facilitate investigating the pHRI in waltz, which is difficult to be addressed by curve fitting methods.

V. CONCLUSION AND FUTURE WORK

Human and robot models are two crucial parts in pHRI; selections of those models can largely affect pHRI's qualities. Because the robot model adopted by a dance partner robot (PBDR) was not sufficiently accurate in representing human's body dynamics in waltz, a linear inverted pendulum (LIPM) model, which has been widely used in biped gait generation, is implemented and evaluated.

For simplicity, waltz closed changes (CCL and CCR) in sagittal plane are converted into a sequence of motions of an LIPM (or two). Several assumptions are made on the controller ((6)), the connection (Fig. 6), and the interaction (Section III-B). By comparing model-generated motions with human dancers' real motions, the validities of the model and the assumptions are supported. For the dance partner robot, since the LIPM model can preserve the basic features in human's body dynamics while offering several additional advantages, it is an appropriate robot model for implementation.

However, our analysis are still far from complete: due to the difficulties in measuring the interaction force $f(t)$ (given in (7) and (8)) and assuming the desired velocities, the analysis in Section III is rather preliminary. In addition, the presented discussions only involve the closed changes, while more dance steps with body rotations are not addressed. These issues need to be considered in our future work.

VI. ACKNOWLEDGMENTS

This work was supported by the Asian Office of Aerospace Research and Development (AOARD), Air Force Office of Scientific Research (AFOSR) under grant number FA2386-10-1-4126.

REFERENCES

[1] H. Kazerooni, "Human/robot interaction via the transfer of power and informationsignals," *IEEE Transactions on System, Man, and Cypernetics*, vol. 20, no. 2, pp. 450–463, 1990.

[2] K. B. Reed, J. Patton, and M. Peshkin, "Replicating Human-Human Physical Interaction," *Proceedings 2007 IEEE International Conference on Robotics and Automation*, pp. 3615–3620, Apr. 2007.

[3] S. Ikemoto, H. B. Amor, T. Minato, H. Ishiguro, and B. Jung, "Physical interaction learning: Behavior adaptation in cooperative human-robot tasks involving physical contact," *RO-MAN 2009 - The 18th IEEE International Symposium on Robot and Human Interactive Communication*, pp. 504–509, Sep. 2009.

[4] Z. Wang, A. Peer, and M. Buss, "An HMM approach to realistic haptic human-robot interaction," *EuroHaptics conference, 2009 and Symposium on Haptic Interfaces for Virtual Environment and Teleoperator Systems. World Haptics 2009. Third Joint*, pp. 374–379, 2009.

[5] J. Hölldampf, A. Peer, and M. Buss, "Virtual partner for a haptic interaction task," in *Human Centered Robot Systems*, ser. Cognitive Systems Monographs. Springer Berlin Heidelberg, 2009, vol. 6, pp. 183–191.

[6] T. Takeda, Y. Hirata, and K. Kosuge, "Dance step estimation method based on HMM for dance partner robot," *IEEE Transactions on Industrial Electronics*, vol. 54, no. 2, pp. 699–706, 2007.

[7] T. Takeda, Y. Hirata, and K. Kosuge, "Dance partner robot cooperative motion generation with adjustable length of dance step stride based on physical interaction," *2007 IEEE/RSJ International Conference on Intelligent Robots and Systems*, pp. 3258–3263, Oct. 2007.

[8] S. Kajita and K. Tani, "Study of dynamic biped locomotion on rugged terrain—theory and basic experiment," *Advanced Robotics, 1991. 'Robots in Unstructured Environments', 91 ICAR., Fifth International Conference on*, pp. 741–746 vol.1, jun. 1991.

[9] S. Kajita, F. Kanehiro, K. Kaneko, K. Yokoi, and H. Hirukawa, "The 3D linear inverted pendulum mode: a simple modeling for a biped walking pattern generation," *Proceedings 2001 IEEE/RSJ International Conference on Intelligent Robots and Systems*, no. 4, pp. 239–246, 2001.

[10] M. Thirunarayan, D. Kerrigan, M. Rabuffetti, U. Croce, and M. Saini, "Comparison of three methods for estimating vertical displacement of center of mass during level walking in patients," *Gait & Posture*, vol. 4, no. 4, pp. 306–314, 1996.

[11] E. M. Gutierrez-Farewik, A. Bartonek, and H. Saraste, "Comparison and evaluation of two common methods to measure center of mass displacement in three dimensions during gait." *Human movement science*, vol. 25, no. 2, pp. 238–56, 2006.